

# LIBRARY Michigan State University

# This is to certify that the dissertation entitled

# APTAMERS FOR PARALLEL MEASUREMENTS OF CELLULAR MOLECULES

presented by

Shengnan Xie

has been accepted towards fulfillment of the requirements for the

Ph.D. degree in Chemical Engineering

Major Professor's Signature

C4/27/10

Date

MSU is an Affirmative Action/Equal Opportunity Employer

**PLACE IN RETURN BOX** to remove this checkout from your record. **TO AVOID FINES** return on or before date due. **MAY BE RECALLED** with earlier due date if requested.

DATE DUE	DATE DUE	DATE DUE
		<del></del>

5/08 K:/Proj/Acc&Pres/CIRC/DateDue.indd

#### APTAMERS FOR PARALLEL MEASUREMENTS OF CELLULAR MOLECULES

Ву

Shengnan Xie

#### **A DISSERTATION**

Submitted to
Michigan State University
in partial fulfillment of the requirements
for the degree of

**DOCTOR OF PHILOSOPHY** 

**Chemical Engineering** 

2010

#### **Abstract**

#### APTAMERS FOR PARALLEL MEASUREMENTS OF CELLULAR MOLECULES

By

#### Shengnan Xie

Measuring the levels of the various molecules present in cells at any time is essential for the thorough and systematic understanding of complex biological processes. Thus, continuing innovation in analytical techniques for making these measurements, especially in parallel, can yield significant improvement in our understanding of biological systems. Moreover, successful analytical approaches often move from being applied purely for laboratory studies to use in clinical diagnoses, where an even greater impact is possible. Among the different types of biological analytes, much current research is focused on developing techniques to enable quantitative and parallel analyses of non-nucleic acid molecules such as proteins and small molecules.

Affinity-based analytical techniques have proven useful for nucleic acid, protein, and small molecule measurements. Aptamers, being nucleic acids that can bind non-nucleic acid molecules with high affinity and specificity, are an emerging class of affinity reagents that have potential advantages for analytical/biosensing applications. The aim of this dissertation was to use aptamers to develop analytical methods that leverage established nucleic acid analytical technologies for the analysis of proteins and small molecules. This work focused on two technologies for the analysis of small molecules and proteins, respectively.

One advantage of aptamers is the opportunity to couple sensing and readout of the analytes. This is particularly true with a unique class of aptamer-based sensing molecules,

termed structure-switching aptamers (SSAs), wherein the binding of the target molecule results in a conformational change of the molecule. Unfortunately, the parameters that determine the fidelity of the signal from SSA biosensors are generally unknown. In the first study, an SSA-based biosensing assay was developed to detect a model small molecule, theophylline, in solution. Through both computational and experimental analysis, it was found that the biosensor fidelity is primarily controlled by the relative stability of the two conformations of the SSA.

Based on this result, a protein biosensor was developed using a dual-aptamer approach. It was predicted that this approach would have improved dynamic range and sensitivity, relative to the SSA-based technique. The dual-aptamer biosensor relied on recognition of the target protein by two unique aptamers targeting different epitopes on the protein. Results showed that the technique achieved simultaneous and quantitative detection of proteins with high specificity. Moreover, the empirical biosensing performance agreed with expectations based on theoretical calculations.

To demonstrate the applicability of the dual-aptamer sensing technique for proteomics research, *in vitro* selection was performed to generate new aptamers. Aptamers for acute phase proteins fibrinogen and C-reactive protein (CRP) were selected and characterized to have nanomolar affinity for the proteins. Furthermore, two fibrinogen aptamers selected from two different pools bound the protein in a non-competitive fashion. The selected aptamers will serve as affinity reagents for developing multiplex protein analytical technique for these APPs. The results also suggested that identifying multiple, non-competitive aptamers for a target protein may be a general phenomenon that can be used to generate pairs of aptamers for our biosensing approach.

To my family

### **ACKNOWLEDGEMENTS**

This dissertation could not have been completed without the help and guidance of my advisor, Prof. S. Patrick Walton. He has provided me with invaluable academic independence yet made sure I am on the right track. I want to thank him for his brilliant ideas, insightful suggestions, and constant encouragement, all of which helped inspired my research. I'm grateful for having the opportunity to have worked with Prof. Walton, especially at the beginning of his professional career which I am sure will be very fruitful. I thank him for being such a great advisor.

I also would like to thank my committee members Prof. Chan, Prof. Worden and Prof. DeWitt. The discussions with all of them have always been productive and helpful. Prof. Chan has kept a close relationship to our research group and provided me with many creative ideas and invaluable suggestions. Prof. Worden helped to build an academic foundation for my biochemical engineering background. I have always been grateful for his suggestions and encouragement throughout my Ph.D. study. The insightful suggestions of Prof. DeWitt have inspired the conception of a large portion of my review paper in proteomics among many other works in this dissertation. I want to express my special appreciation to all of them.

My work would not have been possible without the assistance of Prof. Andrew Ellington at University of Texas-Austin (UT-Austin), who gave me the opportunity to learn selection in his lab. I want to give special thanks to Brad Hall at (UT-Austin) for his hosting and training and Xi Chen for tremendously enlightening discussions. My UT-Austin experiences had a powerful and significant impact on my research for which I am truly appreciative.

I also want to thank former and present members of the Cellular and Biomolecular Laboratory. Special thanks go to Joe Gredell and Hemant Kini, who made my transition from coursework to laboratory work much smoother; I was happy to form good friendships with both of them which I am sure will last through our professional careers. In addition, I want to thank Mark Swartzlander for his assistance with experiments. I am also thankful to Zheng Li and Lufang Sheng, who welcomed me on my first arrival to MSU and offered me so much care and help throughout; for that I am always grateful. I would also like to express my gratitude to Linxia Zhang, Xuerui Yang, Yifei Wu, Xuewei Wang, Hyun Ju Cho, Li Liu, Betul Bilgin, Hirosha Geekiyanage, Amanda Portis and Ming Wu for many many helpful interactions. I will always cherish the days I work with them.

I was fortunate to meet many other friends outside of lab, who have been a constant help and encouragement for me. Special thanks to Jun Sun, who is so knowledgeable and intelligent. I thank him for all the discussions, suggestions and techniques. A special note of thanks goes out to Susan Farhat-for sharing the journey from the beginning to the end-and to Cecelia Chen, for all the years of growing pains, with tears and laughter. I also want to thank Xi Hong, Yaoyan Xi, and Weipeng Liu for their friendships.

I want to express my deep gratitude to my parents who have given me endless unconditional love. Without them I would never have become the person I am today. Finally, I want to thank my beloved fiancé Fei Ren for his patience, support and encouragement. Thank you all for always being there for me.

Thank you.

# **TABLE OF CONTENTS**

LIST OF TABLES	ix
LIST OF FIGURES	x
LIST OF ABBREVIATIONS	xii
CHAPTER 1 INTRODUCTION	1
1.1 Significance	2
1.2 Current technologies for cellular molecule measurements	
1.2.1 Nucleic acid analytical techniques	
1.2.2 Protein analytical technologies	4
1.2.2.1 Planar antibody arrays	
1.2.2.2 Bead-based antibody arrays	9
1.2.2.3 Antibody conjugated-DNA barcoding	
1.2.3 Small molecule analytical technologies	
1.3 Aptamers	
1.3.1 What are aptamers?	
1.3.2 Advantages of aptamers	
1.3.3 Aptamer applications	
1.3.4 Aptamers as in vitro biosensors	
1.3.4.1 Binding-based aptamer biosensors	
1.3.4.2 Structure-switching aptamers	
1.4 The scope of this study	
References	
CHAPTER 2 APPLICATION AND ANALYSIS OF STRUCTURE-SWITCHING	
APTAMERS FOR SMALL MOLECULE QUANTIFICATION	41
2.1 Abstract	42
2.2 Introduction	
2.3 Experimental section	
2.3.1 Synthesis of the MBS	
2.3.2 Binding reactions and theophylline sensing experiments	
2.3.3 Binding affinity and theoretical signal-to-noise ratio calculation	
2.3.4 Reverse transcription and quantitative PCR	
2.4 Results and discussion	
2.4.1 Application of theophylline-responsive MBS	
2.4.2 Analysis of MBS performance	
2.4.3 Thermodynamic constructs for predicting MBS function	
2.5 Conclusions	
References	

CHAPTER 3 DEVELOPMENT OF A DUAL APTAMER-BASED MULTIPLEX	ζ
PROTEIN BIOSENSOR	89
3.1 Abstract	<b>9</b> 0
3.2 Introduction	91
3.3 Experimental section	
3.3.1 Proteins and aptamer sequences	
3.3.2 Dual aptamer sensing assays	
3.3.3 Aptamer affinity characterization	
3.3.4 PCR and qPCR	
3.3.5 Detection in bovine and human sera	
3.4 Results and discussion	
3.5 Conclusions	
References	
CHAPTER 4 IN VITRO SELECTION OF APTAMERS TO ACUTE PHASE PROTEINS	
4.1 Abstract	
4.2 Introduction	
4.3 Experimental section	
4.3.1 Synthesis of randomized RNA pool	
4.3.2 In vitro selection	
4.3.3 Cloning and sequencing	
4.3.4 Affinity characterization by filter binding assays	
4.3.5 Competition assays	
4.4 Results and discussion	144
4.5 Conclusions	161
References	162
CHAPTER 5 CONCLUSIONS AND FUTURE WORK	163
Defenence	1//

# **LIST OF TABLES**

Table 1.1 Comparison of conventional and affinity-based proteomics techniques 7
Table 2.1: Thermodynamic Predictions for MBS design modifications
Table 3.1: K <sub>D</sub> measured for each aptamer for its target protein
Table 3.2: C <sub>t</sub> values used to generate Figure 3.4
Table 4.1: Summary of in vitro selection for the R50-fibrinogen pool
Table 4.2: Summary of <i>in vitro</i> selection for the R70-fibrinogen pool
Table 4.3: Summary of in vitro selection for the R60-CRP pool
Table 4.4: The sequences of the random regions from selected clones of round 6 of the R50-fibringen selection pool
Table 4.5: The sequences of the random regions from selected clones of round 10 of the R70-fibringen selection pool
Table 4.6: The sequences of the random regions from selected clones of round 10 of the R60-CRP selection pool

# **LIST OF FIGURES**

Figure 1.1: Overview of the <i>in vitro</i> selection (SELEX) process
Figure 2.1: MBS design and detection strategy
Figure 2.2: Impact of theophylline on MBS-MBC hybridization
Figure 2.3: MBS-MBC binding affinity characterization
Figure 2.4: Validation of the fidelity of magnetic bead separation
Figure 2.5: Concentrations for optimal S/N, S-N and aggregate score
Figure 2.6: Theophylline and caffeine standard curves at optimal MBS and MBC concentration
Figure 2.7: Validation of qPCR assay for MBS detection
Figure 2.8: Quantification of theophylline concentration
Figure 2.9: Theoretical analysis of S/N, S-N and aggregate score
Figure 2.10: Thermodynamic constructs for MBS-MBC binding in the absence and presence of theophylline
Figure 3.1: Sensing response with respect to detecting aptamer concentration
Figure 3.2: Dual-aptamer detection schematic
Figure 3.3: Validation of qPCR amplification of sensing aptamers
Figure 3.4: Concentrations of sensing aptamers for optimal signal dynamic range 108
Figure 3.5: Affinity characterization of thrombin and PDGF-BB aptamers 109
Figure 3.6: Standard curves for singleplex detection of individual proteins using qPCR.
Figure 3.7: Multiplex detection of proteins using electrophoresis as the readout method.
Figure 3.8: Multiplex detection using qPCR as the readout method
Figure 3.9: Specificity of detection in the presence of competing protein
Figure 3.10: Multiplex detection of proteins in fetal bovine serum and human serum. 125

Figure 3.11: Correlation of various analyses.	129	
Figure 4.1: Affinity improvement of selected pools.	150	
Figure 4.2: Affinity characterization of selected clones.	157	
Figure 4.3: Competition assays for fibrinogen aptamers	159	

## LIST OF ABBREVIATIONS

2-DE - two-dimensional gel electrophoresis

AFP - α-fetoprotein

APP - acute phase proteins

ATP - adenosine triphosphate

BrdU - bromodeoxyuridine

cAMP - cyclic-adenosine monophosphate

CE-LIF - capillary electrophoresis with laser-induced fluorescence

CIAP - Calf Intestinal Alkaline Phosphatase

CRP - C-reactive protein

Ct - threshold cycle

DTT - dithiothreitol

EGFR - epidermal growth factor receptor

ELISA - enzyme-linked immunosorbent assay

ELONA - enzyme-linked oligonucleotide assay

EMSA - electrophoretic mobility shift assay

Erk - extracellular regulated kinase

FBS - fetal bovine serum

GBM - glioblastoma multiform

HCG - human chorionic gonadotropin

HIT - high-throughput immunophenotyping using transcription

hVEGF - human vascular endothelial growth factor

MB - molecular barcode

MBC - molecular barcode complement

MBS - molecular barcode switch

MS - mass spectrometry

PDGF - platelet-derived growth factor

PLA - proximity ligation assay

PSA - prostate specific antigen

QD - quantum dot

qPCR - quantitative Polymerase Chain Reaction

RCA - rolling circle amplification

RT - reverse transcription

S/N - signal-to-noise ratio

SELEX - Systematic Evolution of Ligands by EXponential enrichment

S-N - signal-to-noise difference

SSA - structure-switching aptamer

TPP - thyamine pyrophosphate

UTR - untranslated region

VEGF - vascular endothelial growth factor

# **CHAPTER 1 INTRODUCTION**

Portions reproduced from: Xie, S., Moya, C., Bilgin, B., Jayaraman, A. and Walton, S. P., "Emerging affinity-based techniques in proteomics", *Expert review of proteomics*, 6:573-583 (2009) with permission of Expert Reviews Ltd.

## 1.1 Significance

The advancement of both basic and applied biological research relies on the improvement of analytical techniques for measuring biomolecules, especially in a multiplex fashion. With the completion of human genome project, large amounts of gene sequence information became available. Now, the task is to concretely establish the functions of each of the gene products produced from these sequences. This will require continued advancement in technology and will lead to a more complete understanding of biological processes. In turn, it should accelerate application of this understanding in clinical applications and research.

### 1.2 Current technologies for cellular molecule measurements

Nucleic acid analyses, both in a single and multiplex fashion, are very mature at this point. However, a full description of cellular function also requires the measurement of downstream products of gene expression, such as proteins and metabolites/small molecules. Current research on technology development focuses on developing reliable and flexible techniques for analyzing proteins and small molecules, especially in a high-throughput fashion. In this section, the state of the art technologies will be reviewed, with an emphasis in multiplex detection techniques.

### 1.2.1 Nucleic acid analytical techniques

Analytical technologies for DNAs and RNAs were established early, primarily based on Watson-Crick base pairing of nucleic acids, with, for instance, quantitative polymerase

chain reaction (qPCR) now common practice for nucleic acid analyses [1-5]. The invention of microarrays allowed large quantities of nucleic acids to be simultaneously monitored on a single chip, which resulted in a revolution relative to the historical "one gene-one experiment" method [6]. Microarrays are fabricated with DNAs of known sequence arranged on solid substrates. Typically, fluorescently-labeled sample nucleic acids are hybridized to the complementary sequences immobilized on the substrate, yielding a fluorescent signal from the bound material [7]. By calculating the signal intensity, concentrations of the nucleic acid samples can be quantified. DNA sequences can be either spotted or synthesized onto the substrates. Spotted microarrays are produced by physical deposition of DNA, either cDNAs or oligonucleotides, onto the substrate [8], while oligonucleotide arrays can also be synthesized nucleotide by nucleotide *in situ* [9,10].

Since their invention, microarrays have been widely used for monitoring gene expression [11,12], characterizing DNA polymorphisms [13], and detecting genome-wide chromosomal alterations in cancer and development [10]. DNA microarrays are now standard practice for parallel nucleic acid analyses, and they are also finding novel applications in parallel analyses of other biomolecules (discussed in Section 1.2.2.3, below).

The advancement of high-throughput DNA sequencing technologies has also enabled their applications in nucleic acids analyses [14,15]. For example, the 454 sequencing technology allows for simultaneous sequencing of genomic DNA or a large number of

clones with significant reduction in experimental cost and time. This technology has started to be used for gene expression analysis [16] and identifying DNA methylation patterns in cancer patients [17]. It has also been applied for comprehensive analysis of small RNAs, including their discovery and differential expression profile characterization [18,19].

#### 1.2.2 Protein analytical technologies

Proteins lack the natural complementarity of nucleic acids and so must be analyzed by a variety of techniques that leverage their unique physical and chemical properties.

Individual proteins can be measured by techniques such as electrophoresis, chromatography, spectroscopy, and immunoassays [20]. However, high-throughput analytical techniques for proteins still do not approach the scale of current genomics methods.

Although techniques for separating proteins such as polyacrylamide gel electrophoresis and chromatography have been in practice for a long time, 'large-scale' protein separation was first described by O'Farrell in 1975 [21]. The technique, two-dimensional gel electrophoresis (2-DE), separates proteins in a polyacrylamide gel in two orthogonal dimensions. Proteins are first separated based on their isoelectric point followed by molecular weight/size-based separation. 2-DE has been applied to a diverse range of samples [22-26]. While simple to use and without complex instrumentation, 2-DE has some significant drawbacks. First, not all types of proteins (e.g., membrane proteins, hydrophobic proteins, proteins greater than 150 kDa) are resolved equally well in gel

electrophoresis [27]. Second, the loading capacity of gels is limited, which in turn limits the amount of protein that can be separated and the depth of proteome coverage that can be obtained. This is especially important when working with complex biological fluids such as serum where the range of protein concentrations spans at least five orders of magnitude [28,29]. Although approaches such as sample fractionation, use of 'zoom gels' (i.e., narrow pI range isoelectric focusing gels), and more sensitive staining methods (e.g., fluorescence-based stains) have been developed to overcome these drawbacks, 2-DE is currently used primarily for initially characterizing proteomes prior to more thorough analysis by other methods.

The development of mass spectrometry (MS) methods has addressed some of the drawbacks of gel-based proteomics methods mentioned above, especially in handling complex protein samples and increasing the depth of proteome coverage. Proteins are first separated by gel electrophoresis or by liquid chromatography, prior to proteolytic fragmentation and identification by MS [30]. Alternatively, the entire protein sample can be digested and the generated peptides separated and analyzed [31]. This "shotgun approach" has the advantage of utilizing multiple liquid chromatography techniques (e.g., size exclusion followed by strong-cation exchange chromatography) to separate the complex peptide mixture before MS analysis. However as the number of generated peptides exceeds 2 million [32], the ability to separate ions with very similar mass-to-charge ratios and instrument sensitivity are limiting factors. Therefore, complementary, affinity-based technologies are actively under development for multiplex protein analyses.

Emerging techniques using affinity reagents for the analysis of focused sets of proteins have the potential for improved sensitivity, less effort, and more broadly focused than 2DE/MS techniques (see Table 1.1 for a general comparison of 2-DE/MS-based and affinity-based methods). These methods are highly tunable to meet the needs of the investigator and the system of interest. However, they are only applicable for known protein targets and, furthermore, these targets need to have well characterized, specific affinity reagents. To date, the use of antibodies has predominated affinity-based protein analytical methods. Nonetheless, the interactions between proteins and their non-proteinaceous binding partners such as transcription factor binding sequences [33] and aptamers derived from *in vitro* selection (chapter 1.3), have been screened in various array formats. In this section, the state of the art in antibody-based proteomic strategies will be discussed, focusing primarily on new techniques that are using antibodies in creative ways to circumvent the limitations of existing technologies.

Table 1.1 Comparison of conventional and affinity-based proteomics techniques.

Property	2DE/MS-based	Affinity-based
Applications	Identification, expression, post translational modifications	Expression, interactions, function, post translational modifications
Specificity	Tunable based on separation	Depends on specificity of affinity
	method used	reagents
Sensitivity	Difficulty with low abundance	Nano- to femtomolar protein
	proteins in mixtures	concentration
Breadth of	Can approach all proteins in a	Focused sets of proteins defined
coverage	sample	by researcher
Instrumentation	Significant	Varies broadly depending on
Requirements		technique
Pretreatment	Typically requires removal of high abundance proteins	Often no pretreatment required

#### 1.2.2.1 Planar antibody arrays

Planar antibody arrays were the earliest form of proteomic arrays for profiling protein expression levels. Compared to 2-DE/MS methods, antibody arrays can, in some cases, perform more rapid and sensitive multiplex analyses of the non-fractionated proteome [34]. Antibody arrays can generally be classified into three categories: i) immobilized antibodies to capture labeled proteins from the solution [35]; ii) immobilized proteins detected by labeled antibodies [36,37], and iii) dual antibody sandwich assays [38-40]. Protein arrays have been widely used for cytokine profiling in a variety of studies, including providing comprehensive information for inflammation and aging studies [41,42]. They have also been actively used in biomarker identification for a variety of cancers, including prostate [43], breast [44], hepatic [45], and pancreatic [46]. Analysis of secreted proteins to establish disease biomarker profiles continues to be a primary use of protein arrays.

Antibody microarrays have also been applied to study intracellular signaling. Antibodies to epidermal growth factor receptor (EGFR) and ErbB2/Her2 and their tyrosine phosphorylated forms were used to monitor the concentrations and activities of receptor tyrosine kinases in a ratiometric microarray format [47]. A label-free sandwich approach using near infrared spectroscopy was applied to study extracellular regulated kinase (Erk) 1/2 and Stat3 signaling in cell lines and primary cells over time [48].

Unique methods have been explored to improve the sensitivity and performance of antibody-based methods. One such method, rolling circle amplification (RCA) was used

to maximize the signal response from protein recognition in a multiplexed assay [49]. After protein capture by monoclonal antibodies on the microarray, secondary, biotinylated polyclonal antibodies for the proteins were added. Finally, the secondary antibodies were bound by anti-biotin antibodies conjugated with DNA primers.

Following addition of a circular DNA template, polymerase, and nucleotides, RCA begins and produces long ssDNA strands that were then detected with fluorescently-labeled, complementary oligonucleotides. This technique was used for the simultaneous measurement of 75 cytokines with femto- to picomolar sensitivity. RCA enabled detection of cytokine levels 1000-fold below the sensitivity limit of direct fluorescent detection without amplification. In addition, because of the ligation of the readout to the antibody binding, signal diffusion, often an issue with enzyme catalyzed chemiluminescent readouts, was largely avoided.

#### 1.2.2.2 Bead-based antibody arrays

Solution-phase, multiplexed immunoassays have been developed on microbeads, enabled by flow cytometric detection of the color-coded beads used to immobilize the antibodies [50]. Each bead is then detected by its unique optical signature. The beads can also be conjugated with other capture molecules such as antigens, receptors, or enzyme substrates. A commercially available platform has been developed using beads labeled with two fluorescent dyes each with 10 different intensities (Luminex Corporation, Austin, TX) [51], which limits analyses to a maximum of 100 unique analytes. However, as the limitation is based on bead encoding, rather than sensitivity or specificity, the potential to expand the technique to greater parallelism, certainly exists.

Compared with planar protein arrays, bead-based assays have advantages such as solution phase processing and detection, increased flexibility, and simplified automation [52]. Unlike planar arrays, which are relatively inflexible after synthesis, bead-based arrays can be readily customized through inclusion of different sets of existing or user-customized beads [51]. Because they are typically based on two-molecule detection (e.g., detection of the bead color and fluorescence from the analyte), bead-based assays often do not require a wash step to reduce non-specific background, which maximizes the sensitivity of the assay while simultaneously simplifying sample processing.

Bead-based assays have been applied for a variety of systems, including detection of cytokines [53-58], auto-antibodies [59,60], and biological warfare agents [61]. In one interesting application, the bead system was used for fast analysis of binding specificities of monoclonal antibodies [62]. Protein epitope signature tags from which antibodies were generated were immobilized and mixed. The binding specificity of 84 antibodies was assayed by incubating each antibody with the bead mixture followed by detection with fluorescently labeled secondary antibodies. Results from the bead technique were validated with planar microarrays [62]. The authors were also able to use their validated antibodies with the bead system to measure 20 serum proteins from 200 clinical serum samples in under 2 days [63].

Recently, bead-based profiling was applied for measuring the phosphorylation activity of 62 of 90 tyrosine kinases present in various cancer cell lines [64]. Tyrosine kinase

specific antibodies were coupled to the beads for immobilization of the enzymes. A biotinylated, antiphosphotyrosine antibody was then used for detection of the phosphorylation status of the enzymes from cell lysates. Kinases with similar phosphorylation patterns across multiple cancer cell lines were identified [64]. Importantly, the frequent activation of SRC in glioblastoma was confirmed in follow up experiments with primary glioblastoma multiform (GBM) patient samples. SRC was also indicated as a potential therapeutic target for GBM. This multiplexed method significantly reduced the required cell number and cost per assay and proved to have specificity and sensitivity equivalent to western blotting.

Quantum dots (QDs) have been explored to address the limit on the number of possible fluorescent bead encodings. QDs are inorganic crystals composed of a cadmium selenide core and a zinc sulfide shell. QDs typically have higher brightness, orders of magnitude higher resistance to photobleaching, and narrower emission spectra, compared to organic fluorophores [65]. Moreover, the properties of QDs result from their chemical composition and physical structure, allowing facile manipulation of their characteristics to avoid spectrum overlap and increase their potential for multiplex applications [65]. Polymeric microbeads coded with QDs were developed by infusing QDs into preformed beads in organic solvents [66]. The QD encoded beads were used in a multiplexed detection of autoantibodies of Topol and sm-antigen in serum samples of systemic sclerosis patients [67]. QDs were also used directly as fluorescent labels in immunophenotyping [68]. A 17-color staining panel composed of 7 QDs and 10 other fluorophore labeled antibodies and pMHCI antigens was used to probe surface marker

expression of antigen specific T-cell populations within an HIV-seropositive individual by polychromatic flow cytometry [68]. It was found that every antigen specific subset of cells had a unique phenotypic pattern, providing an example of the potential of QD-based readouts in proteomic applications.

#### 1.2.2.3 Antibody conjugated-DNA barcoding

An alternative to direct readout of protein detection is through the translation of protein signal to the nucleic acid domain through strategies that can collectively be described as antibody conjugated-DNA barcoding. These methods have the advantage that the terminal readout is the quantity of the nucleic acid, rather than the quantity of protein, therefore the readouts can take advantage of convenient, parallel, sensitive, and relatively ubiquitous methods for nucleic acid detection (as discussed in Chapter 1.2.1 above). One manner by which this is accomplished is to assign antibodies with a unique DNA label. An early application of a barcoding strategy was in the use of gold nanoparticles functionalized with an antibody and multiple copies of a biobarcode oligonucleotide [69]. The particles were then applied in a sandwich-like format with magnetic particles conjugated with another monoclonal antibody for the same protein target. Different oligonucleotides were used as identifiers for different target proteins, and, after magnetic separation, the biobarcodes were eluted from the nanoparticles with dithiothreitol (DTT) and measured using a DNA microarray. This method was used in a multiplex assay to measure three established cancer markers: prostate specific antigen (PSA, a prostate cancer marker), human chorionic gonadotropin (HCG, a testicular cancer marker), and αfetoprotein (AFP, a hepatocellular carcinoma marker) at 170 fM concentration in diluted

serum. The extraordinary sensitivity was resulted from the release of multiple biobarcode oligonucleotides for each protein molecule detected. It is possible that even further sensitivity might be possible using PCR to amplify the released oligonucleotides prior to detection.

Antibodies directly conjugated with DNA tags have also been used to measure six proteins simultaneously in what is termed a proximity ligation assay (PLA) [70]. Each protein analyte was probed by a pair of antibodies each modified with an oligonucleotide probe. Upon binding of both antibodies to the target, the probes were in close proximity and were ligated together in the presence of template strands complementary to the two probes. Ligated products were amplified with specific primers to each probe and detected with real time PCR [70]. This assay can sensitively detect proteins at femtomolar concentrations in 1 µl samples (roughly 1000-10000 total molecules of protein per sample). The high sensitivity and low background of this assay was due to the amplification capacity of PCR and the dual binding events required for generating a positive signal, similar to the biobarcode assay described above. However, in this study, the unique barcode sequences were not utilized for discrimination among the protein signals in parallel.

DNA barcoding has been combined with microfluidics for rapid, flexible construction of a tool for plasma protein analysis. Rather than depositing the antibodies directly onto an array, antibodies were conjugated with multiple copies of a ssDNA barcode and were then hybridized to an array functionalized with complementary ssDNA strands [71]. The

ligated DNA barcodes ensured that the antibodies were separated so that any region of the array was specific for a single antigen. The array was then applied in a sandwich format with detection antibodies. Coupling the array to a microfluidic system, direct onchip separation of plasma from blood obviated the need for prior centrifugation, enabling measurement of 12 protein concentrations simultaneously from a 10 µL sample [71].

In the high-throughput immunophenotyping using transcription (HIT) technique, each DNA tag used to label the antibody contained a T7 promoter and was amplified by the T7 RNA polymerase [72]. The labeled RNA tags were then purified and hybridized to a DNA microarray for quantification. Using two 48-plex HIT reactions, 90 surface markers on human naïve T helper cells were profiled. Although the assay format was limited to measuring the surface proteins on pure populations of cells, the concept of using existing DNA microarrays for new purposes suggests an efficient means for the rapid development of new proteomics platforms.

Although antibodies are currently the most commonly used affinity reagent, the majority of human proteins still lack a specific antibody. Moreover, many proteins have a large number of antibodies and their qualities and performances are not easily defined.

Moreover, the costs are also extraordinarily high for proteomics analysis [73]. Therefore, other affinity reagents such as aptamers are being explored as alternative and complementary affinity reagents for protein analytical applications (Chapter 1.3).

#### 1.2.3 Small molecule analytical technologies

Metabolites/small molecules are another essential set of cellular molecules. The systematic study of small molecule profiles resulting from specific cellular processes is usually termed metabolomics. Together with transcriptomic (mRNA) and proteomic (protein) analyses, metabolomic analyses provide a comprehensive description of cellular physiology. The quantification of disease-associated metabolites provides another means of biomarkers that may serve as guidance for development of therapeutics [74].

While certain metabolites and hormones can be detected using immunoassays, and some small molecules such as glucose and alcohols can be measured by enzymatic assays [75], metabolomics analyses in general are the most complex among parallel biomolecule analysis [76]. Identification of individual small molecules within a complex samples requires techniques that can separate the various analytes using methods such as gas or high performance liquid chromatography, followed by mass spectrometry [75,77]. Metabolomics was used to identify metabolite biomarkers for prostate cancer [78]. 1126 metabolites across 262 clinical samples related to prostate cancer were profiled. Sarcosine was identified as a marker metabolite whose concentration was highly elevated during prostate cancer progression to metastasis and whose inhibition was also suggested to attenuate prostate cancer progression [78].

Nonetheless, the metabolome is so complex that no single method can effectively analyze all of the unique molecules within most biological samples. Analysis of data from these methods can also be complicated due to the difficulty in resolving constituents with

chemical or structural similarity [79]. The combination of current and emerging technologies is contributing a more comprehensive description of the entire cellular metabolome.

# 1.3 Aptamers

#### 1.3.1 What are aptamers?

Aptamers are single-stranded nucleic acids that can bind specific target molecules with high affinity and specificity. Two groups published the method to generate aptamers almost simultaneously [80,81]. High-affinity aptamers can be isolated by an in vitro selection process named SELEX (Systematic Evolution of Ligands by EXponential enrichment) (Figure 1.1). The selection starts from a large library (10<sup>14</sup>-10<sup>15</sup>) of randomized RNA or single stranded DNA sequences. The pool is mixed with the target molecules and sequences that bind with the target are separated from the unbound ones. The recovered sequences are amplified by Polymerase Chain Reaction (PCR). This enriched pool is then subjected to another round of selection. This process is repeated for several rounds until the pool primarily consists of aptamers of high affinity to the target molecules. To date, aptamers have been generated against a variety of molecules including amino acids [82], peptides [83], proteins [84,85], small molecules [86,87], metal ions [88], oligosaccharides [89,90], and lipids [91,92]. Therefore, SELEX can be used to isolate oligonucleotide sequences with the capacity to recognize virtually any target biomolecule with high affinity and specificity.

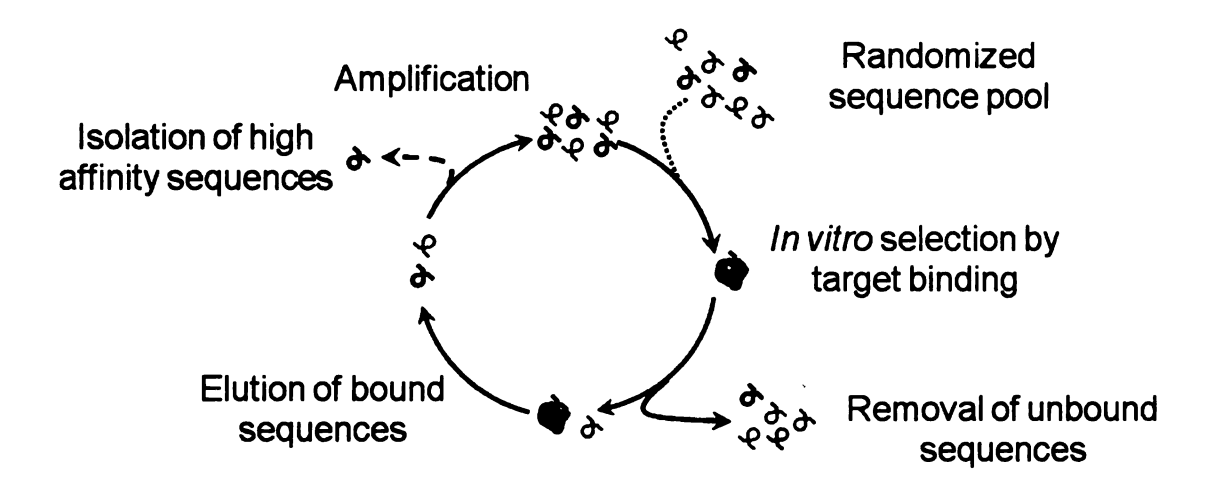


Figure 1.1: Overview of the *in vitro* selection (SELEX) process. A library of single stranded DNA or RNA is incubated with target molecules. Unbound sequences are separated and removed. The target-bound sequences are eluted from the target and amplified to start the next round of selection. This process is repeated until high affinity aptamers are enriched and isolated for characterization.

Interestingly, aptamers have also been discovered in the mRNA of natural organisms and they typically reside in the 5' untranslated regions (UTRs) [93]. These aptamers couple *in vivo* sensing of small molecules and response domains to participate in the response to stimuli. Because their response depends on conformational changes in the molecule, they were termed riboswitches [93]. Since their initial discovery, bioinformatics tools have identified 20 distinct classes of metabolite binding aptamers, primarily in eubacteria, with the thyamine pyrophosphate (TPP) riboswitch class also discovered in eukaryotes [94]. Riboswitches are suggested to play significant roles in regulating the expression of genes that are vital to metabolism [93,95-101]

### 1.3.2 Advantages of aptamers

In comparison to antibodies (proteinaceous affinity molecules), aptamers offer a number of advantages. First, aptamers can be reliably synthesized from known sequences using chemical or enzymatic procedures [102,103]. Second, because aptamers are generated by *in vitro* selection, aptamers targeting any analyte, including those too toxic to allow generation of antibodies, could potentially be generated. Third, the specificity and affinity of aptamers is tunable through manipulation of the selection conditions, such as by incorporating negative selection against similar analytes for an increased target specificity [86]. The high specificity that can be achieved is especially advantageous for multiplex sensing applications. Aptamers can also be generated with chemically-modified nucleotides to enhance their properties for various applications, such as stability to nucleases for measurements in biological fluids [104-106]. Moreover, aptamers can be

readily engineered for various applications using designed selection or through *post hoc* manipulations [107-114]

## 1.3.3 Aptamer applications

Aptamers have been used in various biotechnology and biomedicine applications. One therapeutic aptamer, Macugen, which binds vascular endothelial growth factor (VEGF), is already available in the market [115], and, to date, six more aptamer drugs are in clinical trials [115]. Non-natural riboswitches have also been produced for controlling transcription, translation, and mRNA stability [116,117]. Moreover, aptamers can be immobilized in chromatography columns for affinity purification [118,119].

## 1.3.4 Aptamers as in vitro biosensors

Aptamers are being actively applied as biosensing elements for *in vitro* diagnostics.

Aptamer based biosensors have been developed for a variety of analytes such as small molecules, metal ions and proteins [120]. While the readout mechanisms vary, aptamer-based biosensing methods are becoming invaluable components of current biomolecule analytical technologies.

#### 1.3.4.1 Binding-based aptamer biosensors

Aptamers have been used in a variety of applications for which antibodies are typically applied. In a so-called enzyme-linked oligonucleotide assay (ELONA), an aptamer was used in place of the secondary antibody in a sandwich-type assay for the detection of human vascular endothelial growth factor (hVEGF) [121]. The assay showed a detection

sensitivity of 25 pg/ml (0.55 pM), and a good correlation to the enzyme-linked immunosorbent assay (ELISA) results. A similar approach was used in the detection of thrombin with a detection limit of 1 nM [122]. A quartz crystal biosensor was designed for IgE with a detection limit of 0.5 nM [123]. The same target was analyzed with capillary electrophoresis with laser-induced fluorescence detection (CE-LIF) with a detection limit of 46 pM [124]. Aptamers were also used in designing biosensors using fluorescence anisotropy [125], electrochemical detection [126], micro-fabricated cantilever [127], and surface plasma resonance [128].

While the majority of techniques are in the singleplex format, several groups have since developed aptamer arrays to measure multiple proteins simultaneously [129-131]. A four-element RNA aptamer array was developed in which biotinylated RNA aptamers were deposited onto streptavidin coated slides using contact printing. Analyte proteins were labeled with Cy3 or Cy5 fluorescent dyes and detected in a cell lysate background [130]. A dual protein detection scheme using an electrochemical biosensor was recently demonstrated [132]. A flow cell system enabling real time detection of multiple aptamer binding events was also developed on a bead array format [133].

In native aptamer (and antibody) assays for measuring proteins, non-specific interactions are reduced through washes or other means. However, in doing so, specific signal is also reduced. In an effort to maintain sensitivity with minimal background, photoaptamers were developed [134]. Photoaptamers are selected containing bromodeoxyuridine (BrdU) modifications that readily crosslink to bound proteins upon UV exposure. These were

applied in an aptamer array that measured 17 proteins simultaneously from serum samples [129]. Crosslinked proteins were detected by universal protein stain or specific secondary antibodies. Because of the low background, the detection limits of about one third of the analytes were below picomolar concentration, with several analytes exhibiting an impressive detection limit below 10 fM.

#### 1.3.4.2 Structure-switching aptamers

A unique class of aptamer-based sensors has been termed structure-switching aptamers (SSAs), wherein the binding of the target molecule results in a conformational change of the SSA. As engineering protein biosensors is difficult because it generally requires knowledge of protein tertiary structures, the ability to design SSAs solely based on their primary (sequence) and secondary (intramolecular hybridization) structures is essentially unique to nucleic acids. The sensing can be simultaneously measured by detection of the conformational rearrangement, in some cases without requiring the addition of secondary reagents. Therefore, SSAs are of particular interest for biosensing applications [135-147].

The most straightforward method to construct an SSA is to utilize the aptamer rearrangement upon target binding. For instance, methods were developed such that a *single* modification with a fluorophore was made to the aptamer on a position that underwent significant structural rearrangement upon target binding. The change in the environment around the fluorophore would result in altered signal. The fluorescence signal then was directly dependent on the degree of target binding [113,148]. Aptamer beacons, wherein the spacing between a fluorophore and a quencher changes upon target

binding, have also been applied [149-151]. Electrochemical detection was also used in which the free end of the immobilized aptamer was labeled with a redox moiety, whose distance to the sensor surface changed upon target binding, thereby altering the electron transfer efficiency [152,153]. However, these designs usually result in a high background or limited signal response, due to the relative flexibility of aptamer conformations in the absence of the target.

To minimize background, target induced strand displacement architectures were developed in which a complementary strand was incorporated to hybridize with the designed aptamer construct. In one fluorescence approach, fluorophore-labeled aptamers were hybridized with a quencher labeled antisense strand in the absence of target [154]. Upon target binding to the aptamer strand, the duplex strand was disrupted and fluorescence was observed. Such signaling SSAs were created by both rational design and *in vitro* selection approaches with the detection limit for adenosine triphosphate (ATP) at micromolar concentrations and thrombin at nanomolar concentrations [144,154,155]. As above, an electrochemical approach has also been applied, showing detection of thrombin at nanomolar concentrations [138]. While the readout strategies vary, SSA-based biosensors have to date been used primarily for single analytes. In addition, the parameters controlling the sensitivity and the signal-to-noise ratios for this type of biosensor were poorly understood.

Structural rearrangement upon aptamer-target binding was also used in designing allosteric ribozyme biosensors. Allosteric ribozymes are nucleic acid enzymes composed

of an aptamer domain and a ribozyme domain. Target binding to the aptamer alters the conformation of the construct, leading to a change in ribozyme catalytic activity.

Allosteric ribozymes have been designed for self-cleavage [156-158] and ligation [159].

Modular rational design, *in vitro* selection, and computational strategies have all been used to generate allosteric ribozymes, and their altered activity upon target binding can be transduced to an observable signal for use in biosensing [160,161].

The most prominent example of such class of biosensors is a small molecule array fabricated by depositing seven allosteric ribozymes onto a gold surface [162]. By measuring the fraction of radiolabeled ribozymes that underwent self-cleavage in the presence of different small molecules in a complex cellular environment, the analyte composition and concentration can be determined. The array was used to determine the concentrations of 3'-5' cyclic-adenosine monophosphate (cAMP), a secreted product in bacterial cultures. An aptazyme ligation assay was also developed by immobilizing a biotinylated substrate in a 96-well format and measuring the fraction of radioactive aptazyme ligated to the substrate upon target binding [163]. This assay was used to detect a variety of analytes, such as metabolites, peptides and proteins, at nanomolar concentrations with good specificity. These methods demonstrated the possibility of utilizing an ensemble of aptamers for multiplex sensing applications and corroborated that aptamers retain their specificity in complex, mixed analyte environments. Improved readout methods using fluorescence have also been developed [164,165]. However, their use in multiplexed applications has yet to be demonstrated.

## 1.4 The scope of this study

In this study, we leverage the use of nucleic acid quantification techniques for designing aptamer-based, multiplex analytical technologies for proteins and small molecules. In chapter 2, the development and analysis of an SSA biosensor were discussed, for the detection of a model small molecule theophylline. Quantitative theophylline detection over near three orders of magnitude was achieved with convenient nucleic acid quantification techniques. We investigated the biosensor performance by both computational and experimental approaches and found that the relative stability of the two SSA conformations is the factor limiting the S/N. It was further proposed that the direct binding approach would provide a larger dose response relative to the SSA design.

Based on the prediction, in chapter 3, a dual aptamer-based multiplex protein sensor was developed. Results demonstrated that the technique achieved simultaneous and quantitative detection of thrombin and platelet-derived growth factor-BB (PDGF-BB) at pico- to nanomolar concentrations with high specificity both in buffered solutions and in sera. The biosensing performance derived experimentally confirmed the theoretical prediction.

In chapter 4, we describe the *in vitro* selection of aptamers for the acute phase proteins, C-reactive protein (CRP) and fibrinogen. Two fibrinogen aptamers that bind the protein in a non-competitive fashion were generated. The selected aptamers are designed for use in the biosensing assays we have developed. Our approach provides a universal platform for generating dual-aptamers and designing robust multiplex protein biosensors.

#### References

- 1. Saiki RK, Gelfand DH, Stoffel S *et al.* Primer-directed enzymatic amplification of DNA with a thermostable DNA polymerase. *Science (New York, N.Y*, 239(4839), 487-491 (1988).
- 2. Nolan T, Hands RE, Bustin SA. Quantification of mRNA using real-time RT-PCR. *Nature protocols*, 1(3), 1559-1582 (2006).
- 3. Southern EM. Detection of specific sequences among DNA fragments separated by gel electrophoresis. *Journal of molecular biology*, 98(3), 503-517 (1975).
- 4. Alwine JC, Kemp DJ, Stark GR. Method for detection of specific RNAs in agarose gels by transfer to diazobenzyloxymethyl-paper and hybridization with DNA probes. *Proc Natl Acad Sci U S A*, 74(12), 5350-5354 (1977).
- 5. Schena M, Shalon D, Davis RW, Brown PO. Quantitative monitoring of gene expression patterns with a complementary DNA microarray. *Science (New York, N.Y,* 270(5235), 467-470 (1995).
- 6. Schena M, Shalon D, Davis RW, Brown PO. Quantitative Monitoring of Gene-Expression Patterns with a Complementary-DNA Microarray. *Science*, 270(5235), 467-470 (1995).
- 7. Gershon D. Diy or off-the-shelf? *Nature*, 416(6883), 885-+ (2002).
- 8. Lockhart DJ, Winzeler EA. Genomics, gene expression and DNA arrays. *Nature*, 405(6788), 827-836 (2000).
- 9. Lockhart DJ, Dong HL, Byrne MC *et al.* Expression monitoring by hybridization to high-density oligonucleotide arrays. *Nature biotechnology*, 14(13), 1675-1680 (1996).
- 10. Barrett MT, Scheffer A, Ben-Dor A et al. Comparative genomic hybridization using oligonucleotide microarrays and total genomic DNA. Proceedings of the National Academy of Sciences of the United States of America, 101(51), 17765-17770 (2004).

- 11. Wodicka L, Dong HL, Mittmann M, Ho MH, Lockhart DJ. Genome-wide expression monitoring in Saccharomyces cerevisiae. *Nature biotechnology*, 15(13), 1359-1367 (1997).
- 12. van 't Veer LJ, Bernards R. Enabling personalized cancer medicine through analysis of gene-expression patterns. *Nature*, 452(7187), 564-570 (2008).
- 13. Kennedy GC, Matsuzaki H, Dong SL et al. Large-scale genotyping of complex DNA. *Nature biotechnology*, 21(10), 1233-1237 (2003).
- 14. Cloonan N, Forrest ARR, Kolle G et al. Stem cell transcriptome profiling via massive-scale mRNA sequencing. *Nature Methods*, 5(7), 613-619 (2008).
- 15. Main BJ, Bickel RD, McIntyre LM, Graze RM, Calabrese PP, Nuzhdin SV. Allele-specific expression assays using Solexa. *BMC Genomics*, 10, 9 (2009).
- 16. Torres TT, Metta M, Ottenwalder B, Schlotterer C. Gene expression profiling by massively parallel sequencing. *Genome Research*, 18(1), 172-177 (2008).
- 17. Korshunova Y, Maloney RK, Lakey N et al. Massively parallel bisulphite pyrosequencing reveals the molecular complexity of breast cancer-associated cytosine-methylation patterns obtained from tissue and serum DNA. Genome Research, 18(1), 19-29 (2008).
- 18. Berezikov E, Thuemmler F, van Laake LW et al. Diversity of microRNAs in human and chimpanzee brain. Nat Genet, 38(12), 1375-1377 (2006).
- 19. Kasschau KD, Fahlgren N, Chapman EJ et al. Genome-wide profiling and analysis of Arabidopsis siRNAs. PLoS Biol, 5(3), e57 (2007).
- 20. Engvall E, Perlmann P. Enzyme-linked immunosorbent assay (ELISA) quantitative assay of immunoglobulin-G *Immunochemistry*, 8(9), 871-& (1971).
- 21. O'Farrell PH. High resolution two-dimensional electrophoresis of proteins. Journal of Biological Chemistry, 250, 4007-4021 (1975).

- 22. Duan X, Berthiaume F, Yarmush DM, Jayaraman A, Yarmush ML. A mouse serum two-dimensional gel map: Application to profiling burn injury and infection. *Electrophoresis*, 25, 3055-3065 (2004).
- 23. Duan X, Yarmush ML, Jayaraman A, L YM. Dispensable role for interferon gamma in the acute phase response: A proteomics analysis. *Proteomics*, 4, 1830-1839 (2004).
- 24. Jayaraman A, Roberts KA, Yoon J et al. Identification of neutrophil gelatinase-associated lipocalin (NGAL) as a discriminant marker of the hepatocyte secreted protein response to IL-1β: a proteomic analysis. Biotechnol & Bioeng, 91, 502-515 (2005).
- 25. Nandakumar R, Nandakumar MP, Marten MR, Ross JM. Proteome analysis of membrane and cell wall associated proteins from *Staphylococcus aureus*. *J Proteome Res*, 4, 250-257 (2005).
- 26. Dooley GP, Reardon KF, Prenni JE et al. Proteomic analysis of diaminochlorotriazine adducts in wistar rat pituitary glands and LbetaT2 rat pituitary cells. Chem Res Toxicol, 21, 844-851 (2008).
- 27. Rabilloud T. Membrane proteins and proteomics: Love is possible, but so difficult. *Electrophoresis*, 30, S174-180 (2009).
- 28. Miller I, Crawford J, Gianazza E. Protein stains for proteomic applications: which, when, why? *Proteomics*, 6, 5385-5408 (2008).
- 29. Shen Y, Jacobs JM, Camp DG, 2nd et al. Ultra-high-efficiency strong cation exchange LC/RPLC/MS/MS for high dynamic range characterization of the human plasma proteome. Anal Chem, 76(4), 1134-1144 (2004).
- 30. Iwadate Y. Clinical Proteomics in Cancer Research-Promises and Limitations of Current Two-Dimensional Gel Electrophoresis. *Current Medicinal Chemistry*, 15(23), 2393-2400 (2008).
- 31. Cravatt BF, Simon GM, Yates JR. The biological impact of mass-spectrometry-based proteomics. *Nature*, 450, 991-1000 (2007).

- 32. Ahn NG, Shabb JB, Old WM, Resing KA. Achieving in-depth proteomics profiling by mass spectrometry. *ACS Chem Biol*, 2, 39-52 (2007).
- 33. Xie S, Moya C, Bilgin B, Jayaraman A, Walton SP. Emerging affinity-based techniques in proteomics. *Expert Rev Proteomics*, 6(5), 573-583 (2009).
- 34. Borrebaeck CA, Wingren C. High-throughput proteomics using antibody microarrays: an update. *Expert Rev Mol Diagn*, 7(5), 673-686 (2007).
- 35. Zhou HP, Bouwman K, Schotanus M et al. Two-color, rolling-circle amplification on antibody microarrays for sensitive, multiplexed serum-protein measurements. Genome Biology, 5(4) (2004).
- 36. Wulfkuhle JD, Aquino JA, Calvert VS *et al.* Signal pathway profiling of ovarian cancer from human tissue specimens using reverse-phase protein microarrays. *Proteomics*, 3(11), 2085-2090 (2003).
- 37. Paweletz CP, Charboneau L, Bichsel VE et al. Reverse phase protein microarrays which capture disease progression show activation of pro-survival pathways at the cancer invasion front. Oncogene, 20(16), 1981-1989 (2001).
- 38. Silzel JW, Cercek B, Dodson C, Tsay T, Obremski RJ. Mass-sensing, multianalyte microarray immunoassay with imaging detection. *Clinical Chemistry*, 44(9), 2036-2043 (1998).
- 39. Wiese R, Belosludtsev Y, Powdrill T, Thompson P, Hogan M. Simultaneous multianalyte ELISA performed on a microarray platform. *Clinical Chemistry*, 47(8), 1451-1457 (2001).
- 40. Woodbury RL, Varnum SM, Zangar RC. Elevated HGF levels in sera from breast cancer patients detected using a protein microarray ELISA. *Journal of Proteome Research*, 1(3), 233-237 (2002).
- 41. Lin Y, Huang R, Chen LP et al. Profiling of cytokine expression by biotinlabeled-based protein arrays. *Proteomics*, 3(9), 1750-1757 (2003).
- 42. Kverka M, Burianova J, Lodinova-Zadnikova R et al. Cytokine profiling in human colostrum and milk by protein array. Clin Chem, 53(5), 955-962 (2007).

- 43. Miller JC, Zhou H, Kwekel J et al. Antibody microarray profiling of human prostate cancer sera: antibody screening and identification of potential biomarkers. *Proteomics*, 3(1), 56-63 (2003).
- 44. Shin BK, Wang H, Hanash S. Proteomics approaches to uncover the repertoire of circulating biomarkers for breast cancer. *J Mammary Gland Biol Neoplasia*, 7(4), 407-413 (2002).
- 45. Melle C, Ernst G, Scheibner O et al. Identification of specific protein markers in microdissected hepatocellular carcinoma. J Proteome Res, 6(1), 306-315 (2007).
- 46. Ingvarsson J, Wingren C, Carlsson A *et al.* Detection of pancreatic cancer using antibody microarray-based serum protein profiling. *Proteomics*, 8(11), 2211-2219 (2008).
- 47. Nielsen UB, Cardone MH, Sinskey AJ, MacBeath G, Sorger PK. Profiling receptor tyrosine kinase activation by using Ab microarrays. *Proceedings of the National Academy of Sciences of the United States of America*, 100(16), 9330-9335 (2003).
- 48. Korf U, Derdak S, Tresch A *et al.* Quantitative protein microarrays for time-resolved measurements of protein phosphorylation. *Proteomics*, 8(21), 4603-4612 (2008).
- 49. Schweitzer B, Roberts S, Grimwade B *et al.* Multiplexed protein profiling on microarrays by rolling-circle amplification. *Nat Biotechnol*, 20(4), 359-365 (2002).
- 50. Fulton RJ, McDade RL, Smith PL, Kienker LJ, Kettman JR. Advanced multiplexed analysis with the FlowMetrix(TM) system. *Clinical Chemistry*, 43(9), 1749-1756 (1997).
- 51. Nolan JP, Sklar LA. Suspension array technology: evolution of the flat-array paradigm. *Trends in Biotechnology*, 20(1), 9-12 (2002).
- 52. Templin MF, Stoll D, Bachmann J, Joos TO. Protein microarrays and multiplexed sandwich immunoassays: what beats the beads? *Comb Chem High Throughput Screen*, 7(3), 223-229 (2004).

- 53. Oliver KG, Kettman JR, Fulton RJ. Multiplexed analysis of human cytokines by use of the FlowMetrix system. (Ed.^(Eds) (Amer Assoc Clinical Chemistry, 1998) 2057-2060.
- 54. Carson RT, Vignali DAA. Simultaneous quantitation of 15 cytokines using a multiplexed flow cytometric assay. *Journal of Immunological Methods*, 227(1-2), 41-52 (1999).
- 55. Prabhakar U, Eirikis E, Davis HM. Simultaneous quantification of proinflammatory cytokines in human plasma using the LabMAP (TM) assay. *Journal of Immunological Methods*, 260(1-2), 207-218 (2002).
- 56. Chen R, Lowe L, Wilson JD et al. Simultaneous quantification of six human cytokines in a single sample using microparticle-based flow cytometric technology. Clinical Chemistry, 45(9), 1693-1694 (1999).
- 57. Cook EB, Stahl JL, Lowe L *et al.* Simultaneous measurement of six cytokines in a single sample of human tears using microparticle-based flow cytometry, allergies vs. non-allergies. *Journal of Immunological Methods*, 254(1-2), 109-118 (2001).
- 58. Kellar KL, Kalwar RR, Dubois KA, Crouse D, Chafin WD, Kane BE. Multiplexed fluorescent bead-based immunoassays for quantitation of human cytokines in serum and culture supernatants. *Cytometry*, 45(1), 27-36 (2001).
- 59. Bellisario R, Colinas RJ, Pass KA. Simultaneous measurement of antibodies to three HIV-1 antigens in newborn dried blood-spot specimens using a multiplexed microsphere-based immunoassay. *Early Human Development*, 64(1), 21-25 (2001).
- 60. Opalka D, Lachman CE, MacMullen SA et al. Simultaneous quantitation of antibodies to neutralizing epitopes on virus-like particles for human papillomavirus types 6, 11, 16, and 18 by a multiplexed luminex assay 2. Clinical and Diagnostic Laboratory Immunology, 10(1), 108-115 (2003).
- 61. McBride MT, Gammon S, Pitesky M et al. Multiplexed liquid arrays for simultaneous detection of simulants of biological warfare agents. *Analytical Chemistry*, 75(8), 1924-1930 (2003).

- 62. Schwenk JM, Lindberg J, Sundberg M, Uhlen M, Nilsson P. Determination of binding specificities in highly multiplexed bead-based assays for antibody proteomics. *Mol Cell Proteomics*, 6(1), 125-132 (2007).
- 63. Schwenk JM, Gry M, Rimini R, Uhlen M, Nilsson P. Antibody suspension bead arrays within serum proteomics. *J Proteome Res*, 7(8), 3168-3179 (2008).
- 64. Du JY, Bernasconi P, Clauser KR et al. Bead-based profiling of tyrosine kinase phosphorylation identifies SRC as a potential target for glioblastoma therapy. *Nature Biotechnology*, 27(1), 77-83 (2009).
- 65. Sukhanova A, Nabiev I. Fluorescent nanocrystal-encoded microbeads for multiplexed cancer imaging and diagnosis. *Crit Rev Oncol Hematol*, 68(1), 39-59 (2008).
- 66. Han MY, Gao XH, Su JZ, Nie S. Quantum-dot-tagged microbeads for multiplexed optical coding of biomolecules. *Nature Biotechnology*, 19(7), 631-635 (2001).
- 67. Sukhanova A, Susha AS, Bek A *et al.* Nanocrystal-encoded fluorescent microbeads for proteomics: Antibody profiling and diagnostics of autoimmune diseases. *Nano Letters*, 7(8), 2322-2327 (2007).
- 68. Chattopadhyay PK, Price DA, Harper TF et al. Quantum dot semiconductor nanocrystals for immunophenotyping by polychromatic flow cytometry. *Nature Medicine*, 12(8), 972-977 (2006).
- 69. Stoeva SI, Lee JS, Smith JE, Rosen ST, Mirkin CA. Multiplexed detection of protein cancer markers with biobarcoded nanoparticle probes. *Journal of the American Chemical Society*, 128(26), 8378-8379 (2006).
- 70. Fredriksson S, Dixon W, Ji H, Koong AC, Mindrinos M, Davis RW. Multiplexed protein detection by proximity ligation for cancer biomarker validation. *Nature Methods*, 4(4), 327-329 (2007).
- 71. Fan R, Vermesh O, Srivastava A et al. Integrated barcode chips for rapid, multiplexed analysis of proteins in microliter quantities of blood. Nature Biotechnology, 26(12), 1373-1378 (2008).

- 72. Kattah MG, Coller J, Cheung RK, Oshidary N, Utz PJ. HIT: a versatile proteomics platform for multianalyte phenotyping of cytokines, intracellular proteins and surface molecules. *Nat Med*, 14(11), 1284-1289 (2008).
- 73. Gloriam DE, Orchard S, Bertinetti D et al. A community standard format for the representation of protein affinity reagents. Mol Cell Proteomics, 9(1), 1-10 (2010).
- 74. Arakaki AK, Skolnick J, McDonald JF. Marker metabolites can be therapeutic targets as well. *Nature*, 456(7221), 443-443 (2008).
- 75. Gibson G, Muse S. V. Analysis of cellular constituents. In: *A primer of genome science*. Gibson, G, Muse S. V. (Ed. (Sinauer Associates 2004) 333-337.
- 76. Blow N. Metabolomics: Biochemistry's new look. *Nature*, 455(7213), 697-700 (2008).
- 77. Griffin JL. Understanding mouse models of disease through metabolomics. Current opinion in chemical biology, 10(4), 309-315 (2006).
- 78. Sreekumar A, Poisson LM, Rajendiran TM *et al.* Metabolomic profiles delineate potential role for sarcosine in prostate cancer progression. *Nature*, 457(7231), 910-914 (2009).
- 79. Seetharaman S, Zivarts M, Sudarsan N, Breaker RR. Immobilized RNA switches for the analysis of complex chemical and biological mixtures. *Nature biotechnology*, 19(4), 336-341 (2001).
- 80. Ellington AD, Szostak JW. *In vitro* selection of RNA molecules that bind specific ligands. *Nature*, 346(6287), 818-822 (1990).
- 81. Tuerk C, Gold L. Systematic evolution of ligands by exponential enrichment: RNA ligands to bacteriophage T4 DNA polymerase. *Science*, 249(4968), 505-510 (1990).
- 82. Famulok M. Molecular recognition of amino-acids by RNA-aptamers-an L-citrulline binding RNA motif and its evolution into an L-arginine binder. *Journal of the American Chemical Society*, 116(5), 1698-1706 (1994).

- 83. Giver L, Bartel D, Zapp M, Pawul A, Green M, Ellington AD. Selective optimization of the Rev-binding element of HIV-1. *Nucleic Acids Research*, 21(23), 5509-5516 (1993).
- 84. Hesselberth JR, Miller D, Robertus J, Ellington AD. *In vitro* selection of RNA molecules that inhibit the activity of ricin A-chain. *Journal of Biological Chemistry*, 275(7), 4937-4942 (2000).
- 85. Li N, Wang Y, Pothukuchy A *et al.* Aptamers that recognize drug-resistant HIV-1 reverse transcriptase. *Nucleic Acids Research*, 36(21), 6739-6751 (2008).
- 86. Jenison RD, Gill SC, Pardi A, Polisky B. High-resolution molecular discrimination by RNA. *Science*, 263(5152), 1425-1429 (1994).
- 87. Huizenga DE, Szostak JW. A DNA aptamer that binds adenosine and ATP. *Biochemistry*, 34(2), 656-665 (1995).
- 88. Rajendran M, Ellington AD. Selection of fluorescent aptamer beacons that light up in the presence of zinc. *Analytical and Bioanalytical Chemistry*, 390(4), 1067-1075 (2008).
- 89. Wang Y, Rando RR. Specific binding of aminoglycoside antibiotics to RNA. Chemistry & Biology, 2(5), 281-290 (1995).
- 90. Wallis MG, Vonahsen U, Schroeder R, Famulok M. A novel RNA motif for neomycin recognition. *Chemistry & Biology*, 2(8), 543-552 (1995).
- 91. Khvorova A, Kwak YG, Tamkun M, Majerfeld I, Yarus M. RNAs that bind and change the permeability of phospholipid membranes. *Proceedings of the National Academy of Sciences of the United States of America*, 96(19), 10649-10654 (1999).
- 92. Vlassov A, Khvorova A, Yarus M. Binding and disruption of phospholipid bilayers by supramolecular RNA complexes. *Proceedings of the National Academy of Sciences of the United States of America*, 98(14), 7706-7711 (2001).
- 93. Winkler W, Nahvi A, Breaker RR. Thiamine derivatives bind messenger RNAs directly to regulate bacterial gene expression. *Nature*, 419(6910), 952-956 (2002).

- 94. Roth A, Breaker RR. The Structural and Functional Diversity of Metabolite-Binding Riboswitches. *Annual Review of Biochemistry*, 78, 305-334 (2009).
- 95. Nahvi A, Sudarsan N, Ebert MS, Zou X, Brown KL, Breaker RR. Genetic control by a metabolite binding mRNA. *Chemistry & Biology*, 9(9), 1043-1049 (2002).
- 96. Winkler WC, Cohen-Chalamish S, Breaker RR. An mRNA structure that controls gene expression by binding FMN. *Proceedings of the National Academy of Sciences of the United States of America*, 99(25), 15908-15913 (2002).
- 97. Mandal M, Boese B, Barrick JE, Winkler WC, Breaker RR. Riboswitches control fundamental biochemical pathways in Bacillus subtilis and other bacteria. *Cell*, 113(5), 577-586 (2003).
- 98. Winkler WC, Nahvi A, Sudarsan N, Barrick JE, Breaker RR. An mRNA structure that controls gene expression by binding S-adenosylmethionine. *Nat. Struct. Biol.*, 10(9), 701-707 (2003).
- 99. Sudarsan N, Wickiser JK, Nakamura S, Ebert MS, Breaker RR. An mRNA structure in bacteria that controls gene expression by binding lysine. *Genes Dev.*, 17(21), 2688-2697 (2003).
- 100. Winkler WC, Nahvi A, Roth A, Collins JA, Breaker RR. Control of gene expression by a natural metabolite-responsive ribozyme. *Nature*, 428(6980), 281-286 (2004).
- 101. Mandal M, Lee M, Barrick JE et al. A glycine-dependent riboswitch that uses cooperative binding to control gene expression. Science, 306(5694), 275-279 (2004).
- 102. Lee JF, Hesselberth JR, Meyers LA, Ellington AD. Aptamer database. *Nucleic Acids Research*, 32, D95-D100 (2004).
- 103. Gold L, Polisky B, Uhlenbeck O, Yarus M. Diversity of oligonucleotide functions. *Annu Rev Biochem*, 64, 763-797 (1995).
- 104. Lin Y, Qiu Q, Gill SC, Jayasena SD. Modified RNA sequence pools for *in vitro* selection. *Nucleic Acids Res*, 22(24), 5229-5234 (1994).

- 105. Pieken WA, Olsen DB, Benseler F, Aurup H, Eckstein F. Kinetic characterization of ribonuclease-resistant 2'-modified hammerhead ribozymes. *Science*, 253(5017), 314-317 (1991).
- 106. Kang J, Lee MS, Copland JA, 3rd, Luxon BA, Gorenstein DG. Combinatorial selection of a single stranded DNA thioaptamer targeting TGF-beta1 protein. *Bioorg Med Chem Lett*, 18(6), 1835-1839 (2008).
- 107. Win MN, Smolke CD. A modular and extensible RNA-based gene-regulatory platform for engineering cellular function. *Proceedings of the National Academy of Sciences of the United States of America*, 104(36), 14283-14288 (2007).
- 108. Lynch SA, Desai SK, Sajja HK, Gallivan JP. A high-throughput screen for synthetic riboswitches reveals mechanistic insights into their function. *Chemistry & Biology*, 14(2), 173-184 (2007).
- 109. Bayer TS, Smolke CD. Programmable ligand-controlled riboregulators of eukaryotic gene expression. *Nature Biotechnology*, 23(3), 337-343 (2005).
- 110. Win MN, Smolke CD. Higher-order cellular information processing with synthetic RNA devices. *Science*, 322(5900), 456-460 (2008).
- 111. Xie S, Walton SP. Application and analysis of structure-switching aptamers for small molecule quantification. *Anal Chim Acta*, 638(2), 213-219 (2009).
- 112. Lynch SA, Gallivan JP. A flow cytometry-based screen for synthetic riboswitches. *Nucleic Acids Research*, 37(1), 184-192 (2009).
- 113. Jhaveri S, Rajendran M, Ellington AD. *In vitro* selection of signaling aptamers. *Nature biotechnology*, 18(12), 1293-1297 (2000).
- 114. Stojanovic MN, Kolpashchikov DM. Modular aptameric sensors. *J Am Chem Soc*, 126(30), 9266-9270 (2004).
- 115. Bouchard PR, Hutabarat RM, Thompson KM. Discovery and development of therapeutic aptamers. *Annu Rev Pharmacol Toxicol*, 50, 237-257 (2010).

- 116. Win MN, Liang JC, Smolke CD. Frameworks for Programming Biological Function through RNA Parts and Devices. *Chemistry & Biology*, 16(3), 298-310 (2009).
- 117. Weigand J, Suess B. Aptamers and riboswitches: perspectives in biotechnology. *Applied Microbiology and Biotechnology*, 85(2), 229-236 (2009).
- 118. Romig TS, Bell C, Drolet DW. Aptamer affinity chromatography: combinatorial chemistry applied to protein purification. *Journal of Chromatography B-Analytical Technologies in the Biomedical and Life Sciences*, 731(2), 275-284 (1999).
- 119. Deng Q, German I, Buchanan D, Kennedy RT. Retention and separation of adenosine and analogues by affinity chromatography with an aptamer stationary phase. *Analytical Chemistry*, 73(22), 5415-5421 (2001).
- 120. Mairal T, Ozalp VC, Sanchez PL, Mir M, Katakis I, O'Sullivan CK. Aptamers: molecular tools for analytical applications. *Analytical and Bioanalytical Chemistry*, 390(4), 989-1007 (2008).
- 121. Drolet DW, MoonMcDermott L, Romig TS. An enzyme-linked oligonucleotide assay. *Nature biotechnology*, 14(8), 1021-1025 (1996).
- 122. Baldrich E, Restrepo A, O'Sullivan CK. Aptasensor development: Elucidation of critical parameters for optimal aptamer performance. *Analytical Chemistry*, 76(23), 7053-7063 (2004).
- 123. Liss M, Petersen B, Wolf H, Prohaska E. An aptamer-based quartz crystal protein biosensor. *Analytical Chemistry*, 74(17), 4488-4495 (2002).
- 124. German I, Buchanan DD, Kennedy RT. Aptamers as ligands in affinity probe capillary electrophoresis. *Analytical Chemistry*, 70(21), 4540-4545 (1998).
- 125. Potyrailo RA, Conrad RC, Ellington AD, Hieftje GM. Adapting selected nucleic acid ligands (aptamers) to biosensors. *Analytical Chemistry*, 70(16), 3419-3425 (1998).

- 126. Kim YS, Jung HS, Matsuura T, Lee HY, Kawai T, Gu MB. Electrochemical detection of 17 beta-estradiol using DNA aptamer immobilized gold electrode chip. *Biosensors & Bioelectronics*, 22(11), 2525-2531 (2007).
- 127. Savran CA, Knudsen SM, Ellington AD, Manalis SR. Micromechanical detection of proteins using aptamer-based receptor molecules. *Analytical Chemistry*, 76(11), 3194-3198 (2004).
- 128. Wang JL, Zhou HS. Aptamer-based Au nanoparticles-enhanced surface plasmon resonance detection of small molecules. *Analytical Chemistry*, 80(18), 7174-7178 (2008).
- 129. Bock C, Coleman M, Collins B et al. Photoaptamer arrays applied to multiplexed proteomic analysis. *Proteomics*, 4(3), 609-618 (2004).
- 130. Collett JR, Cho EJ, Ellington AD. Production and processing of aptamer microarrays. *Methods*, 37(1), 4-15 (2005).
- 131. Stadtherr K, Wolf H, Lindner P. An aptamer-based protein biochip. *Anal Chem*, 77(11), 3437-3443 (2005).
- 132. Hansen JA, Wang J, Kawde AN, Xiang Y, Gothelf KV, Collins G. Quantum-dot/aptamer-based ultrasensitive multi-analyte electrochemical biosensor. *Journal of the American Chemical Society*, 128(7), 2228-2229 (2006).
- 133. Kirby R, Cho EJ, Gehrke B et al. Aptamer-based sensor arrays for the detection and quantitation of proteins. Analytical Chemistry, 76(14), 4066-4075 (2004).
- 134. Golden MC, Resing KA, Collins BD, Willis MC, Koch TH. Mass spectral characterization of a protein-nucleic acid photocrosslink. *Protein Sci*, 8(12), 2806-2812 (1999).
- 135. Rankin CJ, Fuller EN, Hamor KH, Gabarra SA, Shields TP. A simple fluorescent biosensor for theophylline based on its RNA aptamer. *Nucleosides Nucleotides Nucleic Acids*, 25(12), 1407-1424 (2006).
- 136. Hamaguchi N, Ellington A, Stanton M. Aptamer beacons for the direct detection of proteins. *Anal. Biochem.*, 294(2), 126-131 (2001).

- 137. Nutiu R, Li Y. Aptamers with fluorescence-signaling properties. *Methods (San Diego, Calif,* 37(1), 16-25 (2005).
- 138. Xiao Y, Piorek BD, Plaxco KW, Heeger AJ. A reagentless signal-on architecture for electronic, aptamer-based sensors via target-induced strand displacement. *J Am Chem Soc*, 127(51), 17990-17991 (2005).
- 139. Wu ZS, Guo MM, Zhang SB *et al.* Reusable electrochemical sensing platform for highly sensitive detection of small molecules based on structure-switching signaling aptamers. *Analytical chemistry*, 79(7), 2933-2939 (2007).
- 140. Zuo X, Song S, Zhang J, Pan D, Wang L, Fan C. A target-responsive electrochemical aptamer switch (TREAS) for reagentless detection of nanomolar ATP. *Journal of the American Chemical Society*, 129(5), 1042-1043 (2007).
- 141. Radi AE, O'Sullivan CK. Aptamer conformational switch as sensitive electrochemical biosensor for potassium ion recognition. *Chem Commun (Camb)*, (32), 3432-3434 (2006).
- 142. Bauer G, Suess B. Engineered riboswitches as novel tools in molecular biology. *J Biotechnol*, 124(1), 4-11 (2006).
- 143. Wang J, Jiang Y, Zhou C, Fang X. Aptamer-based ATP assay using a luminescent light switching complex. *Analytical chemistry*, 77(11), 3542-3546 (2005).
- 144. Nutiu R, Li Y. *In vitro* selection of structure-switching signaling aptamers. *Angewandte Chemie (International ed*, 44(7), 1061-1065 (2005).
- 145. Rajendran M, Ellington AD. Selection of fluorescent aptamer beacons that light up in the presence of zinc. *Anal Bioanal Chem*, 390(4), 1067-1075 (2008).
- 146. Yang L, Fung CW, Cho EJ, Ellington AD. Real-time rolling circle amplification for protein detection. *Anal Chem*, 79(9), 3320-3329 (2007).
- 147. Yang L, Ellington AD. Real-time PCR detection of protein analytes with conformation-switching aptamers. *Anal Biochem*, 380(2), 164-173 (2008).

- 148. Jhaveri SD, Kirby R, Conrad R et al. Designed signaling aptamers that transduce molecular recognition to changes in fluorescence intensity. *Journal of the American Chemical Society*, 122(11), 2469-2473 (2000).
- 149. Yamamoto R, Kumar PKR. Molecular beacon aptamer fluoresces in the presence of Tat protein of HIV-1. *Genes to Cells*, 5(5), 389-396 (2000).
- 150. Stojanovic MN, de Prada P, Landry DW. Aptamer-based folding fluorescent sensor for cocaine. *J Am Chem Soc*, 123(21), 4928-4931 (2001).
- 151. Fang XH, Sen A, Vicens M, Tan WH. Synthetic DNA aptamers to detect protein molecular variants in a high-throughput fluorescence quenching assay. *Chembiochem*, 4(9), 829-834 (2003).
- 152. Xiao Y, Lubin AA, Heeger AJ, Plaxco KW. Label-free electronic detection of thrombin in blood serum by using an aptamer-based sensor. *Angewandte Chemie-International Edition*, 44(34), 5456-5459 (2005).
- 153. Baker BR, Lai RY, Wood MS, Doctor EH, Heeger AJ, Plaxco KW. An electronic, aptamer-based small-molecule sensor for the rapid, label-free detection of cocaine in adulterated samples and biological fluids. *J Am Chem Soc*, 128(10), 3138-3139 (2006).
- 154. Nutiu R, Li Y. Structure-switching signaling aptamers: transducing molecular recognition into fluorescence signaling. *Chemistry*, 10(8), 1868-1876 (2004).
- 155. Nutiu R, Li Y. Structure-switching signaling aptamers. J Am Chem Soc, 125(16), 4771-4778 (2003).
- 156. Tang J, Breaker RR. Rational design of allosteric ribozymes. *Chemistry & Biology*, 4(6), 453-459 (1997).
- 157. Soukup GA, Breaker RR. Engineering precision RNA molecular switches.

  Proceedings of the National Academy of Sciences of the United States of America, 96(7), 3584-3589 (1999).
- 158. Zivarts M, Liu Y, Breaker RR. Engineered allosteric ribozymes that respond to specific divalent metal ions. *Nucleic Acids Research*, 33(2), 622-631 (2005).

- 159. Robertson MP, Ellington AD. Design and optimization of effector-activated ribozyme ligases. *Nucleic Acids Research*, 28(8), 1751-1759 (2000).
- 160. Breaker RR. Engineered allosteric ribozymes as biosensor components. Current Opinion in Biotechnology, 13(1), 31-39 (2002).
- 161. Hall B, Hesselberth JR, Ellington AD. Computational selection of nucleic acid biosensors via a slip structure model. *Biosensors & Bioelectronics*, 22(9-10), 1939-1947 (2007).
- 162. Seetharaman S, Zivarts M, Sudarsan N, Breaker RR. Immobilized RNA switches for the analysis of complex chemical and biological mixtures. *Nature Biotechnology*, 19(4), 336-341 (2001).
- 163. Hesselberth JR, Robertson MP, Knudsen SM, Ellington AD. Simultaneous detection of diverse analytes with an aptazyme ligase array. *Analytical Biochemistry*, 312(2), 106-112 (2003).
- 164. Sekella PT, Rueda D, Walter NG. A biosensor for theophylline based on fluorescence detection of ligand-induced hammerhead ribozyme cleavage. *RNA-Publ. RNA Soc.*, 8(10), 1242-1252 (2002).
- 165. Ferguson A, Boomer RM, Kurz M et al. A novel strategy for selection of allosteric ribozymes yields RiboReporter (TM) sensors for caffeine and aspartame. *Nucleic Acids Research*, 32(5), 1756-1766 (2004).

# CHAPTER 2 APPLICATION AND ANALYSIS OF STRUCTURE-SWITCHING APTAMERS FOR SMALL MOLECULE QUANTIFICATION

Portions reproduced from: Xie, S. and Walton, S. P., "Application and analysis of structure-switching aptamers for small molecule quantification", *Analytica Chimica Acta*, **638**:213-219 (2009) with permissions from Elsevier.

### 2.1 Abstract

Modern tools for the analysis of cellular function aim for the quantitative measurement of all members of a given class of biological molecules. Of the analyte classes, nucleic acid measurements are typically the most tractable, both on an individual analyte basis and in parallel. Thus, tools are being sought to enable measurement of other cellular molecules using nucleic acid biosensors. Of the variety of potential nucleic acid biosensor strategies, structure-switching aptamers (SSAs) present a unique opportunity to couple sensing and readout of the target molecule. However, little has been characterized about the parameters that determine the fidelity of the signal from SSA biosensors. In this study, a small molecule biosensor based on an SSA was engineered to detect the model small molecule, theophylline, in solution. Quantitative theophylline detection over nearly three orders of magnitude was achieved by scintillation counting and quantitative PCR. Further analysis showed that the biosensor fidelity is primarily controlled by the relative stability of the two conformations of the SSA.

#### 2.2 Introduction

Evolution in the analysis of biological function occurs in concert with the development and application of new analytical techniques. Quantification techniques for DNA or RNA molecules were established early, based on Watson-Crick base pairing of nucleic acids, with, for instance, quantitative polymerase chain reaction (qPCR) now common practice for nucleic acid analyses [1-5]. Sensing techniques for non-nucleic acid molecules such as proteins and small molecules, especially parallel techniques, are markedly less mature. The importance of small molecule analyses is illustrated by current efforts in metabolomics, as understanding the profile of small molecules generated by metabolism provides a comprehensive picture of the effects of upstream transcriptional and translational changes. Moreover, a great number of drugs are small molecules, so specific and accurate measurement of their levels is essential to the rapeutic monitoring of disease treatment. Currently, small molecule measurements are primarily performed using spectroscopic analyses combined with chromatography [6,7]. Analysis of data from these methods can be limited due to the difficulty in resolving constituents with chemical or structural similarity. Thus, more flexible methods for small molecule analyses are being sought.

In recent years, aptamers have shown promise in small molecule and protein biosensing applications [8-14]. Aptamers are nucleic acid affinity molecules with exceptional specificity for a target for which they were specifically selected [15,16]. In comparison to antibodies, aptamers offer a number of advantages for sensing applications. First, the sequences for a large number of aptamers have been reported [17,18], and these

sequences can be easily synthesized chemically or enzymatically with high reproducibility and purity. Moreover, because aptamers are generated by *in vitro* selection, in theory, aptamers targeting any analyte could be generated. Second, the specificity and affinity of aptamers is tunable through manipulation of the selection conditions, such as by incorporating negative selection against similar analytes that would confound accurate detection [19]. The degree of specificity that can be achieved is especially advantageous for multiplex sensing applications. Third, aptamers can be generated with chemically-modified nucleotides to enhance their properties for various applications, such as stability to nucleases for measurements in biological fluids [20,21]. Finally, aptamers can be readily engineered for specific signaling function using designed selection or through *post hoc* manipulations [22,23].

A unique class of aptamer-based sensors has been termed structure-switching aptamers (SSAs), wherein the binding of the target molecule results in a conformational change of the SSA. Given their simultaneous sensing and readout, SSAs are of particular interest for biosensing applications [24-31]. A common mode for the structure-switching behavior is based upon helix-rearrangement coupled with strand displacement [29,32,33]. The ability to design SSA sequences *a priori* to utilize this rearrangement is essentially unique to nucleic acids. This enables flexible and facile design of SSA biosensors with coupled readouts, such as to mimic molecular beacons [34-36] or to engineer cellular responses [37,38].

The utility of SSA-based sensing techniques, as with all analytical methods, is defined largely by the signal-to-noise ratio of the technique. Both rational design strategies and high-throughput screening techniques have been investigated to generate SSAs with high signal-to-noise ratio [38,39]. However, little has been characterized about the parameters impacting the signal fidelity of an SSA. Thus, there is a clear need to identify these parameters and use them as theoretical guidance in generating SSA biosensors with optimal function. In this work, a modular-designed SSA that acts by strand displacement was applied to quantify the concentration of a model small molecule, theophylline. This SSA was designed for future parallel analyses through the inclusion of a molecular barcode (MB) [40] and was therefore termed a molecular barcode switch (MBS). These MBs have been shown to provide quantitative accuracy in parallel nucleic acid analyses [41,42]. An oligonucleotide complementary to the MB domain of the MBS (molecular barcode complement, MBC) was used to probe the conformational change upon target binding and to utilize the change for the concentration readout. It was observed that the affinity between the MBS and the complementary strand relative to the internal stability of the MBS structure was a principal factor limiting the achievable signal-to-noise ratio. Using the designed construct, theophylline concentrations as low as 0.5 µM can be reproducibly detected in solution. The observed lower detection limit for the ophylline exceeded that of caffeine by over three orders of magnitude, confirming analytical specificity. As previous studies have coupled PCR amplification with aptamer-based protein measurement [39,43-45], here we also report the applicability of PCR for small molecule quantification.

## 2.3 Experimental section

#### 2.3.1 Synthesis of the MBS

A double-stranded DNA was prepared by Klenow extension from a synthesized single-stranded DNA template and the reverse primer. The sequence of the single-stranded DNA template was (5'-

TAATACGACTCACTATAACCTAACTCGAAGTGAAGCCCACTTCGAGTTAGGTGA
TACCAGCATCGTCTTGATGCCCTTGGCAGCACCTAACT-3', underlined: T7
promoter; italicized: MB sequence; bold: reverse primer binding site) and the reverse
primer was (5'-AGTTAGGTGCTGCCAAGGGC-3'). The double-stranded DNA was *in*vitro transcribed using Ampliscribe T7 High Yield Transcription Kit (Epicentre, Madison,
WI). Reactions were incubated at 42 °C for 2 hrs, and RNA transcripts were purified on
10% polyacrylamide gels, eluted, ethanol precipitated, and resuspended in TE (10 mM
Tris, pH 7.0, 1 mM EDTA). The 20-nt MBC has a sequence of 5'-

GGCTTCACTTCGAGTTAGGT-Biotin-3'. All oligonucleotides were synthesized and purified by IDT (Coralville, IA). Assays with varying length of MBC showed no significant binding to the MBS when the MBC was shorter than 14-nt. Longer MBC sequences tended to cause higher background binding. Therefore, an MBC of 20-nt in length was chosen to generate the maximum signal-to-noise ratio (S/N). For subsequent separation using streptavidin-coated magnetic beads (see below), the MBC was biotinylated at the 3'end. For reverse transcription-qPCR (RT-qPCR), the forward primer

sequence was (5'-TAGGTGATACCAGCATCGTC-3'). Several sets of primers were tested to produce the least mispriming products (data not shown). To avoid mispriming products due to the self-complementary sequence of the MBS, primers were chosen to be outside the range of the MB domain, resulting in a 45 bp product.

#### 2.3.2 Binding reactions and theophylline sensing experiments

Binding reactions were performed in a buffer of 50 mM Tris-HCl (pH 8.0), 100 mM NaCl, and 5 mM MgCl<sub>2</sub>. Varying concentrations of theophylline (Sigma Aldrich, St. Louis, MO) were added to thermally annealed MBSs and incubated at room temperature for 30 min. MBCs were then added and incubated at room temperature. The total binding reaction volume was 30  $\mu$ L. The MBC incubation time was 10 min for theophylline sensing applications and 20 hrs for deriving equilibrium dissociation constants (K<sub>D</sub>).

Separation of MBS-MBC complexes was achieved by either electrophoretic mobility shift assay (EMSA) or streptavidin-coated magnetic beads. For EMSA, the MBCs were 5'-labeled with <sup>33</sup>P-γ-ATP using T4 polynucleotide kinase (Ambion, Austin, TX) followed by purification by Quick Spin Columns (Roche, Indianapolis, IN). Prior to gel loading, glycerol (final concentration 10% v/v) was added to each binding reaction. 15 μL were then loaded for electrophoresis. Electrophoresis was performed at 90 V in 10% polyacrylamide gels in 1X TBE Extended Range Buffer (Bio-Rad, Hercules, CA) for 1 hr at room temperature. Gels were then dried on Whatman filter paper at 80 °C for 45 min under vacuum. Dried gels were exposed to phosphorimaging screens for 16 hrs followed

by quantification on a Storm 860 (GE Healthcare/Amersham Biosciences, Piscataway, NJ). Band intensities were quantified, and the fraction bound was calculated as the band intensity of the MBS-MBC complex divided by the total intensity of the bands for the complex and the free MBCs.

For magnetic bead separations, binding reactions were performed with 5'-33P labeled MBSs when using scintillation counting as the read out and with unlabeled strands when using RT-qPCR. Binding reactions were added to streptavidin-coated magnetic beads (Dynal; Oslo, Norway), and a magnet was applied to retain the beads while the supernatant was removed. The final concentration of beads was 20 µg/µL. 30 µL binding reactions were then added to 5 µL of bead solution and incubated at room temperature for 5 min. Kinetic experiments showed 5 min was sufficient to yield 95-99% binding of biotinylated MBC to the beads (data not shown). A magnet was then applied to retain the beads while the supernatant was removed. The beads were then washed three times with 30 μL 1x binding buffer. Retained MBSs were eluted from the magnetic beads in 30 μL nuclease-free water at 65°C for 5 min. The magnet was applied to retain the beads, and the supernatant was collected for scintillation counting or RT-qPCR quantification. All scintillation counts were background corrected by subtracting counts of scintillation vials containing no radioactivity. Scintillation counting validation experiments were performed using 333 nM MBC and varying MBS concentrations. The MBS and MBC were mixed for 1 hr at room temperature followed by a 5-min incubation with the magnetic beads. The theophylline detection limit for scintillation counting was defined to be signal at least three standard deviations above background. By linear interpolation of data near the

lower detection limit, a minimum detectable theophylline concentration of 0.5  $\mu$ M was obtained.

Experiments for determining optimal sensing conditions were performed in binding reactions with varying concentration pairs of MBC (0.1, 1.0, 10, 50, and 100 nM) and MBS (0.1, 1.0, 10, and 50 nM) in the presence (2 mM) or absence of theophylline.

Magnetic beads were used to separate the bound MBSs, followed by scintillation counting as described. MBS fractional binding in the presence of 2 mM and 0 mM theophylline were defined as signal and noise, respectively. Signal-to-noise ratios (S/N) and their differences (S-N) were calculated from the measured data for each concentration pair. Contour plots were generated by Sigmaplot. The aggregate score was obtained by scaling the ratios and differences as a fraction of the range from the minimum to the maximum and then summing the two scaled values. The resulting sums were then scaled from 0 to 1 to obtain the displayed results.

### 2.3.3 Binding affinity and theoretical signal-to-noise ratio calculation

For experiments to determine dissociation constants, the  $K_D$  values were calculated from curve fits using Origin software based on:

$$f = \frac{[MBS]_0}{K_D + [MBS]_0}$$
 (2.1)

where f is the fraction bound of MBC as calculated from the quantified gel images. This fit requires that the concentration of free MBS is nearly constant at its initial value throughout the experiment. MBC concentrations were minimized to maximize the

validity of this assumption [46]. Data from at least three experimental runs were fit simultaneously to generate a single parameter fit to all the data.

Theoretical fractional MBS binding at each MBS and MBC concentration pair was calculated as follows:

$$f = \frac{([MBS]_0 + [MBC]_0 + K_D) - \sqrt{([MBS]_0 + [MBC]_0 + K_D)^2 - 4[MBS]_0[MBC]_0}}{2[MBS]_0} (2.2)$$

where f is the MBS fraction bound and K<sub>D</sub> is the dissociation constant of MBS-MBC binding. This arises from the equilibrium reaction equation wherein one free MBS and one free MBC combine to form one complex. S/N and S-N were then calculated by solving (2.2) using the appropriate K<sub>D</sub>, [MBS]<sub>0</sub>, and [MBC]<sub>0</sub> values for each condition.

## 2.3.4 Reverse transcription and quantitative PCR

Following binding and elution from the magnetic beads as described above, MBSs were reverse-transcribed using the reverse primer and Superscript III (Invitrogen, Carlsbad, California) per the manufacturer's instructions. The cDNA was amplified by qPCR using iQ SYBR Green Supermix (Bio-Rad, Hercules, CA) in a MyiQ Real Time PCR detection system (Bio-Rad, Hercules, CA). The purity of the resulting qPCR products was confirmed by gel electrophoresis. Threshold cycle (Ct) values for the qPCR standard curve were generated with ten-fold dilutions of initial MBS template. Initial template concentrations ranged from 485 aM to 485 pM, in 50 µL qPCR reactions.

#### 2.4 Results and discussion

#### 2.4.1 Application of the ophylline-responsive MBS

The goal of any analytical strategy is precise, accurate, and quantitative measurement of the analyte(s) of interest. SSAs have been proposed as a basis for solution-phase and solid-substrate mediated single and parallel analyses [24,25,34,47]. Here, a theophylline-sensitive SSA was constructed where the quantity of aptamer that undergoes a conformational change provided the readout of the theophylline concentration (Figure 2.1). The SSA consists of two domains, the aptamer domain and the readout domain. This modular design approach is well-established [37,38] and provides a basis for convenient multiplex detection of SSAs by careful design of the readout domain.

In the described detection strategy, the readout is based on the enhanced binding affinity of MBCs to MBSs bound to their target relative to MBSs without bound target (Figure 2.1). This is due to the structural rearrangement of the aptamer domain upon target binding. Upon rearrangement, intermolecular hybridization in the MB domain can compete more easily with native intramolecular hybridization. Streptavidin-coated magnetic beads loaded with MBC sequences are used to isolate MBSs with bound analyte for subsequent quantification by qPCR, microarray, or other convenient nucleic acid analytical strategy. The technique thus provides an indirect but still quantitative measurement of the theophylline concentration. Using gel-shift experiments (Figures 2.2 (a)), it was verified that the binding of MBC by MBS is dependent on theophylline concentration. Maximal binding of the MBC occurred at 200 µM - 2 mM concentration of theophylline (Figure 2.2 (b)), thus subsequent experiments where saturating MBS-

theophylline interactions were desired were performed at 2 mM theophylline. Binding with 2 mM caffeine showed fractional MBC binding equal to that with 2  $\mu$ M theophylline (Figure 2.2 (a), lane 10), which is consistent with the difference in the affinity of the aptamer for these two species [19]. Thus, the specificity of the aptamer for theophylline over caffeine was maintained in the MBS design, further support for use of the modular MBS construction strategy. It is worthwhile to note that even in the absence of theophylline, the fractional MBC hybridization with the MBS was 0.25 (Figure 2.2 (a), lane 3). This suggests that caution must be taken in the development of SSA-based analyses to ensure minimal background.



Figure 2.1: MBS design and detection strategy. In the native conformation of the MBS, the MB sequence forms a 15 bp intramolecular stem. Upon the ophylline binding with the aptamer domain (light gray), competition by the free 3'-end of the MBS becomes more favored, increasing the exposure of the MB domain (dark gray) for hybridization with an MBC. Using biotinylated MBCs and streptavidin-coated magnetic beads, the MBSs with available MB domains can be selectively removed from the solution and quantified by standard nucleic acid analytical techniques.

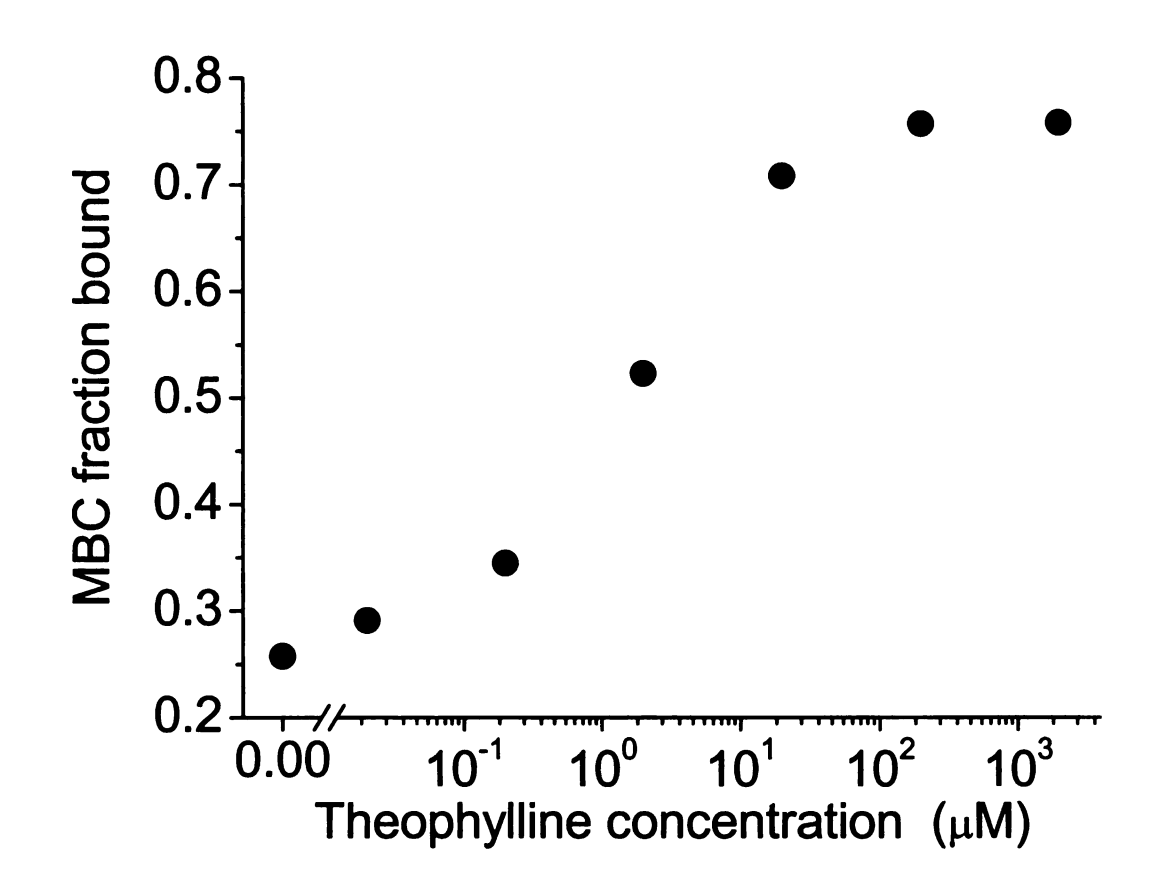
Theophylline

1 2 3 4 5 6 7 8 9 10

Figure 2.2: Impact of theophylline on MBS-MBC hybridization. (a) Theophylline at concentrations of 0-2 mM (lanes 3-9) was incubated with MBSs followed by hybridization with radiolabeled MBCs. Signal from the upper band indicates an MBS-MBC complex. Complexes with and without theophylline cannot be distinguished. Lane 1: MBC alone. Lane 2: 5 nM MBC with 2 mM theophylline. Lane 3-9: 5 nM MBC, 16 nM MBS and 0, 20 nM, 200 nM, 2 μM, 20 μM, 200 μM, and 2 mM theophylline. Lane 10: 5 nM MBC, 16 nM MBS and 2 mM caffeine. Image contrast was adjusted to improve image clarity but band intensities used for fraction bound calculations were not altered. (b) Quantification of band intensity from (a). Quantification was followed by calculation of the fraction of signal in the upper band relative to the total of the upper and lower bands.

Figure 2.2 continued.

(b)



To assess further if structural rearrangement of the MBS upon the ophylline binding was responsible for the change in MBS-MBC binding affinity, gel shift assays were conducted in the absence and presence of 2 mM theophylline. Initially, a wide range of MBS concentrations were chosen to estimate roughly the K<sub>D</sub> of MBS-MBC complex formation. Subsequent experiments focused on the range surrounding the concentration resulting in 50% binding for a more accurate evaluation of the K<sub>D</sub>. As expected, with increasing MBS concentration, MBC fractional binding increases (Figures 2.3), yielding K<sub>D</sub> values for MBS-MBC hybridization in the absence and presence of theophylline of 9.9 nM and 1.0 nM, respectively. This change in affinity reflects the change in the relative stability of the two MBS conformations due to theophylline binding. The basal level of binding between the MBS and MBC that occurred in the absence of theophylline was therefore predefined by their K<sub>D</sub> and the concentration of the two strands. It should also be noted that even at saturating theophylline concentration, the MB domain was not necessarily completely exposed to hybridize with its complement. This is reflected in a much lower affinity between the strands than might be expected for hybridization of sequences of this length [46]. Nonetheless, the significantly enhanced binding of the MBC indicates increased accessibility of the MB sequence on the MBS, indicative of the expected structural rearrangement.

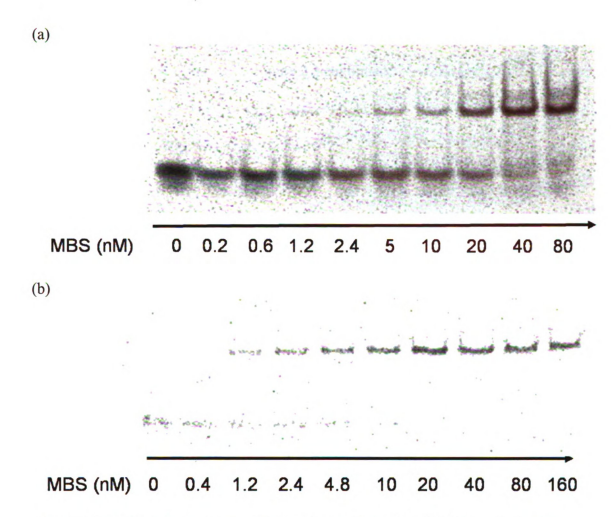
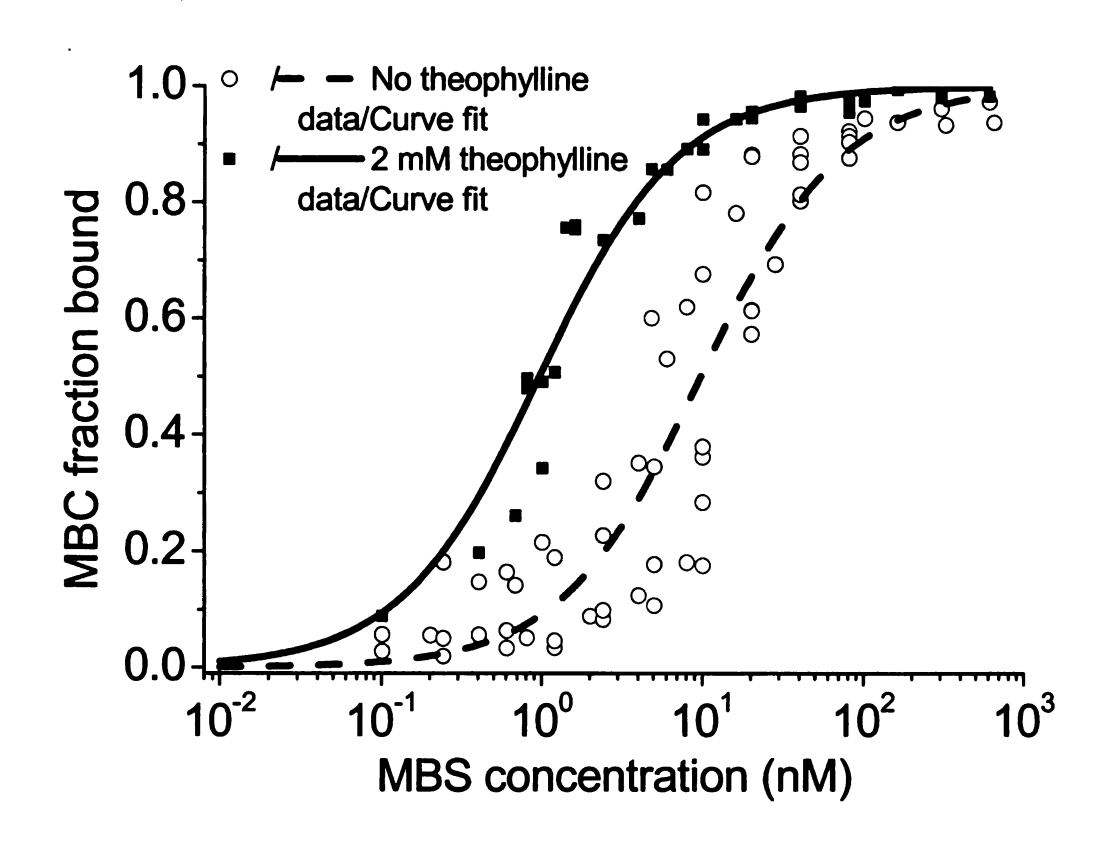


Figure 2.3: MBS-MBC binding affinity characterization. EMSAs were used to measure the  $K_D$  for the complex in the absence (a) and in the presence (b) of 2 mM theophylline. 1-2 fmol of MBC (final concentration of 33 pM-67 pM) was incubated with increasing concentrations of MBS. (c) Quantification of MBS-MBC binding affinity. The fraction of MBC bound was calculated. Data from at least three gels for each condition were plotted simultaneously and fit with a single parameter. In the absence and presence of theophylline, the measured  $K_D$  values were 9.9  $\pm$  1.0 nM ( $R^2$ =0.884) and 1.0  $\pm$  0.1 nM ( $R^2$ =0.957), respectively.

Figure 2.3 continued.

(c)



It was now desired to test the possibility of accurate solution phase analyte detection using the MBS rearrangement. The analytical method as described (Figure 2.1) requires that the quantity of retained MBSs following separation by magnetic beads be quantitatively reliable over a broad dynamic range. Given that MBSs are both the detectors and the readout in this scheme, two methods can be used for quantification that are convenient with nucleic acids, scintillation counting and qPCR. Using radiolabeled MBSs, the quantitative reliability of the magnetic bead separation over the concentration range of interest was first confirmed (Figure 2.4). Across a four order-of-magnitude span, the separation and detection of labeled MBSs was quantitatively accurate as compared to the initial input of labeled MBS. Thus, a standard curve built from the signal obtained from the separated and washed MBSs does provide accurate and sensitive quantification of the initial quantity of MBSs.

Using scintillation counting, the conditions for optimal sensing of theophylline with this MBS-MBC design were determined. The signal was defined as the fractional binding of MBS to MBC in the presence of saturating concentration of theophylline (2 mM) and noise as the fractional binding in the absence of theophylline. By varying the concentrations of MBS and MBC, changes in S/N (Figure 2.5 (a)) were determined experimentally. The highest measured S/N was found to be 2.9 at MBS and MBC concentrations of 10 nM. Synthetic riboswitches that acts as theophylline sensors *in vivo* [38] or in *in vitro* translation [48] systems showed higher S/N values than we obtained in our *in vitro* system. One explanation could be that, in these systems, enzymatic events, such as translation, provide the readout for sensor function. The S/N can therefore be

improved, for instance, by the accumulation of proteins that occurs following each signaling event. The relatively-lower frequency of events in the absence of signal also limits the noise from these readouts, further increasing the S/N. Nonetheless, our system provides <u>i)</u> the sensitivity and precision required for accurate measurement of theophylline at concentrations spanning the medically-relevant regime and ii) a basis for exploring the important parameters of SSA-based biosensor design.

The signal-to-noise differences (S-N, Figure 2.5 (b)) at varying concentrations of MBS and MBC were also determined. The largest value was achieved at 1 nM MBS and 50 nM MBC. Using these conditions results in a 2.1-fold increase in signal relative to 10 nM MBS and 10 nM MBC, but it comes at the cost of a 3.8-fold increase in the noise, resulting in a lower S/N. As S/N measures the relative discrimination of the two signals and S-N measures the difference in their absolute levels, both metrics are valuable in choosing the conditions for optimal sensing. We therefore summed the scaled values of these two parameters to define an aggregate score for sensing (Figure 2.5 (c)). The maximal aggregate score was, as with S/N, obtained at MBS and MBC concentrations of 10 nM. Thus, subsequent experiments to examine the quantitative capacity and sensitivity for theophylline sensing by the technique were performed at these MBS and MBC concentrations.

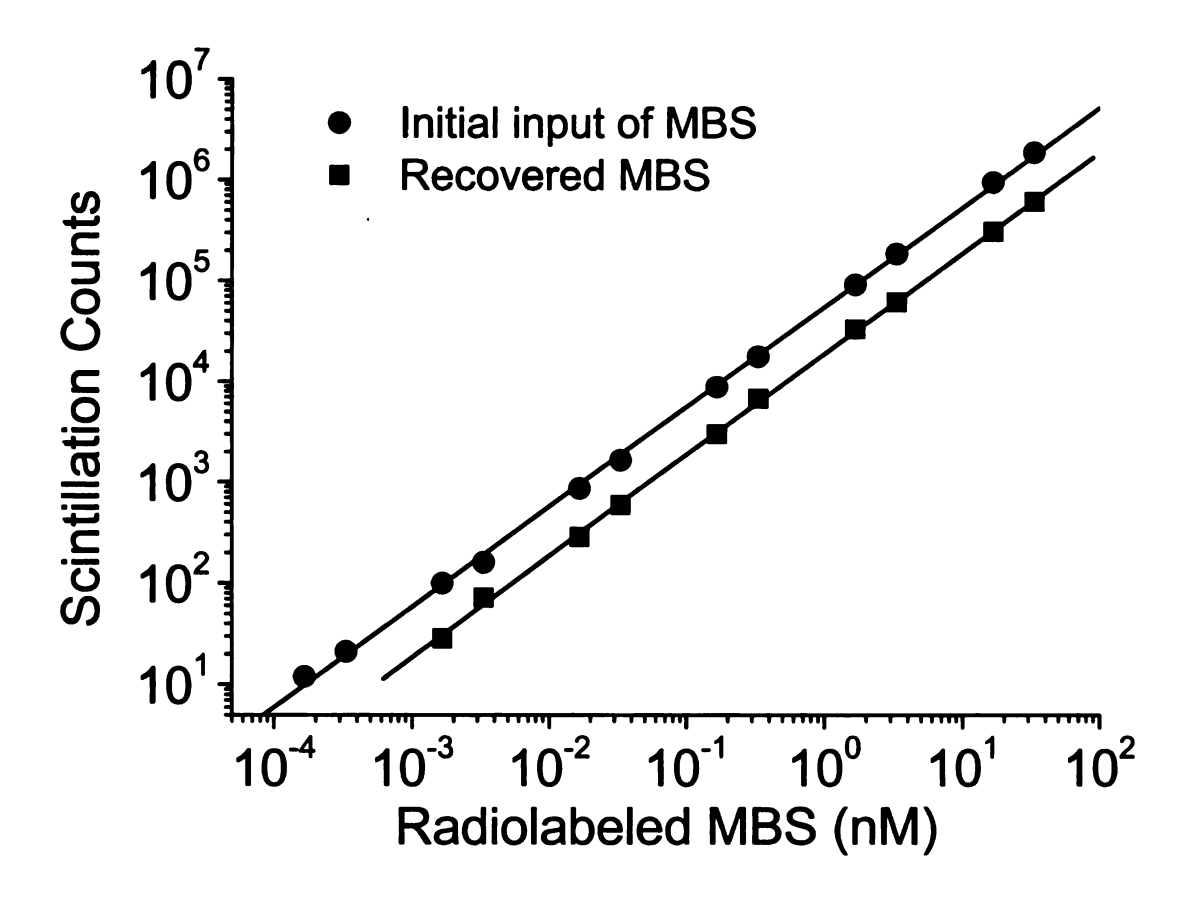


Figure 2.4: Validation of the fidelity of magnetic bead separation. The measured scintillation counts from a serial dilution of MBS concentration counted directly (circles) and after binding by MBCs and elution from magnetic beads (squares) are shown. The signal from the separated MBSs is consistently ~30 % of the signal of the directly-counted MBSs.

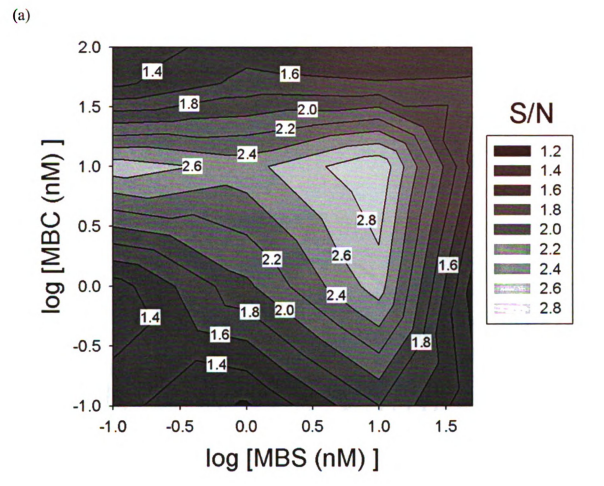
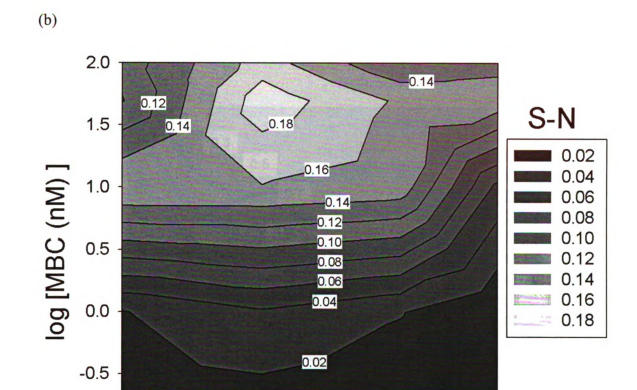


Figure 2.5: Concentrations for optimal S/N, S-N and aggregate score. The fractional MBS binding was calculated as counts from the cluted MBSs normalized to the total counts recovered from the supernatant, washes, and clution. The fractional MBS binding in the presence of 2 mM (signal) and 0 mM (noise) theophylline was measured from which (a) signal-to-noise ratio (S/N), (b) Signal-to-noise difference (S-N) and (c) aggregate score were calculated as described in the experimental section (Chapter 2.3.3). Using MBS and MBC concentrations of 10 nM provided the maximal experimental S/N and aggregate score.

Figure 2.5 continued.



0.5

log [MBS (nM)]

1.0

1.5

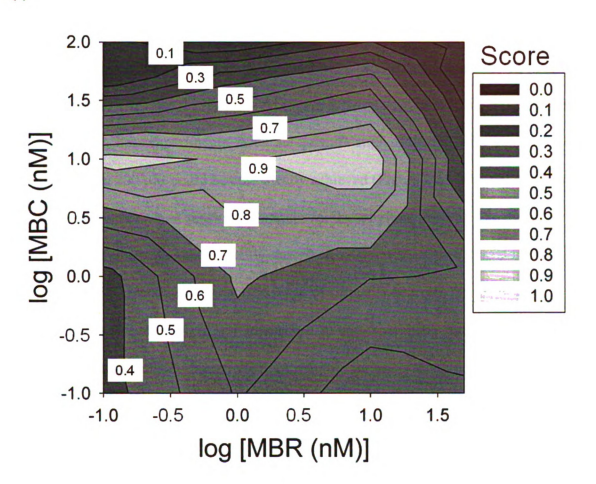
-1.0 <del>-</del>1.0

-0.5

0.0

Figure 2.5 continued.





With the analytical process validated, theophylline concentrations were measured using the described technique. Radiolabeled MBS was incubated in the presence of serial dilutions of theophylline ranging from 0.2 µM to 2 mM. MBC was then added for 10 min, the incubation time that provided the best resolution of bound and free MBS (data not shown). Hence, the interaction of the MBS and MBC is kinetically-limited, rather than equilibrium-limited, as at equilibrium the 20-nt MBC would outcompete the 15-nt cis regulator strand and raise the background (lower S/N) relative to the time frame chosen empirically for these experiments. Accurate quantification of the ophylline concentration from 0.5 µM to 200 µM could be consistently achieved (Figure 2.6). This detection limit is lower than other current sensing techniques for theophylline [49-51]. The dynamic range is also greater than other recently-described aptamer-based theophylline sensing techniques [33,52], and easily spans the range of clinically-relevant theophylline concentrations (55-111 µM) [53]. Furthermore, in our experiments, only 3 µL samples were used, less than the minimum volumes required for many theophylline measurement techniques [54]. As caffeine can convolute the signal for theophylline sensors, the function of the technique in response to caffeine was verified, and it was found that the specificity of separation and detection was maintained at lower than 1 mM analyte concentrations (Figure 2.6). Only 2 mM caffeine had measurable signal significantly above background. This concentration is one order-of-magnitude higher than the analytically important plasma caffeine range (25 to 100 µM) [52]. Therefore, the designed theophylline sensing technique can selectively discriminate highly structurallysimilar molecules at appropriate and useful concentrations.

The advantages of radioactive readouts are their sensitivity and dynamic range. In many circumstances, however, use of radioactivity is undesirable. With the designed MBS sensors, it was important to determine if qPCR could be used as an amplifiable readout of theophylline concentration. PCR-based readouts are particularly useful for parallel applications, as demonstrated previously with MBs [41,42]. The fidelity of qPCR from MBS templates was first confirmed (Figure 2.7), showing a linear response over six orders of magnitude of template concentration. Theophylline concentrations were then measured using qPCR as the readout (Figure 2.8). Theophylline was incubated with unlabeled MBS and biotinylated MBC. The complexes were separated with streptavidin magnetic beads, and eluted MBSs were reverse transcribed and amplified by qPCR. As expected, the results showed decreasing Ct values with increasing theophylline concentration. The detection limit determined by student t-test is 1 µM, and the dynamic range is from 1  $\mu M$  to 20  $\mu M$ . The maximal signal-to-noise ratio was ~3.2 (2<sup>(12.5-10.8)</sup>), similar to what was found with the scintillation counting readout (Figure 2.6), and no significant response was observed for caffeine over the same concentration span.

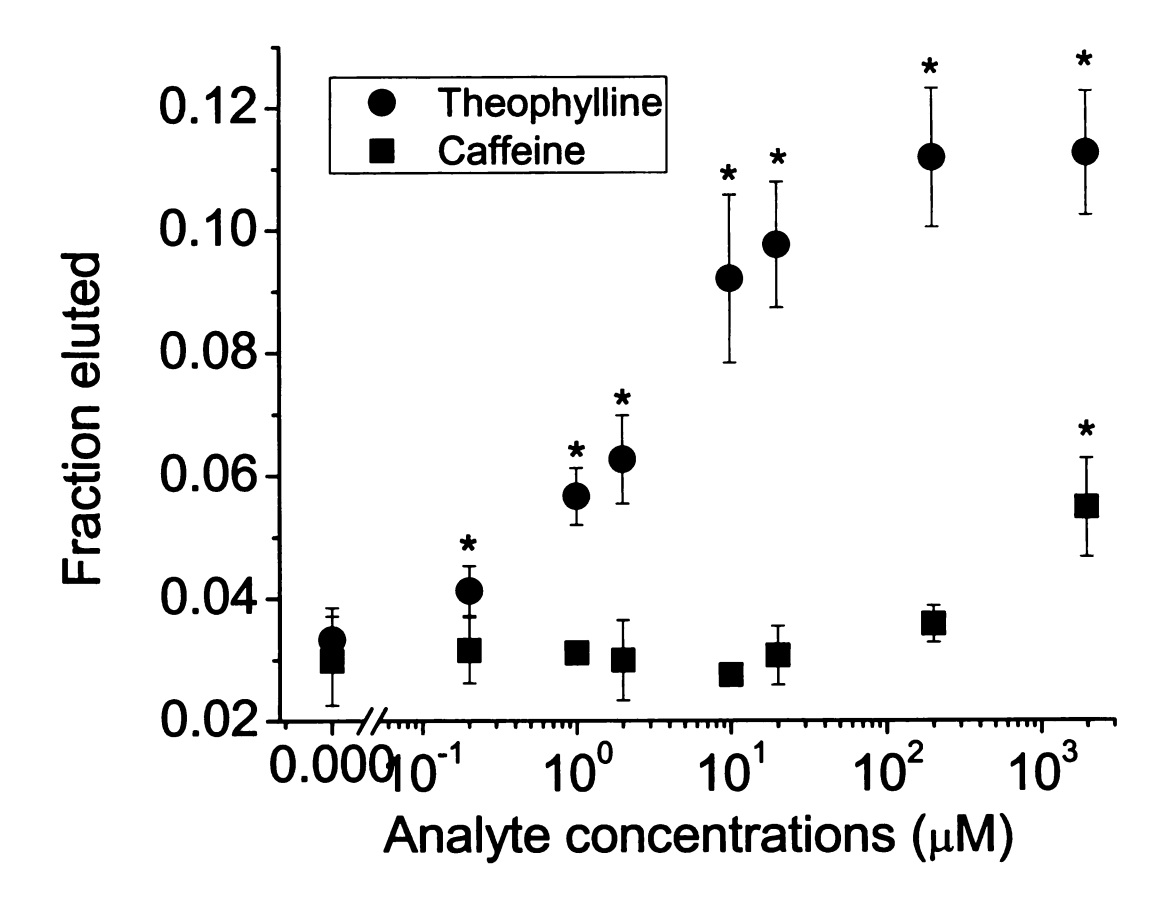


Figure 2.6: Theophylline and caffeine standard curves at optimal MBS and MBC concentration. Using 10 nM MBC and 10 nM MBS, the standard curves for theophylline (circles) and caffeine (squares) show a dynamic range for theophylline of over two orders of magnitude, while maintaining nearly four order-of-magnitude discrimination against the structurally-similar caffeine (\* denotes signal significantly higher than background, p < 0.05). For simplicity, the fractional MBS binding at each analyte concentration was calculated as counts of eluted MBSs relative to counts of total MBS input. Relative values were equivalent to those normalized to the total counts recovered from the sum of supernatant, wash and elution from beads.

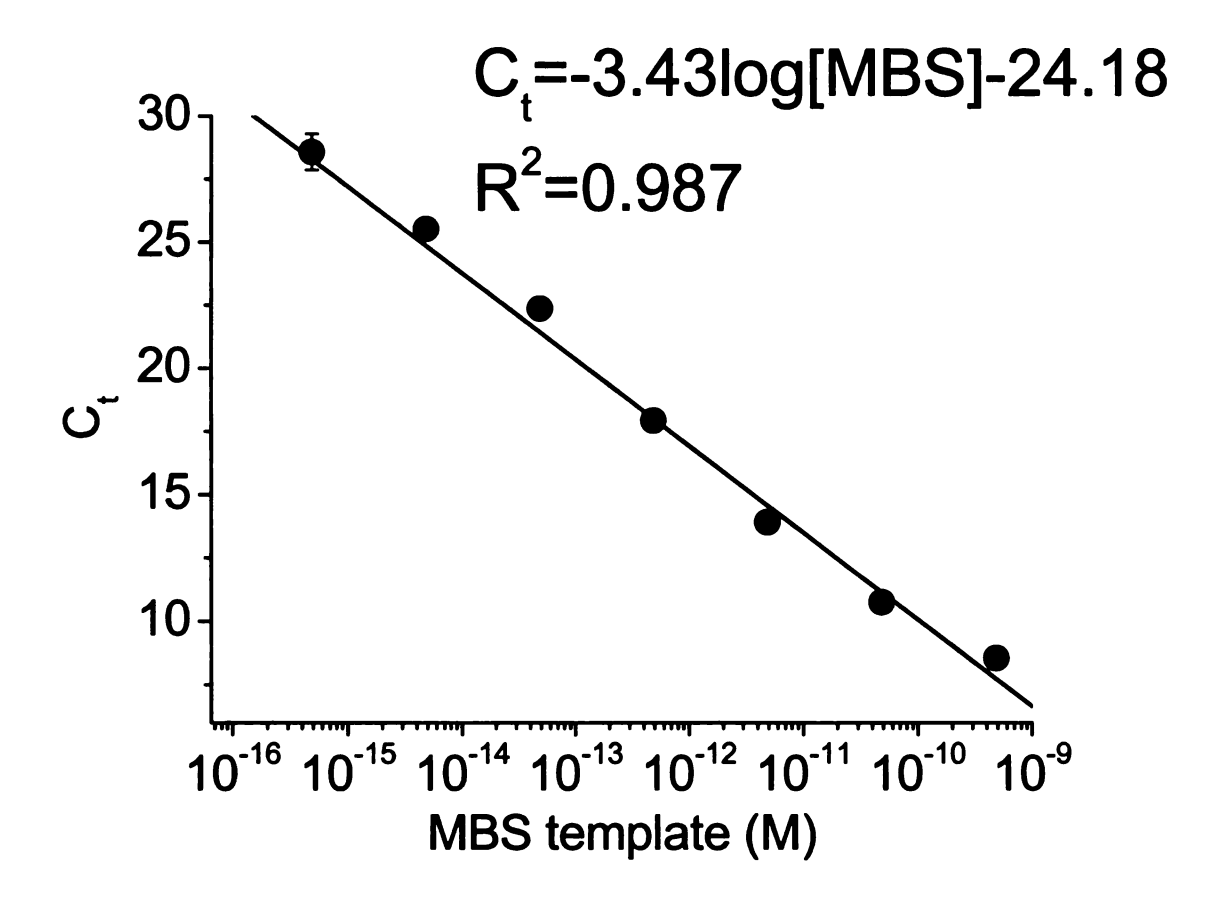


Figure 2.7: Validation of qPCR assay for MBS detection. Serial dilutions of MBS were reverse transcribed and quantified by qPCR. The curve fit shows a slope of -3.4 (R<sup>2</sup>=0.987), indicating nearly 100% amplification efficiency across the tested dynamic range, covering six orders of magnitude from 24.2 zmol to 24.2 fmol of template. For most points, the error bars lie within the plot symbols.

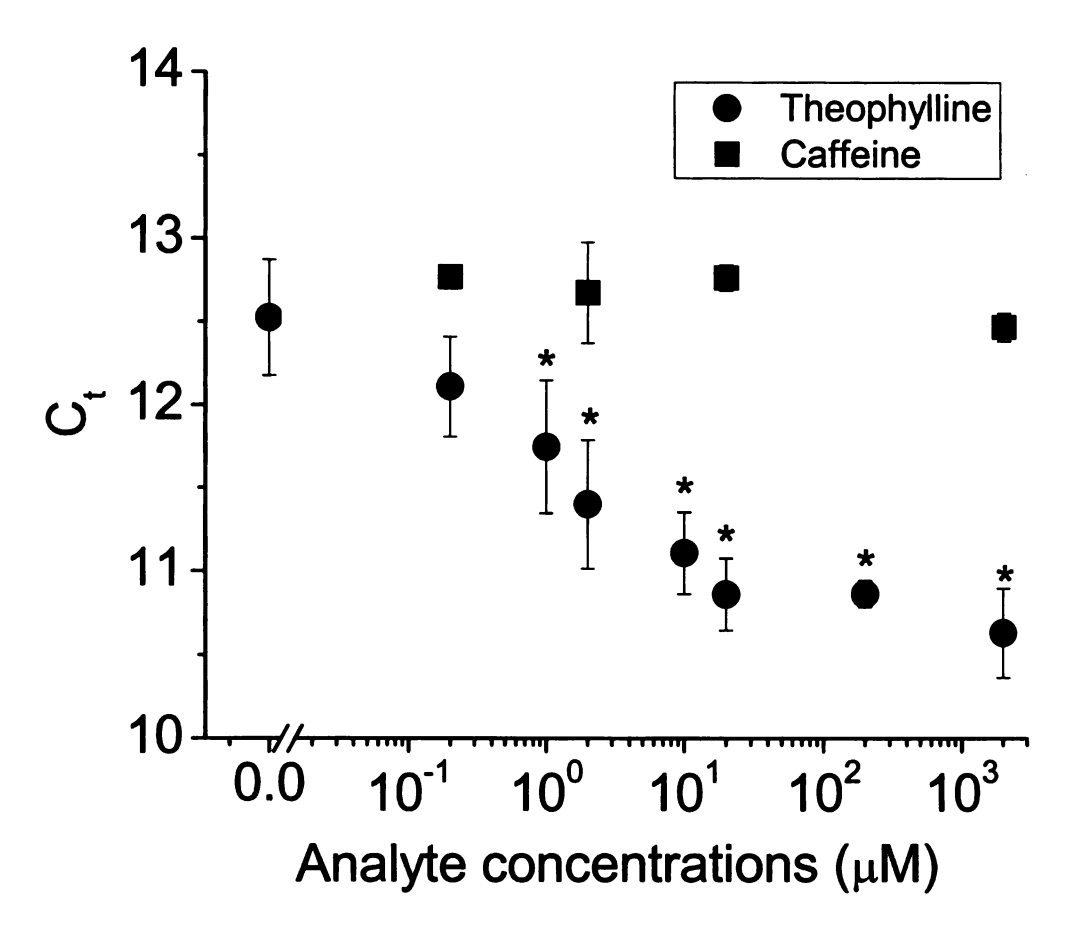


Figure 2.8: Quantification of theophylline concentration. After binding and magnetic bead separation, RT-qPCR was performed on eluted MBSs. Concentration sensitivity for theophylline (circles) was demonstrated across over two orders of magnitude in concentration spanning the clinically-relevant theophylline concentration range (\* denotes signal significantly higher than background, p < 0.05). No significant response was seen for caffeine (squares) over the same concentration span.

#### 2.4.2 Analysis of MBS performance

Having determined the maximal S/N experimentally using two methods, it was of interest to analyze further the variables limiting the resolution of our SSA-based method. Using the measured values for the binding affinities in the presence and absence of the ophylline. the theoretical equilibrium behavior of the system was calculated. Assuming that, when theophylline is present, it is fully-equilibrated with the MBS, the fractional binding of MBS to the MBC was calculated at specified initial concentrations of MBS and MBC. S/N, S-N, and the aggregate score were then calculated using a K<sub>D</sub> of 1 nM (saturating theophylline condition) and a K<sub>D</sub> of 9.9 nM (no theophylline condition) (Figures 2.9). The ratio (Figure 2.9 (a)) reaches a maximum approaching 10 at low MBS and MBC concentrations. This ratio depends exactly on the 10-fold change in affinity between the two conditions for our MBS design; i.e., K<sub>D</sub> becomes the dominant term in equations (2.1) and (2.2). At limiting concentrations of both MBC and MBS, fractional binding scales exactly as the inverse of K<sub>D</sub>. However, this resolution could only be achieved with superb analytical sensitivity, due to the extraordinarily small quantities of analytes at such concentrations (e.g., only 10<sup>5</sup> MBS molecules would be contained in a 3 µL sample at a concentration of  $10^{-4}$  pM).

(a)

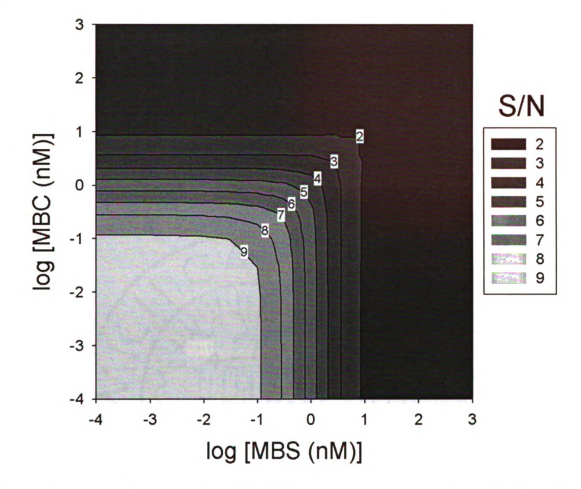


Figure 2.9: Theoretical analysis of S/N, S-N and aggregate score. Using the  $\rm K_D$  values for MBS-MBC complex formation in the presence of saturating levels of theophylline and in the absence of theophylline, the equilibrium MBS fraction binding at varying MBS and MBC concentrations was calculated using equation (2.2). S/N values (a), S-N (b) and aggregate score (c) were then calculated as in Figure 2.5. (d) The scaled aggregate score at 10 nM MBS shows a maximum at 10 nM MBC, as in the experimental results.

Figure 2.9 continued.

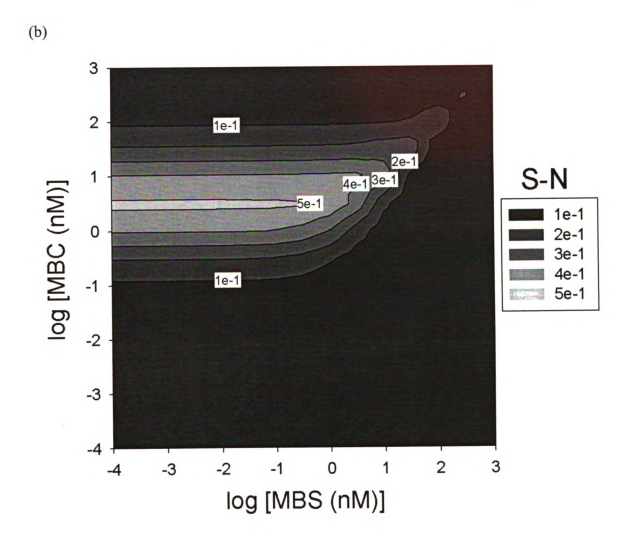
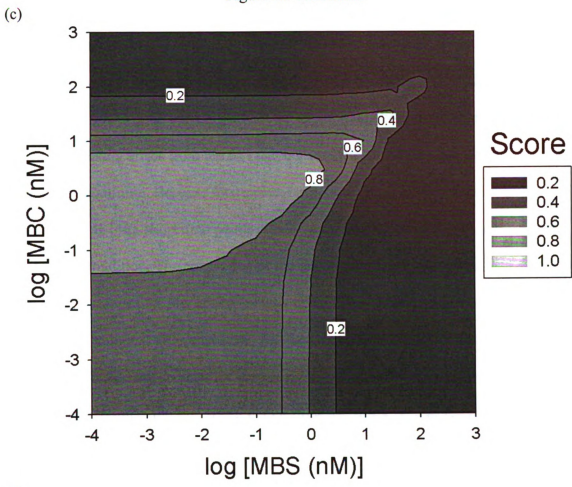
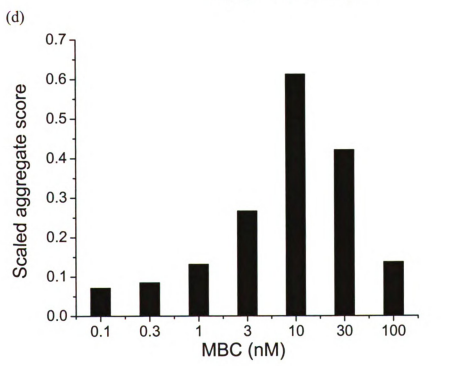


Figure 2.9 continued.





As the concentrations increase, especially above the K<sub>D</sub> values, the concentrations dominate in equation (2.1) and (2.2), minimizing the impact of the affinity difference and causing the ratio to approach 1 (Figure 2.9 (a)). At 10 nM MBS and MBC, the theoretical S/N value is 1.9, in good agreement with the experimentally-derived value of 2.9. The discrepancy likely arises from the fact that our experimental data were not taken at the equilibrium condition. Because intermolecular hybridization affinity can scale with association rate [46], short time points would therefore improve the ratio relative to the equilibrium condition. The correlation of the experimental and theoretical data across the concentration ranges for low concentrations of MBC and MBS is not as strong. This is likely due to technical differences between the calculations and the experiments. The theoretical plots do not account for the lower detection limits for scintillation counting. In addition, to maximize the true signal eluted from the beads, the complexes were washed, which immediately shifts the equilibrium to reduce the number of bound MBSs that are recovered. On a fractional basis, the loss of bound MBSs during the wash steps will reduce the signal recovered at low MBS and MBC concentrations far more dramatically than at high concentrations. Hence, both signals approach the detection background. This is likely the reason the experimental ratios decline at lower than 10 nM concentrations. While the S/N achieved experimentally was sufficient to provide sensitive and accurate theophylline detection, the theoretical analysis suggests that improvements to the resolution of the technique may still be achievable.

Examining the theoretical difference, it peaks at MBC concentrations between the  $K_D$  values, at limiting MBS concentrations (Figure 2.9 (b)). This is expected due to the

maximum absolute distance between the binding curves at these conditions (similar to the separation between the curves along the vertical line at [MBS] ≈ 3 nM on Figure 2.3 (c)). The experimental S-N showed a peak value at MBC and MBS concentrations (50 nM and 1 nM, respectively) higher than those of the theoretical peak, but the peak experimental S-N value of 0.18 is in line with the theoretical value of 0.2 at these concentrations. For the aggregate score, the experimental peak score also occurred at MBS and MBC concentrations both above those of the theoretical peak (compare Figures 2.5 (c) and 2.9 (c)). However, looking only at 10 nM concentration of MBS, we see the maximum aggregate score at 10 nM MBC (Figure 2.9 (d)), to some degree supporting our experimental results. For the experimental conditions, the theoretical aggregate score was ~60% of the global theoretical maximum, another indication that technical improvements to our analytical strategy may be possible.

# 2.4.3 Thermodynamic constructs for predicting MBS function

Typically, to design an SSA biosensor, multiple designs are tested to identify which has the most desirable properties by some metric, such as S/N [24]. Our analyses argue strongly that the experimental behavior of the MBS can be reliably captured by a relatively simple theoretical model in which only the affinities of the SSA for its complement in the presence and absence of target are required. The analysis described above relies on the experimentally derived K<sub>D</sub> values to predict the expected S/N. As minimum free energy structures have proven useful in unimolecular nucleic acid sensor design [55] and interaction free energies between molecules tend to be at least relatively correct as compared to experimental data [46], we also preliminarily investigated whether

a thermodynamic construct using minimum free energy structure predictions, based on our previous work [56], would allow us to predict  $K_D$  values as another means of evaluating alternative designs for the MBS and MBC that would provide higher S/N (Figure 2.10 and Table 2.1).

Improvements in S/N should result from increases in the affinity of the MBS for the MBC in the presence of analyte relative to the affinity in the absence of analyte. To avoid testing every possible MBS and MBC design experimentally, a thermodynamic construct was defined to calculate the predicted affinities of different MBC and MBS designs. In solutions containing theophylline, the MBS will exist largely in the minimum free energy conformation available to the MBS alone (Figure 2.10, construct 1) or that available to the MBS bound to theophylline (Figure 2.10, construct 2). Changes in the experimental S/N should then mimic changes in the relative affinities calculated for the two constructs.

Figure 2.10: Thermodynamic constructs for MBS-MBC binding in the absence and presence of theophylline. The ratios of the predicted  $K_D$  values are representative of the expected S/N in the experimental technique.

Table 2.1: Thermodynamic Predictions for MBS design modifications.

Modifications to MBS	ΔG <sup>o</sup> UN1	ΔG <sup>o</sup> UN2	$\Delta\Delta G^{o}_{TO} = \Delta G^{o}_{UN1} - \Delta G^{o}_{UN2}$	K <sub>D1</sub> / K <sub>D2</sub>
Initial sequence	31.8	31.1	0.7	3.21
Stabilize MB by adding 4 bp	36.1	35.4	0.7	3.21
Stabilize MB by adding 5 bp	39.2	38.4	0.8	3.79
Stabilize MB by adding 10 bp	49.1	48.4	0.7	3.21
Destabilizing MB by deleting 1 bp	28.5	27.8	0.7	3.21
Destabilizing MB by deleting 5 bp	22.1	21.4	0.7	3.21
Destabilizing MB by mutating 1 base	25.8	25.1	0.7	3.21
Lengthening the aptamer 3' stem by 2 bases	31.8	31.5	0.3	1.65
Shortening the aptamer 3' stem by 5 bases	31.8	31.4	0.4	1.95
Extending the 5' MB by G	32.2	31.1	1.1	6.25
Extending the 5' MB by GGG	33.5	31.1	2.4	54.60

Using mfold to perform the structural calculations (in a similar fashion to our earlier work) [56], the free energy for MBS-MBC hybridization was calculated in the absence and presence of theophylline as follows:

$$\Delta G^{o}_{TO} = \Delta G^{o}_{UN} + \Delta G^{o}_{OS} + \Delta G^{o}_{OH} + \Delta G^{o}_{RE}$$

where:  $\Delta G^{0}_{TO}$  = the overall free energy change due to the structural rearrangement upon MBC hybridization

 $\Delta G^{0}_{UN}$  = the cost to unfold the native MBS structure

 $\Delta G^{o}_{OS}$  = the cost to unfold the native MBC structure

 $\Delta G^{0}_{OH}$  = the energy released upon intermolecular MBS-MBC hybridization

 $\Delta G^{o}_{RE}$  = the energy released upon rearrangement of the complex to the available conformation with the lowest free energy

Predicted K<sub>D</sub> values for the interactions can then be calculated from:

$$\Delta G^{o}_{TO} = RT ln K_{D}$$

For a given MBS-MBC pair,  $\Delta G^o_{OS}$ ,  $\Delta G^o_{OH}$ , and  $\Delta G^o_{RE}$  are equal, therefore manipulations like varying the length or sequence of the MBC does not alter the predicted relative affinities of the constructs and is not expected to improve the S/N in practice. The relative affinities, and, hence, the expected S/N, are then defined only by

the change in the cost of unfolding the construct with the ophylline bound (for the construct used in developing the biosensor,  $\Delta G^o_{UN1} = 31.1$  kcal/mole) vs. that without the ophylline ( $\Delta G^o_{UN2} = 31.8$  kcal/mole). For our MBS-MBC pair, the resulting predicted  $K_D$  values, 0.76 nM and 2.4 nM, respectively, are in reasonable agreement with our measured values of 1.0 nM and 9.9 nM, supporting this analysis as a valid method for screening MBS and MBC manipulations.

Though we did not expect, based on our analysis, that changing the MBC length would alter the S/N in an equilibrium circumstance, we also tested this experimentally. As stated in the experimental section (Chapter 2.3.1), we found that using MBC sequences shorter than 14 nt did not provide adequate signal, as might be expected from the higher (less negative)  $\Delta G^o_{TO}$  values due to higher  $\Delta G^o_{OH}$  values. Sequences longer than 20 nt had high background binding due to the relatively stronger intermolecular hybridization (more negative  $\Delta G^o_{OH}$  values) with increasing MBC length as compared to the intramolecular structural stability ( $\Delta G^o_{UN}$  values). Ultimately, a 20 nt MBC sequence was chosen, because the detection range provided by this sequence effectively balances the need for adequate signal while minimizing background,

Computationally, we also modified other domains of the MBS and predicted the change in predicted affinity (Table 2.1). When the aptamer stem, which is involved in both theophylline binding and barcode displacement, was modified, the results showed that

lengthening the aptamer stem increased the cost of unfolding the 3'-tail of the theophylline bound conformation, reducing the predicted affinity. Shortening the stem length reduced the displacement of the MB portion of the construct, again decreasing the predicted affinity. As such, neither case was anticipated to improve MBS function experimentally.

However, we did observe that stabilizing the MB stem by extending the 5'-end of the MB sequence can improve the relative affinity ratio. We synthesized an MBS with 3Gs at the 5'-end, which is predicted to improve the relative affinity ratio by nearly 20-fold. A theophylline dose response assayed by electrophoretic mobility shift at equilibrium showed a S/N of approximately 9, an improvement over our initial design, in line with the calculated results. However, the improvement was due to a reduction of noise rather than an increase in signal. Presumably, the increased structural stability of the MBS reduced the association kinetics for the MBS-MBC pair. Therefore, the non-equilibrium readout using the magnetic beads did not have sufficient signal using this construct to get a reproducible signal. This then becomes a readout problem rather than a sensor design problem. The construct described allowed us to best demonstrate our technique with our current protocols.

## 2.5 Conclusions

A theophylline quantification technique was designed using an SSA in combination with scintillation counting or qPCR. In this manner, the SSA converted the analyte signal into

a nucleic acid signal for subsequent amplification and quantification. Analytical accuracy and specificity were readily achieved by this technique. Analysis of the controlling parameters of the system indicated that further performance enhancements may be achievable through careful SSA design and protocol optimization.

## References

- 1. Saiki RK, Gelfand DH, Stoffel S *et al.* Primer-directed enzymatic amplification of DNA with a thermostable DNA polymerase. *Science (New York, N.Y*, 239(4839), 487-491 (1988).
- 2. Nolan T, Hands RE, Bustin SA. Quantification of mRNA using real-time RT-PCR. *Nature protocols*, 1(3), 1559-1582 (2006).
- 3. Southern EM. Detection of specific sequences among DNA fragments separated by gel electrophoresis. *Journal of molecular biology*, 98(3), 503-517 (1975).
- 4. Alwine JC, Kemp DJ, Stark GR. Method for detection of specific RNAs in agarose gels by transfer to diazobenzyloxymethyl-paper and hybridization with DNA probes. *Proc Natl Acad Sci U S A*, 74(12), 5350-5354 (1977).
- 5. Schena M, Shalon D, Davis RW, Brown PO. Quantitative monitoring of gene expression patterns with a complementary DNA microarray. *Science (New York, N.Y*, 270(5235), 467-470 (1995).
- 6. Griffin JL. Understanding mouse models of disease through metabolomics. Current opinion in chemical biology, 10(4), 309-315 (2006).
- 7. Gibson G, Muse S. V. Analysis of cellular constituents. In: *A primer of genome science*. Gibson, G, Muse S. V. (Ed. (Sinauer Associates 2004) 333-337.
- 8. Jayasena SD. Aptamers: an emerging class of molecules that rival antibodies in diagnostics. *Clin Chem*, 45(9), 1628-1650 (1999).
- 9. Tombelli S, Minunni M, Mascini M. Analytical applications of aptamers. *Biosensors & bioelectronics*, 20(12), 2424-2434 (2005).
- 10. Navani NK, Li Y. Nucleic acid aptamers and enzymes as sensors. *Current opinion in chemical biology*, 10(3), 272-281 (2006).
- 11. Zhou L, Ou LJ, Chu X, Shen GL, Yu RQ. Aptamer-based rolling circle amplification: a platform for electrochemical detection of protein. *Analytical chemistry*, 79(19), 7492-7500 (2007).

- 12. Lee SJ, Youn BS, Park JW et al. ssDNA aptamer-based surface plasmon resonance biosensor for the detection of retinol binding protein 4 for the early diagnosis of type 2 diabetes. Analytical chemistry, 80(8), 2867-2873 (2008).
- 13. Zhang J, Wang L, Pan D *et al.* Visual cocaine detection with gold nanoparticles and rationally engineered aptamer structures. *Small*, 4(8), 1196-1200 (2008).
- 14. Du Y, Li B, Wei H, Wang Y, Wang E. Multifunctional label-free electrochemical biosensor based on an integrated aptamer. *Analytical chemistry*, 80(13), 5110-5117 (2008).
- 15. Ellington AD, Szostak JW. *In vitro* selection of RNA molecules that bind specific ligands. *Nature*, 346(6287), 818-822 (1990).
- 16. Tuerk C, Gold L. Systematic evolution of ligands by exponential enrichment: RNA ligands to bacteriophage T4 DNA polymerase. *Science (New York, N.Y*, 249(4968), 505-510 (1990).
- 17. Gold L, Polisky B, Uhlenbeck O, Yarus M. Diversity of oligonucleotide functions. Annu Rev Biochem, 64, 763-797 (1995).
- 18. Lee JF, Hesselberth JR, Meyers LA, Ellington AD. Aptamer database. *Nucleic Acids Res*, 32(Database issue), D95-100 (2004).
- 19. Jenison RD, Gill SC, Pardi A, Polisky B. High-resolution molecular discrimination by RNA. *Science (New York, N.Y*, 263(5152), 1425-1429 (1994).
- 20. Lin Y, Qiu Q, Gill SC, Jayasena SD. Modified RNA sequence pools for *in vitro* selection. *Nucleic Acids Res*, 22(24), 5229-5234 (1994).
- 21. Pieken WA, Olsen DB, Benseler F, Aurup H, Eckstein F. Kinetic characterization of ribonuclease-resistant 2'-modified hammerhead ribozymes. *Science (New York, N.Y*, 253(5017), 314-317 (1991).
- 22. Jhaveri S, Rajendran M, Ellington AD. *In vitro* selection of signaling aptamers. *Nat Biotechnol*, 18(12), 1293-1297 (2000).

- 23. Stojanovic MN, Kolpashchikov DM. Modular aptameric sensors. *Journal of the American Chemical Society*, 126(30), 9266-9270 (2004).
- 24. Nutiu R, Li Y. Aptamers with fluorescence-signaling properties. *Methods (San Diego, Calif,* 37(1), 16-25 (2005).
- 25. Stojanovic MN, de Prada P, Landry DW. Aptamer-based folding fluorescent sensor for cocaine. *Journal of the American Chemical Society*, 123(21), 4928-4931 (2001).
- 26. Wu ZS, Guo MM, Zhang SB *et al.* Reusable electrochemical sensing platform for highly sensitive detection of small molecules based on structure-switching signaling aptamers. *Analytical chemistry*, 79(7), 2933-2939 (2007).
- 27. Zuo X, Song S, Zhang J et al. A target-responsive electrochemical aptamer switch (TREAS) for reagentless detection of nanomolar ATP. Journal of the American Chemical Society, 129(5), 1042-1043 (2007).
- 28. Radi AE, O'Sullivan CK. Aptamer conformational switch as sensitive electrochemical biosensor for potassium ion recognition. *Chem Commun (Camb)*, (32), 3432-3434 (2006).
- 29. Xiao Y, Piorek BD, Plaxco KW, Heeger AJ. A reagentless signal-on architecture for electronic, aptamer-based sensors via target-induced strand displacement. *Journal of the American Chemical Society*, 127(51), 17990-17991 (2005).
- 30. Bauer G, Suess B. Engineered riboswitches as novel tools in molecular biology. *J Biotechnol*, 124(1), 4-11 (2006).
- 31. Wang J, Jiang Y, Zhou C, Fang X. Aptamer-based ATP assay using a luminescent light switching complex. *Analytical chemistry*, 77(11), 3542-3546 (2005).
- 32. Nutiu R, Li Y. Structure-switching signaling aptamers: transducing molecular recognition into fluorescence signaling. *Chemistry (Weinheim an der Bergstrasse, Germany)*, 10(8), 1868-1876 (2004).
- 33. Rankin CJ, Fuller EN, Hamor KH, Gabarra SA, Shields TP. A simple fluorescent biosensor for theophylline based on its RNA aptamer. *Nucleosides Nucleotides Nucleic Acids*, 25(12), 1407-1424 (2006).

- 34. Nutiu R, Li Y. Structure-switching signaling aptamers. *Journal of the American Chemical Society*, 125(16), 4771-4778 (2003).
- 35. Nutiu R, Li Y. *In vitro* selection of structure-switching signaling aptamers. *Angewandte Chemie (International ed*, 44(7), 1061-1065 (2005).
- 36. Rajendran M, Ellington AD. Selection of fluorescent aptamer beacons that light up in the presence of zinc. *Anal Bioanal Chem*, 390(4), 1067-1075 (2008).
- 37. Bayer TS, Smolke CD. Programmable ligand-controlled riboregulators of eukaryotic gene expression. *Nat Biotechnol*, 23(3), 337-343 (2005).
- 38. Lynch SA, Desai SK, Sajja HK, Gallivan JP. A high-throughput screen for synthetic riboswitches reveals mechanistic insights into their function. *Chem Biol*, 14(2), 173-184 (2007).
- 39. Yang L, Ellington AD. Real-time PCR detection of protein analytes with conformation-switching aptamers. *Anal Biochem*, (2008).
- 40. Shoemaker DD, Lashkari DA, Morris D, Mittmann M, Davis RW. Quantitative phenotypic analysis of yeast deletion mutants using a highly parallel molecular bar-coding strategy. *Nat Genet*, 14(4), 450-456 (1996).
- 41. Giaever G, Chu AM, Ni L *et al.* Functional profiling of the Saccharomyces cerevisiae genome. *Nature*, 418(6896), 387-391 (2002).
- 42. Walton SP, Mindrinos MN, Davis RW. Analysis of hybridization on the molecular barcode GeneChip microarray. *Biochem Biophys Res Commun*, 348(2), 689-696 (2006).
- 43. Fredriksson S, Gullberg M, Jarvius J et al. Protein detection using proximity-dependent DNA ligation assays. *Nat Biotechnol*, 20(5), 473-477 (2002).
- 44. Fischer NO, Tarasow TM, Tok JB. Protein detection via direct enzymatic amplification of short DNA aptamers. *Anal Biochem*, 373(1), 121-128 (2008).

- 45. Zhang H, Wang Z, Li XF, Le XC. Ultrasensitive detection of proteins by amplification of affinity aptamers. *Angew Chem Int Ed Engl*, 45(10), 1576-1580 (2006).
- 46. Walton SP, Stephanopoulos GN, Yarmush ML, Roth CM. Thermodynamic and kinetic characterization of antisense oligodeoxynucleotide binding to a structured mRNA. *Biophysical journal*, 82(1 Pt 1), 366-377 (2002).
- 47. Seetharaman S, Zivarts M, Sudarsan N, Breaker RR. Immobilized RNA switches for the analysis of complex chemical and biological mixtures. *Nat Biotechnol*, 19(4), 336-341 (2001).
- 48. Ogawa A, Maeda M. Aptazyme-based riboswitches as label-free and detector-free sensors for cofactors. *Bioorganic & medicinal chemistry letters*, 17(11), 3156-3160 (2007).
- 49. Sekella PT, Rueda D, Walter NG. A biosensor for theophylline based on fluorescence detection of ligand-induced hammerhead ribozyme cleavage. *Rna*, 8(10), 1242-1252 (2002).
- 50. Ferapontova EE, Shipovskov S, Gorton L. Bioelectrocatalytic detection of theophylline at theophylline oxidase electrodes. *Biosensors & bioelectronics*, 22(11), 2508-2515 (2007).
- 51. Saka K, Uemura K, Shintani-Ishida K, Yoshida K. Acetic acid improves the sensitivity of theophylline analysis by gas chromatography-mass spectrometry. *J Chromatogr B Analyt Technol Biomed Life Sci*, 846(1-2), 240-244 (2007).
- 52. Ferapontova EE, Olsen EM, Gothelf KV. An RNA aptamer-based electrochemical biosensor for detection of theophylline in serum. *Journal of the American Chemical Society*, 130(13), 4256-4258 (2008).
- 53. Hendeles L, Weinberger M, Johnson G. Monitoring serum theophylline levels. *Clin Pharmacokinet*, 3(4), 294-312 (1978).
- 54. Mounie J, Richard L, Ribon B et al. Methods of theophylline assay and therapeutic monitoring of this drug. Annales de biologie clinique, 48(5), 287-293 (1990).

- 55. Hall B, Hesselberth JR, Ellington AD. Computational selection of nucleic acid biosensors via a slip structure model. *Biosensors & bioelectronics*, 22(9-10), 1939-1947 (2007).
- 56. Walton SP, Stephanopoulos GN, Yarmush ML, Roth CM. Prediction of antisense oligonucleotide binding affinity to a structured RNA target. *Biotechnol Bioeng*, 65(1), 1-9 (1999).

# CHAPTER 3 DEVELOPMENT OF A DUAL APTAMER-BASED MULTIPLEX PROTEIN BIOSENSOR

Portions reproduced from: Xie, S. and Walton, S. P., "Development of a dual aptamer-based multiplex protein biosensor", *Biosensors and Bioelectronics* (2010), doi:10.1016/j.bios.2010.04.034 with permissions from Elsevier.

#### 3.1 Abstract

Parallel biosensors for proteins are becoming more essential for the thorough and systematic investigation of complex biological processes. These tools also enable improved clinical diagnoses relative to single protein analyses due to their greater information content. If implemented correctly, affinity-based techniques can provide unique advantages in terms of sensitivity and flexibility. Aptamers are increasingly being used as the affinity reagents of choice for protein biosensing applications. Here, we describe the development and characterization of an aptamer-based method for parallel protein analyses that relies on recognition of the target protein by two unique aptamers targeting different epitopes on the protein. It was predicted that this approach would have improved dynamic range and sensitivity, relative to the SSA-based technique. Our results show that the technique achieved simultaneous and quantitative detection of thrombin and platelet-derived growth factor-BB (PDGF-BB) with high specificity both in buffered solutions and in serum samples. Moreover, the empirical biosensing performance agreed with expectations based on theoretical calculations.

# 3.2 Introduction

Improvements in clinical, laboratory, and biodefense applications rely on the continuing development of biosensing techniques for various biomolecules. In particular, considerable current work is focused on novel tools for parallel biosensors. While nucleic acid detection tools are relatively mature at this point, further evolution in the area of protein biosensing technologies, especially in a multiplex fashion, is required.

While classical parallel protein analytical techniques, such as two-dimensional gel electrophoresis followed by mass spectroscopy (2DE/MS) [1], will continue to be valuable tools for discovery-oriented protein measurements, affinity-based techniques have emerged as popular approaches for the detection of single and focused sets of proteins [2]. Antibody-based multiplex sensing assays have been developed in various planar and bead array formats and are becoming accepted methods for protein expression and interaction studies [3-5]. However, the function of these arrays may be impaired by the high local concentrations of surface-bound antibodies and non-specific interactions between the substrate and the antibodies or analytes [6]. Additional limitations of antibody-based proteomics methods, in general, include batch-to-batch variation in antibody quality and the cost of antibody generation and purification [7]. Therefore, novel approaches are being sought that can complement or expand existing antibody-based techniques.

Aptamers are gaining popularity as alternative affinity reagents for biosensing applications [8-16]. Aptamers are single-stranded nucleic acids that bind other molecules with high specificity and affinity [17,18] and may provide unique advantages for multiplex analytical applications [6,19,20]. Aptamers are selected *in vitro* and in theory can be selected to bind almost any target with automated and high-throughput techniques for aptamer selection having been demonstrated [21]. Furthermore, aptamers are nucleic acids rather than proteins and therefore can be easily synthesized commercially or enzymatically with high reproducibility and minimal batch-to-batch variation [22,23], which is valuable for the development of reproducible biosensors.

The majority of current aptamer-based biosensor designs are specific for a single analyte [14,24-32]. While chip-based aptamer arrays for multiplexed protein measurements are currently in development both by academic and commercial groups [19,20,33-37], Aptamer-based sensing combined with capillary electrophoresis has been used to measure four proteins simultaneously [38]. Nonetheless, the development of additional solution-phase and bead-based assays is still valuable, as they can potentially be customized for specific sets of target proteins and may have sensitivity advantages over current techniques.

In this work, we describe proof-of-concept development of a solution-phase biosensor for *multiplex* protein measurements that relies on dual-aptamer analyte recognition. We have shown previously that the detection dynamic range based on aptamer conformational

rearrangement can be limited [16]. We hypothesized that altering the sensing design to use increased aptamer concentrations, two specific recognition events, and an affinity-based separation would have improved sensitivity, specificity, and dynamic range compared to the structure-switching aptamer approach. Applying our new technique to measure the concentrations of thrombin and platelet-derived growth factor (PDGF-BB), we found a reproducible, linear dynamic response to analyte concentrations over a three order-of-magnitude range of concentration. For both proteins, accurate and reproducible measurements were obtained using multiple readouts in both buffered solutions and in complex mixtures.

## 3.3 Experimental section

### 3.3.1 Proteins and aptamer sequences

Thrombin was purchased from Haematologic Technologies (Essex Junction, VT). PDGF-BB was purchased from R & D Systems (Minneapolis, MN). Haptoglobin, fibrinogen, C-reactive protein and lysozyme were from Sigma Aldrich (St Louis, MO). The sequences for the thrombin sensing and capture aptamers were 5'-

GATGTCCACGAGGTCTCTATTGCATTCGCACTTCCGATTTTTTCAGTCCGTGGTA
GGGCAGGTTGGGGTGACTCGTACGCTGCAGGTCGAC-3' (MB-T, 91 nt, italicized:
MB sequence) and 5'-

T), respectively. The sequences for the PDGF-BB sensing and capture aptamers were 5'-

GATGTCCACGAGGTCTCTGCGGCATCAACAATCTCGAATTTTTTTACTCAGGGCA
CTGCAAGCAATTGTGGTCCCAATGGGCTGAGTATCGTACGCTGCAGGTCGAC3' (MB-P, 106 nt, italicized: MB sequence) and 5'-

TACTCAGGGCACTGCAAGCAATTGTGGTCCCAATGGGCTGAGTATTTTTT-Bio-

3' (Bio-P), respectively. Each of these aptamers was derived from sequences available in the literature [32, 39-41]. Aptamer-protein affinities were measured by filter binding assays. Capture aptamers were synthesized with 3'-biotins spaced from the aptamer sequence by oligo(dT) sequences. Primer sequences specific for MB-T were 5'-ATTGCATTCGCACTTCCGAT-3' (T5'p) and 5'-AGTCACCCCAACCTGCCCTA-3' (T3'p). Primer sequences specific for MB-P were 5'-GCGGCATCAACAATCTCGAA-3' (P5'p) and 5'-ATACTCAGCCCATTGGGACC-3' (P3'p). Aptamer specific primers were used for single-protein and multiplex qPCR readouts. The 5' and 3' primers were chosen to be specific to the MBs and to the aptamer 3' ends, respectively. Using the hybridization server on mfold [42], both sets of template specific primers were confirmed not to cross-prime the other sensing aptamer template (data not shown). Universal primer sequences for both sensing aptamers were 5'-GATGTCCACGAGGTCTCT-3' (U5'p) and 5'-GTCGACCTGCAGCGTACG-3' (U3'p). Universal primers were used for multiplex experiments using electrophoresis readouts. All oligonucleotides were synthesized and purified from Integrated DNA Technologies, Inc (Coralville, IA).

#### 3.3.2 Dual aptamer sensing assays

Prior to use, aptamers were annealed at 95°C for 3 min and cooled to room temperature over a period of 30 min. Proteins and annealed aptamers were mixed in binding buffer (50 mM Tris-HCl (pH 7.5), 100 mM NaCl, 1 mM MgCl<sub>2</sub>, 0.1% BSA, and 5  $\mu$ g/ml poly(dI-dC)) in a total volume of 30  $\mu$ L. Binding reactions were incubated at room temperature for 30 min followed by the addition of streptavidin coated magnetic beads (Dynal/Invitrogen, Oslo, Norway) for an additional 30 min at room temperature. A magnet was then applied to retain the beads, and the supernatant was removed. The beads were then washed three times with 100  $\mu$ L of wash buffer (binding buffer plus 0.02% Tween 20). Retained sensing aptamers were eluted from the magnetic beads in 100  $\mu$ L of water at 95°C for 5 min. Some or all of the recovered sensing aptamers were amplified by PCR.

Experiments determining the optimal concentration of thrombin or PDGF-BB sensing aptamer were performed in binding reactions with varying concentrations of sensing aptamer (5, 50, 250, 500, 1000 and 2500 nM) and 500 nM of capture aptamer in the presence and absence of 500 nM protein. After binding and separation as described above, sensing aptamers were eluted and amplified by qPCR. The metric for optimal sensing was  $\Delta C_t$  where  $\Delta C_t = (C_t \text{ value in the absence of protein}) - (C_t \text{ value in the presence of protein})$ . Higher  $\Delta C_t$  values indicate better recovery of sensing aptamers with minimal background.

#### 3.3.3 Aptamer affinity characterization

Affinities of aptamers to the target proteins were characterized with a filter binding assay. Aptamers were 5'-labeled with <sup>32</sup>P-γ-ATP using T4 polynucleotide kinase (Ambion, Austin, TX) followed by purification by Quick Spin Columns (Roche, Indianapolis, IN). Aptamers were added to serial dilutions of target proteins in binding buffer at 1 nM final concentration and incubated at room temperature for 30 min. The solutions were passed through a dot blot apparatus with a nitrocellulose membrane on top of a nylon membrane. The membranes were exposed to phosphor screens overnight, and the amount of radioactivity of each dot was quantified by Storm 860 (Amersham Biosciences/GE Healthcare, Piscataway, NJ). Fractional binding at each protein concentration was calculated as the dot intensity on the nitrocellulose membrane divided by the total dot intensity of the two membranes. The dissociation constant (K<sub>D</sub>) of the aptamer protein interaction was determined by curve fitting using equation (3.1)

$$f = \frac{P_0}{K_D + P_0} \tag{3.1}$$

where f is the fraction bound as calculated from the quantified dot blot image. P<sub>0</sub> is the initial concentration of the protein added to each binding reaction.

# 3.3.4 PCR and qPCR

For electrophoresis readout experiments, eluted sensing aptamers were added with universal primers U5'p and U3'p at 500 nM each and amplified for 20 cycles with iQ Supermix (Bio-Rad, Hercules, CA) in 50 µL reactions. The PCR program was 94°C for

45 s,  $54^{\circ}$ C for 45 s and  $72^{\circ}$ C for 1 min. PCR products were analyzed by electrophoresis (5  $\mu$ L mixed with 2  $\mu$ L of loading buffer and electrophoresed at 100 V for 1 hr in 10 % acrylamide gels). Gels were stained with SYBR Gold nucleic acid gel stain (Invitrogen, Carlsbad, CA) and visualized in a Molecular Imager ChemiDoc XRS System (Bio-Rad, Hercules, CA).

For qPCR readout experiments, primers specific for sensing aptamers (e.g. T5'p and T3'p for MB-T; P5'p and P3'p for MB-P) were added at 500 nM each and amplified for 40 cycles with iQ SYBR Green Supermix (Bio-Rad, Hercules, CA) in 50  $\mu$ L reactions using the same PCR program as above. Threshold cycle numbers (Ct) for deriving sensing aptamer qPCR standard curves were generated from PCRs containing MB-T or MB-P template serially diluted from 3 × 10<sup>8</sup> to 3000 or 300 initial template molecules. In all standard curves and the correlation analysis, error bars represent at least duplicate experiments with each experiment assayed twice by PCR (four total PCRs). Signal-tonoise ratio was calculated as the fold difference in signal obtained from the maximal signal relative to the background. For qPCR data, this is 2 raised to the power (Ct value for background - Ct value for maximal sensitive concentration)

#### 3.3.5 Detection in bovine and human sera

Binding reactions were performed as described above except in undiluted fetal bovine serum (FBS) (GIBCO, Invitrogen, Carlsbad, CA) or human serum (Sigma, St. Louis, MO)

with thrombin and PDGF-BB spiked in. After separation and elution, the recovered aptamers were amplified with sensing aptamer specific primers to derive C<sub>t</sub> values.

#### 3.4 Results and discussion

In developing aptamer-based biosensors, or any affinity-based biosensor, sensing of the analyte depends on the complex formation between the analyte and the detector molecule, in our case an aptamer. Because the formation of the 1-to-1 complex is an equilibrium process, the degree to which complex forms is controlled by the affinity (e.g., the  $K_D$ ) of the interaction and the concentrations of the analyte and aptamer. For significant complex formation to occur, either the analyte or aptamer concentration must be in the range of or above the  $K_D$  of the interaction. Thus, a critical decision must be made regarding the detecting aptamer concentration (Figure 3.1). The formation of the aptamer-analyte complex is an equilibrium reaction (equation (3.2)) with the dissociation constant  $K_D$  (equation (3.3)).

$$Apt + Ana \xrightarrow{K_D} Apt \cdot Ana$$
 (3.2)

$$K_D = \frac{[Apt][Ana]}{[Apt \cdot Ana]} \tag{3.3}$$

The concentration of the bound complex can be calculated by solving the quadratic equation (3.4), by expressing the concentrations of the free aptamer and analyte as their initial concentrations minus the concentration of the bound complex.

$$[Apt \cdot Ana] = \frac{1}{2} \left[ \left( [Apt]_O + [Ana]_O + K_D \right) - \sqrt{\left( [Apt]_O + [Ana]_O + K_D \right)^2 - 4[Apt]_O [Ana]_O} \right]$$
(3.4)

where  $[Apt \cdot Ana]$  is the concentration of the aptamer-analyte bound complexes.  $[Apt]_0$  and  $[Ana]_0$  are the initial concentration of the aptamer and analyte added to each binding reaction.

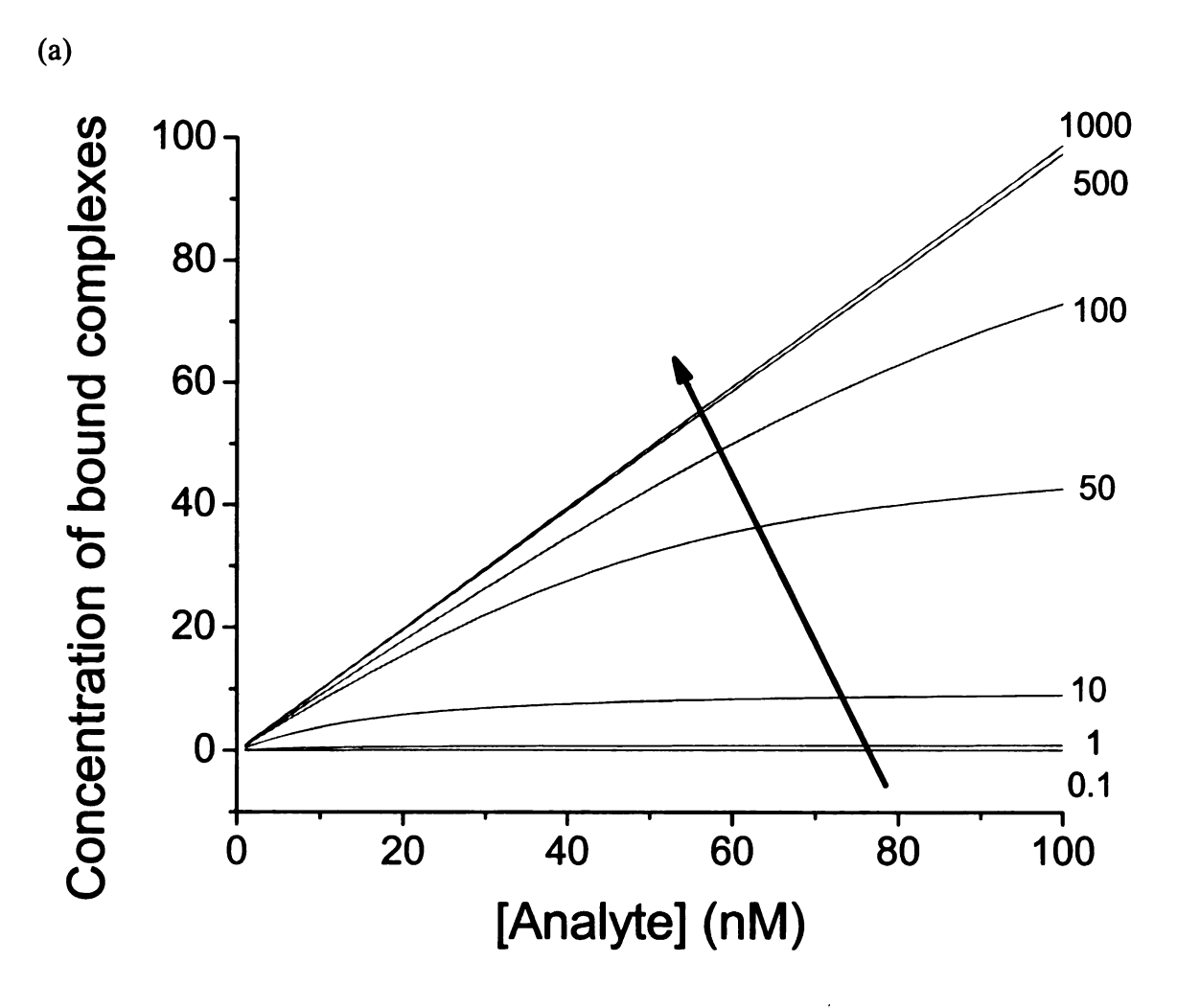
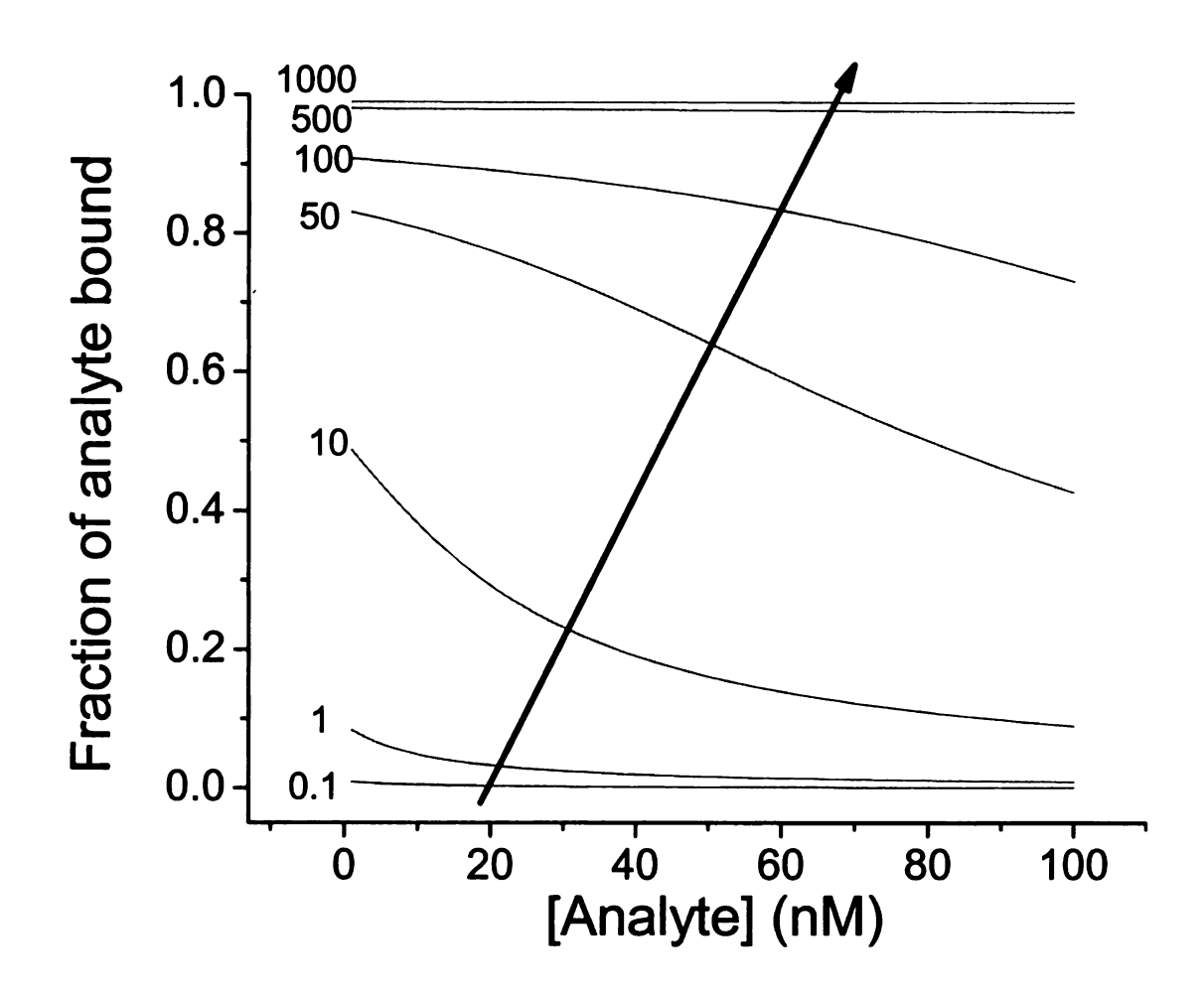


Figure 3.1: Sensing response with respect to detecting aptamer concentration. (a) Shown is the concentration of analyte-aptamer complexes at varying analyte and aptamer concentrations. (b) Shown is the fraction of analyte bound at varying analyte and aptamer concentrations. Simulations were performed using equation (3.4), assuming  $K_D=10 \text{ nM}$  and [Analyte]<sub>0</sub> from 1 to 100 nM. [Aptamer]<sub>0</sub> values used in the simulation are listed next to the corresponding curves. Solid arrows indicate increasing detecting aptamer concentrations.

Figure 3.1 continued.





Using an aptamer concentration below the analyte concentration (limiting aptamer), the concentration of aptamer-analyte complexes cannot exceed the sensing aptamer concentration. The dynamic range of the technique is limited, and the total signal recovered saturates at the limiting aptamer concentration (Figure 3.1 (a)). In contrast, when the sensing aptamer concentration is in excess relative to the analyte concentration. the concentration of analyte-aptamer complexes increases linearly with analyte concentration over the entire range of analyte concentrations. The fraction of the analyte that is bound for the limiting aptamer case decreases as the concentration of analyte increases, while it remains close to 1 when the aptamer is in excess (Figure 3.1(b)). Thus, the relative information content of the excess aptamer approach (fraction of the analyte bound with excess aptamer relative to the fraction bound with limiting aptamer) far exceeds that of the limiting aptamer approach. Therefore, using excess sensing aptamer provides the potential for greater dynamic range (a) and higher sensitivity (b) relative to limiting aptamer approaches. Both the dynamic range and total signal are maximized over the entire analyte concentration range (Figure 3.1).

That said, in techniques where the aptamers are labeled for detection, for instance by fluorescence, the feasibility of using excess aptamer is usually reduced by the presence of a high concentration of unbound aptamer whose signal masks that of the analyte-aptamer complexes. The dynamic range and sensitivity advantages of the excess aptamer design must then be weighed against the need for a stringent separation, wherein the aptameranalyte complexes (the signal) are potentially less than 1% of the total aptamers present (the background) (Figure 3.1). As discussed above, the necessary separation can be

achieved by methods such as microarrays or electrophoresis [36,38]. Here, we describe a method where we have combined aptamer-based separation and aptamer-based detection, using excess aptamers, to design a parallel protein analytical technique (Figure. 3.2) with specificity for the target protein and the potential for excellent sensitivity and broad dynamic range.

In our technique, one aptamer, termed the *capture aptamer*, is biotinylated to immobilize the protein onto streptavidin-coated magnetic beads, while the other aptamer, termed the *sensing aptamer*, is used for quantification of the protein concentration by PCR, microarray, or any other nucleic acid readout. Detection of the sensing aptamer rather than the protein directly leverages the simplicity of multiplex PCR [43,44], through the incorporation of universal primer sequences on all sensing aptamers. The use of PCR also provides straightforward signal amplification, a unique advantage of nucleic acid analytical approaches [4]. In addition, we have incorporated molecular barcodes (MBs) into our sensing aptamers which permits facile parallel detection of the sensing aptamers by sequence alone, as has been shown using oligonucleotide microarrays [45-47]. Readout of the concentration of the MB sequence then serves as an indirect readout of the concentration of the protein target. In this study, we demonstrate proof-of-concept use of our technique for multiplex detection of thrombin and PDGF-BB (Figure 3.2).

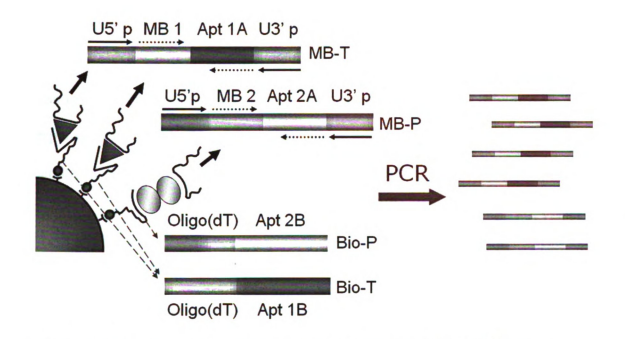


Figure 3.2: Dual-aptamer detection schematic. Thrombin and PDGF-BB are represented by triangles and double-ellipses, respectively. The sensing aptamers (MB-T, MB-P) containing thrombin aptamer (Apt 1A) and PDGF-BB aptamer (Apt 2A) are each labeled with an MB tag (MB1 and MB2) and flanked by a pair of universal primers (5'p and 3'p). Universal primers are labeled as solid arrows and aptamer specific primers are labeled as dashed arrows. Capture aptamers (Bio-T and Bio-P) containing thrombin aptamer (Apt 1B) and PDGF-BB aptamer (Apt 2B) are biotinylated to be attached to streptavidin-coated magnetic beads. Oligo(dT)s are used as the spacer between the aptamer sequences and the beads. After separation, eluted sensing aptamers are amplified by multiplex PCR and quantified.

The fidelity of the sensing aptamers as qPCR templates were first confirmed using serial dilutions of sensing aptamers and template specific primers (similar results were obtained using universal primers) (Figure 3.3). PCR for both templates showed the expected loglinear response over at least a five order-of-magnitude dynamic range (Figure 3.3). Responses plateaued outside of the regions shown on the plot (data not shown). The quantitative response of sensing aptamer concentration relative to protein concentration was then examined. To identify the optimal conditions for protein sensing,  $\Delta C_t$  values (defined as the difference in C<sub>t</sub> value in the presence and absence of 500 nM protein) were measured at various sensing aptamer conditions for both proteins (Figure 3.4). Capture aptamer concentrations were fixed at 500 nM, which should bind 46% of the thrombin and 81% of PDGF-BB based on the measurement of aptamer-protein affinities (Figure 3.5 and Table 3.1). At varying sensing aptamer concentrations, binding reactions were set up, the beads were washed, and the retained sensing aptamers were eluted. Ct values were derived experimentally, and  $\Delta C_t$  values were calculated for each protein. A maximum  $\Delta C_t$  of 16.1 was observed for thrombin at 250 nM sensing aptamer (MB-T) concentration. Similarly, a maximum  $\Delta C_t$  of 7.5 was observed at 50 nM sensing aptamer (MB-P) concentrations for PDGF-BB. In each case, higher concentrations of sensing aptamer resulted in higher non-specific retention of sensing aptamers in the absence of protein (Table 3.2), while lower concentrations had reduced sensitivity in the presence of protein. The larger maximal ΔC<sub>t</sub> observed for thrombin versus PDGF-BB is a result of higher background using the PDGF-BB aptamers (Table 3.2).

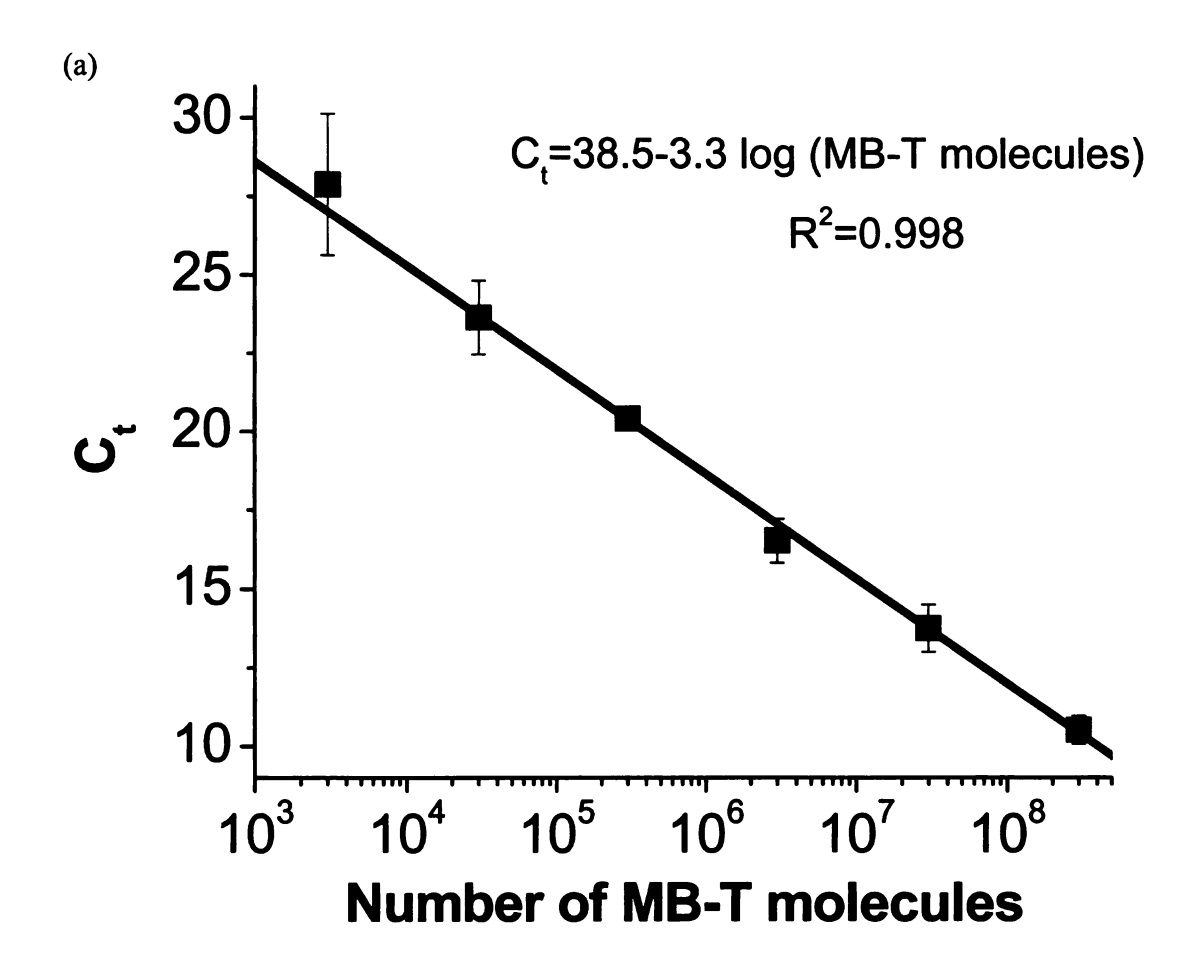
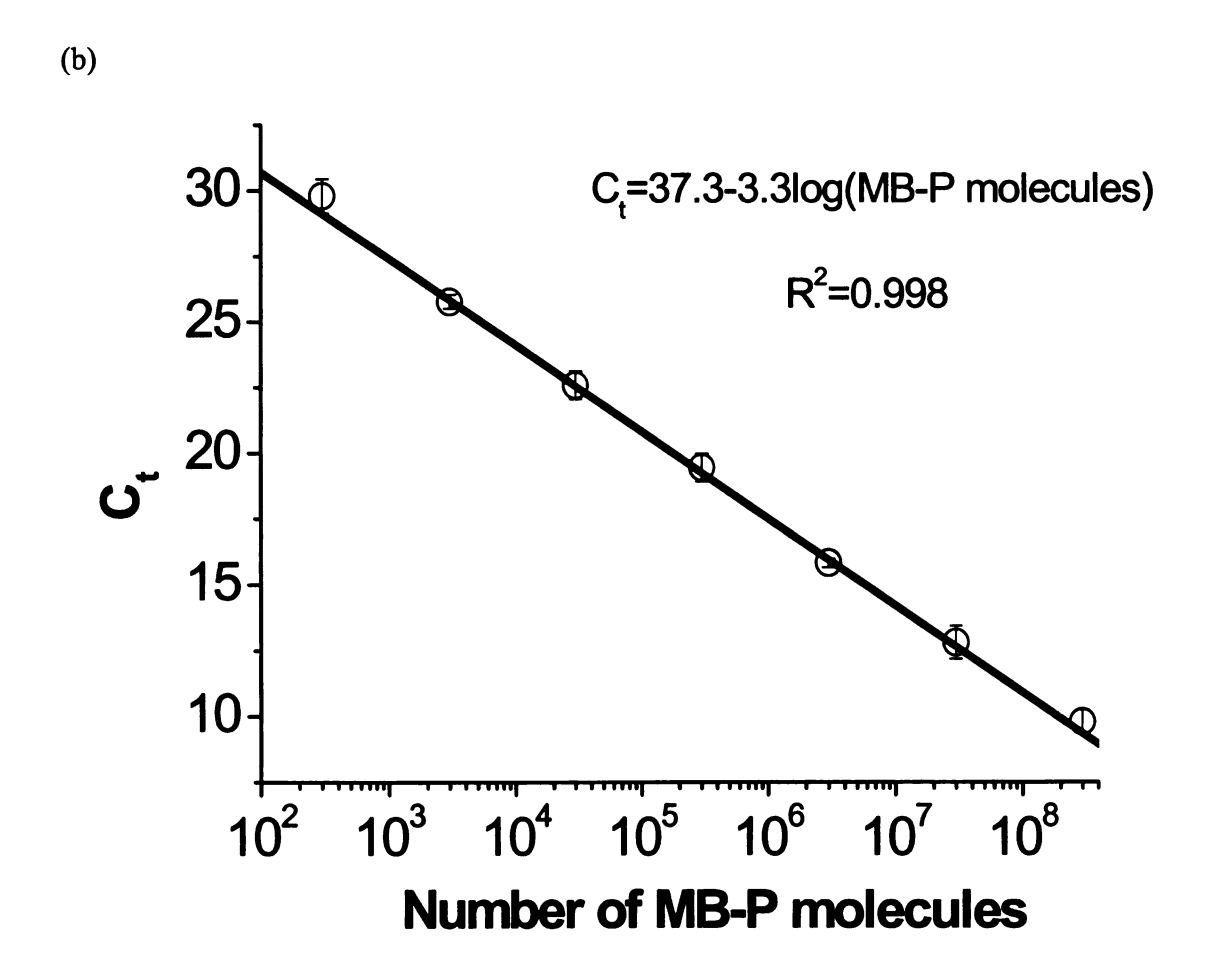


Figure 3.3: Validation of qPCR amplification of sensing aptamers. Serial dilutions of MB-T (a) and MB-P (b) were amplified by qPCR with template-specific primers. The curve fit for both template showed a slope of -3.3 (R<sup>2</sup>=0.998), indicating an amplification efficiency of nearly 100% over the tested dynamic range, covering five orders of magnitude from 5 zmol to 0.5 fmol of MB-T in (a), and six orders of magnitude from 0.5 zmol to 0.5 fmol of MB-P in (b).

Figure 3.3 continued.



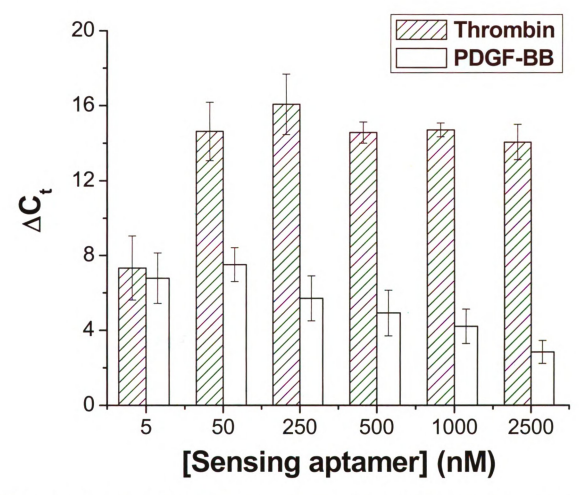


Figure 3.4: Concentrations of sensing aptamers for optimal signal dynamic range.  $\Delta C_t \ values \ were \ derived \ as \ described \ in the experimental section (Chapter 3.3.2) \ for thrombin (hatched columns) \ and PDGF-BB (open columns). Subsequent studies with the technique used concentrations of MB-T and MB-P of 250 nM and 50 nM, respectively, to maximize <math display="inline">\Delta C_t$  and minimize reagent consumption.

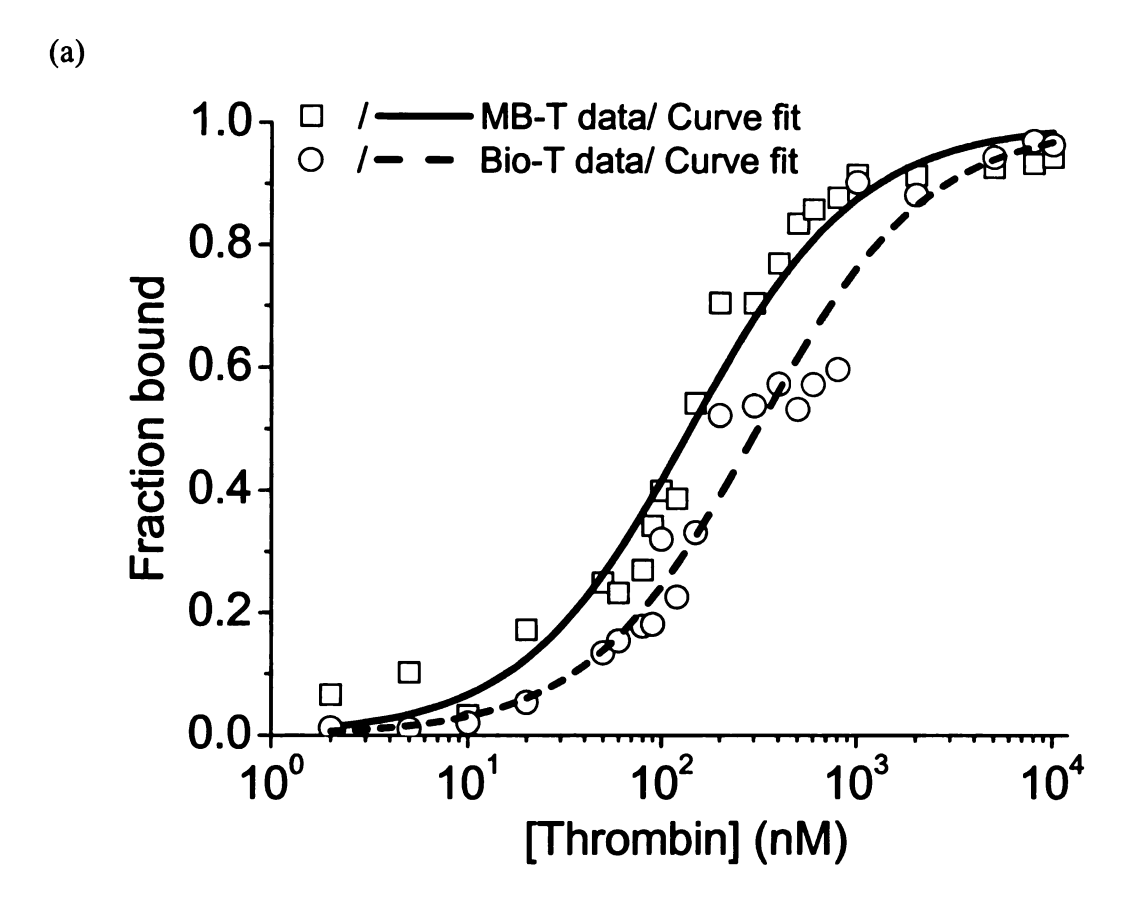


Figure 3.5: Affinity characterization of thrombin and PDGF-BB aptamers.

Radiolabeled aptamers were added to serially diluted thrombin (a) or PDGF-BB (b) and separated with dot blot assays. K<sub>D</sub> values were derived with non-linear least square fitting as described in the experimental section (Chapter 3.3.3).

Figure 3.5 continued.

(b)

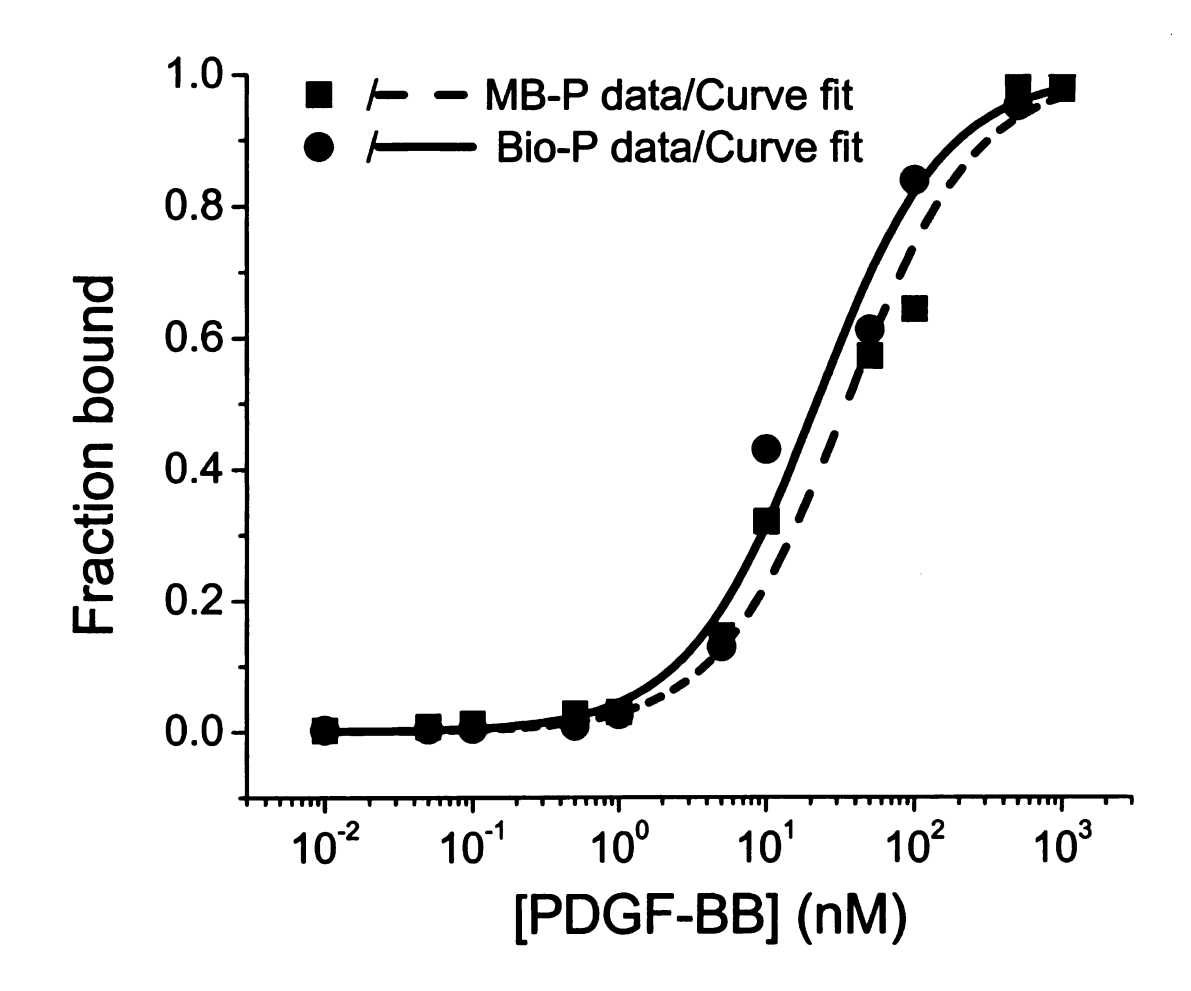


Table 3.1: K<sub>D</sub> measured for each aptamer for its target protein.

Aptamer	MB-T	Bio-T	MB-P	Bio-P
K <sub>D</sub> (nM)	140.1	310.5	34.7	21.6

(The MB-T and Bio-T sequences contain unique aptamer domains while MB-P and Bio-P have the same aptamer domain.)

Table 3.2:  $C_t$  values used to generate Figure 3.4.

мв-т	Background C <sub>t</sub>			C <sub>t</sub> at 500 nM protein				ΔCt				Ave	STDEV	
(nM)	Rl	R2	R3	R4	R1	R2	R3	R4	R1	R2	R3	R4	Ct	$C_{t}$
5	27.7	30.9	30.7	28.5	22.9	22.7	22.1	20.8	4.8	8.2	8.6	7.7	7.3	1.7
50	26.5	29.5	29.1	27.8	13.9	14.8	12.8	12.8	12.5	14.7	16.3	15.0	14.6	1.6
100	23.4	23.9	25.6	26.6	12.4	13.0	11.5	10.9	11.0	10.9	14.1	15.8	12.9	2.4
250	26.1	26.3	27.6	25.6	10.1	12.0	9.4	9.8	16.0	14.3	18.2	15.8	16.1	1.6
500	25.1	25.0	25.6	23.5	11.0	10.5	10.2	9.1	14.1	14.5	15.4	14.4	14.6	0.6
1000	24.9	25.5	23.9	24.0	9.8	11.3	9.1	9.3	15.2	14.3	14.8	14.7	14.7	0.4
2500	23.9	24.9	23.9	24.8	10.7	11.0	10.2	9.4	13.3	13.9	13.7	15.4	14.1	0.9

МВ-Р	l	Backgro	C <sub>t</sub> at 500 nM protein				ΔC <sub>t</sub>				Ave	STDEV		
(nM)	R1	R2	R3	R4	R1	R2	R3	R4	R1	R2	R3	R4	Ct	C <sub>t</sub>
5	24.8	25.6	23.7	24.8	18.8	20.3	16.1	16.6	6.0	5.4	7.6	8.2	6.8	1.4
50	20.1	21.2	19.4	20.6	13.0	14.7	11.6	12.0	7.1	6.5	7.8	8.6	7.5	0.9
100	18.4	19.9	18.3	19.9	13.5	13.9	12.4	11.4	4.9	6.0	5.9	8.5	6.3	1.5
250	16.4	17.9	16.5	17.8	11.6	13.3	9.7	11.1	4.8	4.5	6.8	6.7	5.7	1.2
500	14.9	16.4	14.6	16.2	10.8	12.6	9.4	9.7	4.1	3.8	5.2	6.5	4.9	1.2
1000	14.8	15.8	14.1	15.2	11.0	12.7	9.6	9.9	3.8	3.2	4.6	5.3	4.2	0.9
2500	14.3	14.7	13.6	13.6	11.8	12.3	10.8	9.9	2.5	2.3	2.8	3.7	2.8	0.6

(Concentrations highlighted in bold were determined to be the optimum.)

The optimal concentrations derived above (as selected from the concentrations with the maximum  $\Delta C_t$  value) were then used to generate standard curves for single protein measurements (Figure 3.6). Serial dilutions of thrombin and PDGF-BB were added to binding reactions containing capture and sensing aptamers. After separation, the eluted sensing aptamers were quantified by qPCR. The technique showed sensitivity down to 1 nM protein concentration for thrombin and 10 nM for PDGF-BB. Sensitive detection extended over at least a two order-of-magnitude dynamic range. A linear dose response was observed over the sensing dynamic range, resulting a signal-to-noise ratio of ~ 24000 ( $2^{(25.4-10.9)}$ ) for thrombin, and ~84 ( $2^{(19.3-12.9)}$ ) for PDGF-BB, an improvement over single aptamer approaches [48-51] as well as over a related surface-based aptamer approach [14]. While maximizing dynamic range is valuable for any sensing technique, other factors, such as specificity for the analyte of interest, must be examined in technique development.

We then examined whether the concentration sensitivity would be maintained using the assay in multiplex format (Figure 3.7). After addition of either or both proteins, binding, and washing, sensing aptamers were eluted and amplified by multiplex PCR using the universal primers. PCR products were separated by electrophoresis and visualized. When thrombin was added alone, a band corresponding to the 91 bp MB-T amplification product was observed (Figure 3.7, lane 2). Likewise, when PDGF-BB was added alone, a band representing the 106 bp MB-P was observed (Figure 3.7, lane 3). Upon addition of both proteins, both bands appeared and band intensity increased dose-dependently with increasing protein concentrations (Fig 3.7, lanes 4-6). No signal was returned from either

aptamer pair in the presence of haptoglobin, fibrinogen, C-reactive protein, or lysozyme, further demonstrating good specificity for detection of only the specific protein targets (Figure 3.7, lanes 7-10).

Dose-response curves for multiplex detection of both proteins were derived with serial dilutions of both proteins ranging from 333 pM to 333 nM (Figure 3.8). Eluted sensing aptamers were quantified with qPCR using MB-T or MB-P specific primers. In the multiplex format, the detection limits were 333 pM for thrombin and 3.3 nM for PDGF-BB, respectively, essentially in agreement with the single protein measurements. In both cases, we expect technical improvements in binding, washing, and elution protocols could extend the dynamic range both higher and lower in concentration. That said, the current dynamic range exceeds that of a recently described fluorescence-based method by an order of magnitude [52], while the sensitivity approaches that of a capillary electrophoresis based technique [38].

Given that our initial multiplexing experiments were performed with both proteins at identical concentration in all tests, we examined the concentration sensitivity in the presence of high and low concentrations of the competing proteins (Figure 3.9). Serial dilutions of one protein were measured in multiplex in the presence and absence of 500 nM (Figure 3.9 (a, c)) or 333 nM (Figure 3.9 (b, d)) of the other protein. After separation, eluted aptamers were amplified by PCR and assayed by electrophoresis (Figure 3.9 (a, c)). In all cases and concentrations, the signal returned from each aptamer pair was essentially

identical to that detected in the single-protein case (compare corresponding  $C_t$  values from Figure 3.6 and 3.9 (b, d)).

(a)

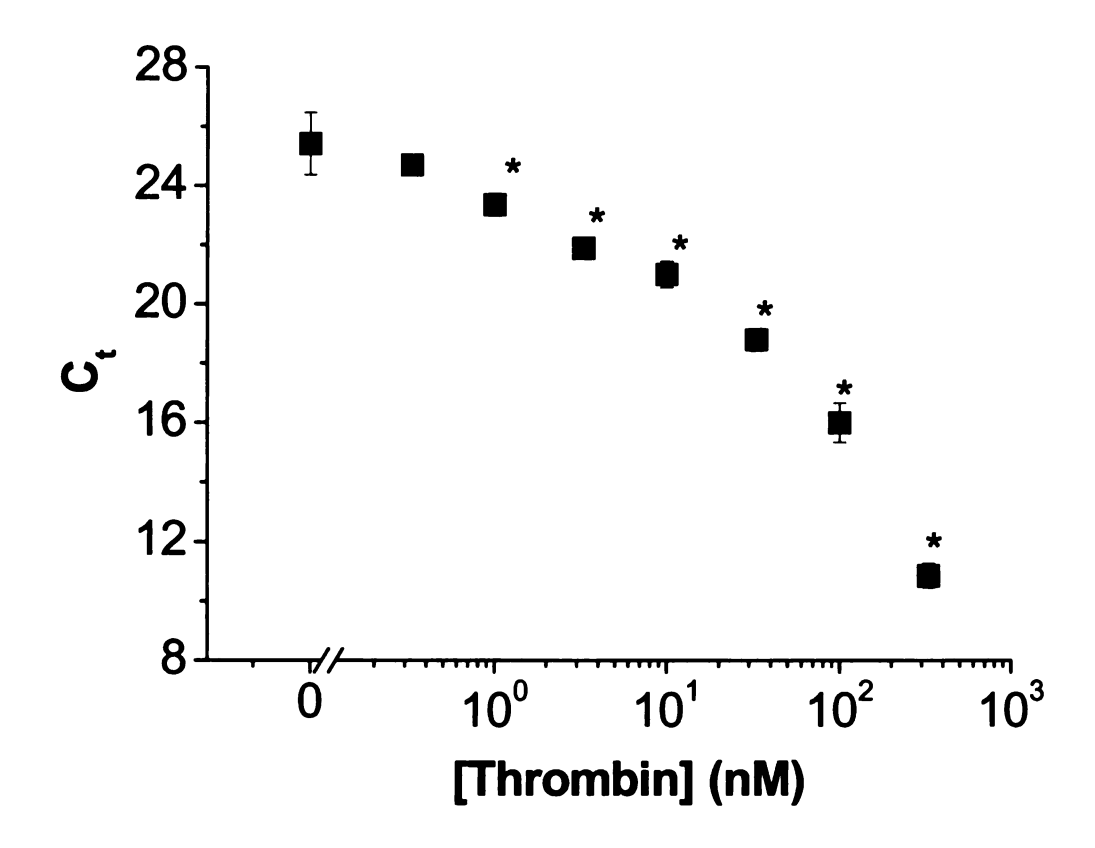
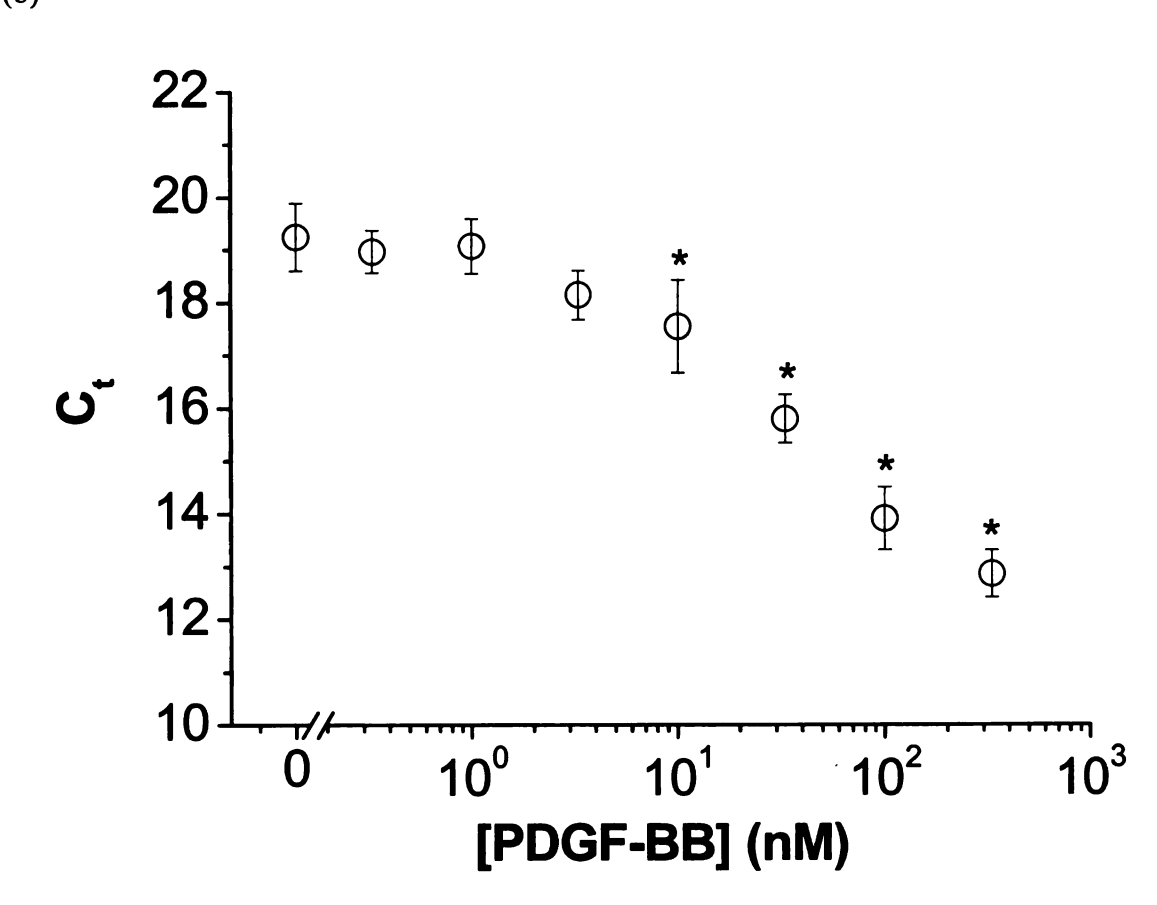
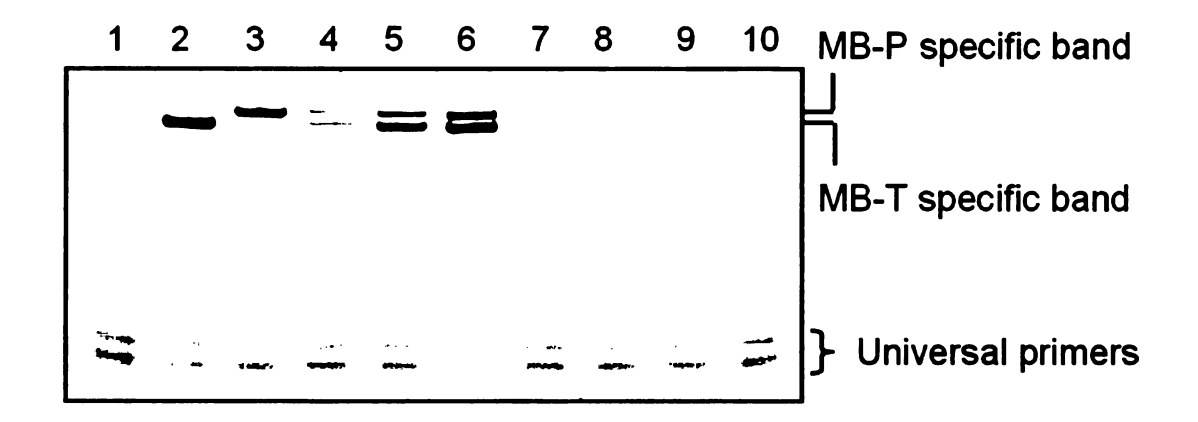


Figure 3.6: Standard curves for singleplex detection of individual proteins using qPCR. (a) The standard curve for thrombin showed a three order-of-magnitude dynamic range. This was generated using 500 nM Bio-T and 250 nM MB-T. (b) The PDGF-BB standard curve showing over a two order-of-magnitude dynamic range was derived using 500 nM Bio-P and 50 nM MB-P. (\* denotes  $C_t$  values significantly lower than background by student's t-test, (p < 0.01)). Lower detection limits were 1 nM and 10 nM for thrombin and PDGF-BB, respectively.

Figure 3.6 continued.







**Figure 3.7: Multiplex detection of proteins using electrophoresis as the readout method.** Control or target protein samples were added to binding buffer containing 250

nM MB-T, 500 nM Bio-T, 50 nM MB-P and 500 nM Bio-P. After binding and separation, eluted sensing aptamers were amplified with universal primers for 20 cycles. PCR products were separated by acrylamide gel and detected by gel staining. Higher bands are the products from amplification of the PDGF-BB and thrombin sensing aptamers.

Remaining primers run to the bottom of the gel. Lane 1: Buffer; Lane 2: 333 nM thrombin; Lane 3: 333 nM PDGF-BB; Lanes 4-6: both thrombin and PDGF-BB at 33, 100 and 333 nM from left to right; Lanes 7-10: haptoglobin, fibrinogen, C-reactive protein and lysozyme each at 333 nM. Image contrast was adjusted to reduce background.

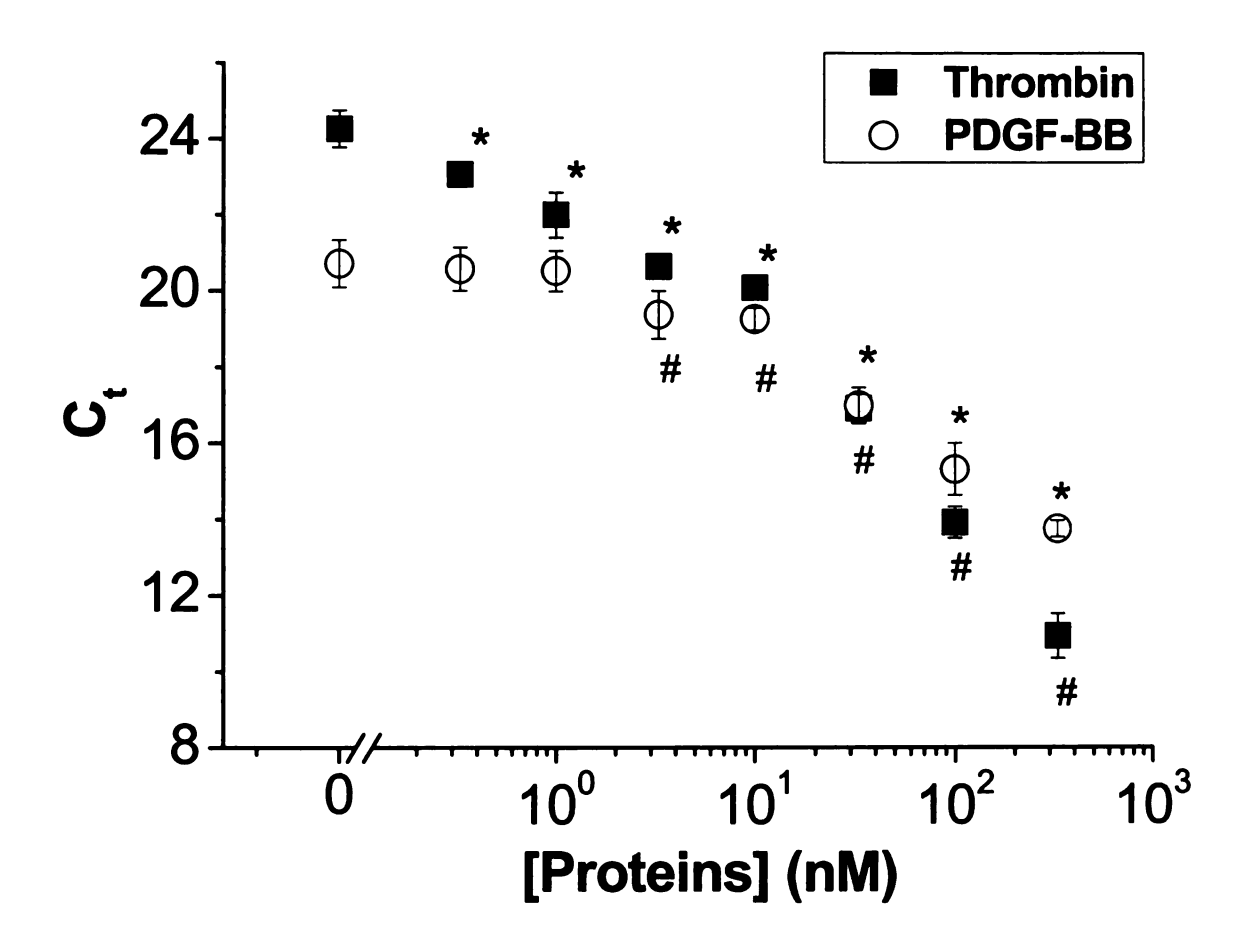


Figure 3.8: Multiplex detection using qPCR as the readout method. Both sets of aptamer pairs were added with serial dilutions of protein mixtures containing both thrombin and PDGF-BB. After binding, separation, and elution, eluted sensing aptamers were amplified with qPCR using template specific primers. (\* and # denote  $C_t$  values significantly lower than background for thrombin and PDGF-BB, respectively (p < 0.01)). Lower detection limits were 330 pM and 3.3 nM for thrombin and PDGF-BB, respectively.

(a)

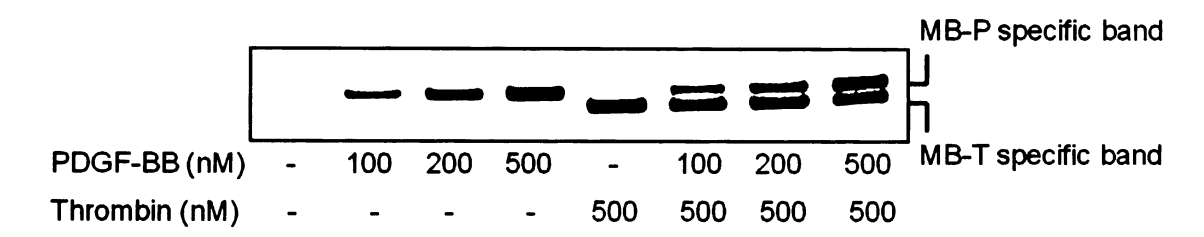


Figure 3.9: Specificity of detection in the presence of competing protein. Both pairs of aptamers were added to serial dilutions of PDGF-BB in the absence or presence of thrombin (a-b) or to serial dilutions of thrombin in the absence or presence of PDGF-BB (c-d). After separation, eluted sensing aptamers were amplified with universal primers (a, c) or sensing aptamer specific primers (b, d) and read out using either electrophoresis (a, c) or qPCR (b, d). For (a) and (c), all four aptamers were used at 500 nM concentration to assess how much cross reactivity occurred at high aptamer concentrations. Little cross-reactivity was seen in either case. For (b) and (d), the optimal sensing aptamer concentrations (from Figure 3.3) were used.

Figure 3.9 continued.

(b)

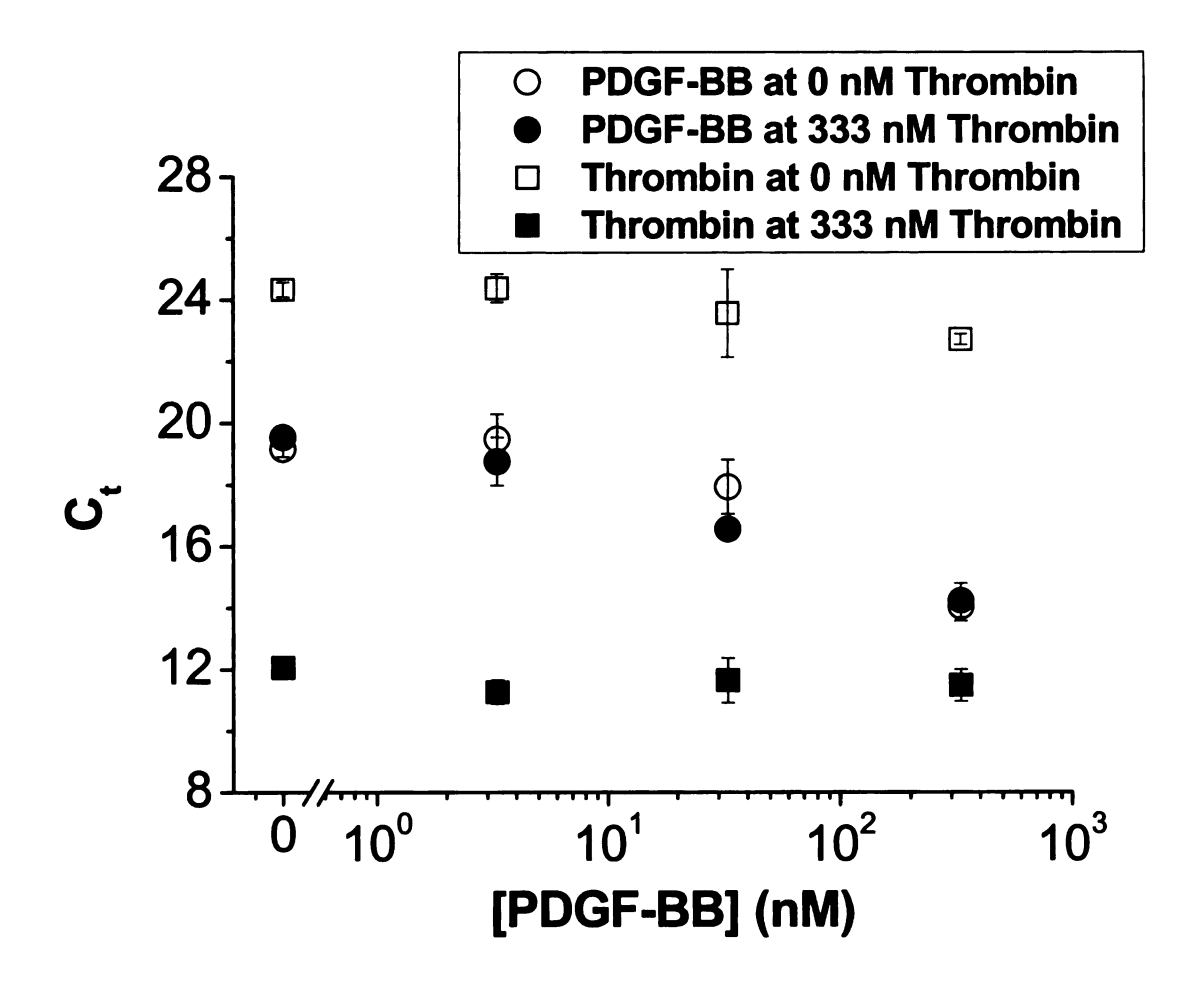
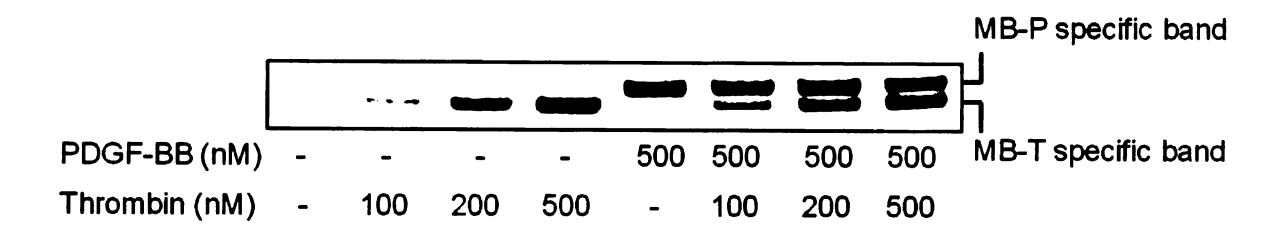
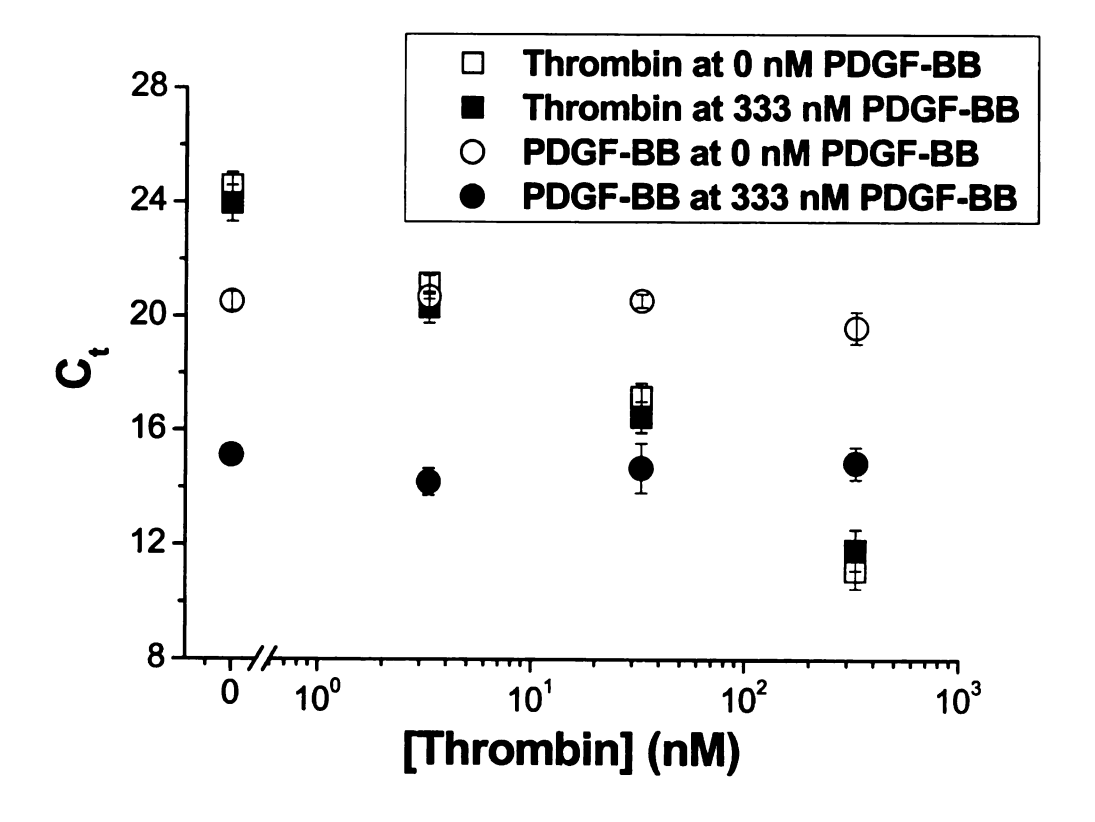


Figure 3.9 continued.

(c)



(d)



Standard curves were also derived in complex biological fluids, fetal bovine serum (FBS) and human serum (Figure 3.10). Results showed that both proteins can still be detected in undiluted serum at low nanomolar concentrations. It was important to confirm that the results in the complex environment agreed with the standard curves derived for the individual proteins in buffered solution (Figure 3.11). For thrombin, the multiplex data derived in buffer, FBS and human serum all agreed well with the singleplex data, showing that competition of the multiplex measurement did not impact the accuracy of our method (Figure 3.11 (a)). For PDGF-BB, the majority of the data derived from multiplex measurements underestimates the PDGF-BB concentration by about two-fold as compared to the singleplex measurement (Figure 3.11 (b)). This implies a greater effect of the binding environment on PDGF-BB detection as compared to thrombin, perhaps due to greater non-specific binding of the sensing aptamer. Nonetheless, the sensitivity and accuracy of concentration detection for the protein are largely maintained.

It could be argued that our method requires more processing as compared to other aptamer-based protein sensing methods [38]. Moreover, detection with our technique does not provide the sensitivity of more traditional methods such as ELISA [53]. However, we feel that our approach has potential utility that makes it worthwhile to continue optimization of the approach. In particular, our method is designed specifically for parallel analyses due to the requirement for multiple specific interactions, the affinity-based separation, and incorporation of the MBs. Thus, our technique avoids any issues that might arise using other analytical approaches, such as the inability to separate proteins of similar size, charge, or hydrophilicity. Currently our sample size (3 µL) is far

lower than that required for most other methods [38,53,54]. Finally, as we continue to lower our background signal through technical improvements, we will also more fully leverage the parallel signal amplification provided by multiplex PCR, giving us the potential for sensitivities far in excess of current methods.

## 3.5 Conclusions

In this study, a novel technique for parallel protein measurement using dual-aptamer recognition was developed. Simultaneous and quantitative detection of thrombin and platelet-derived growth factor (PDGF-BB) was achieved with good specificity and reproducibility in both buffered solutions and a serum background. We have demonstrated that the technique is flexible and has the potential for straightforward customization to sets of proteins, depending on the availability of aptamer pairs for each protein and their specificity and compatibility. The sensitivity and dynamic response of the approach warrants further selection and characterization of aptamer pairs and their use in the described approach.

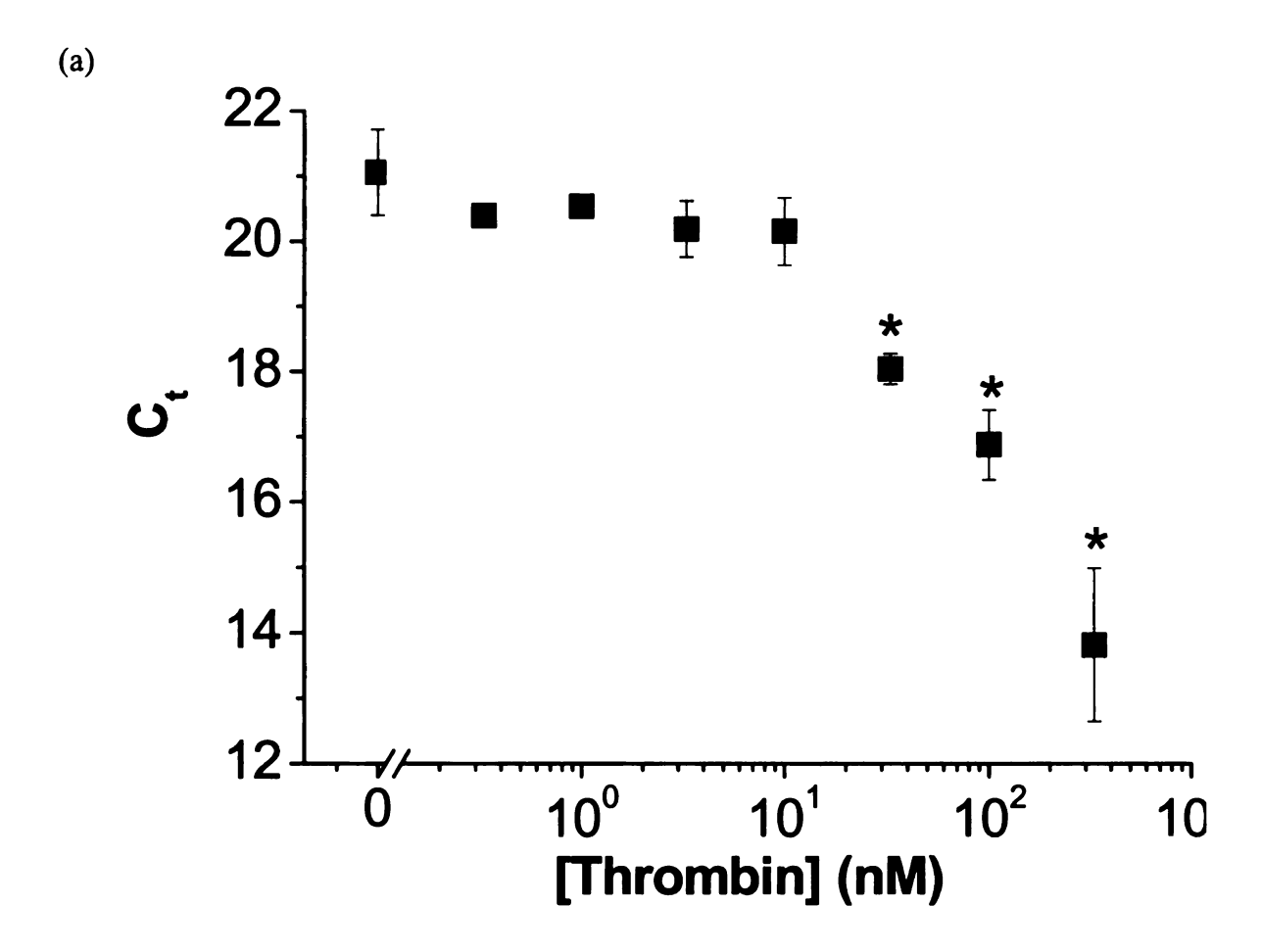


Figure 3.10: Multiplex detection of proteins in fetal bovine serum and human serum. Both pairs of aptamers were added at the optimal concentrations to fetal bovine serum (a-b) and human serum (c-d) spiked with varying concentrations of both thrombin and PDGF-BB. After separation and elution, the eluted sensing aptamers were amplified with qPCR using template-specific primers. (\* denotes  $C_t$  values significantly lower than background, (p < 0.01))

Figure 3.10 continued.

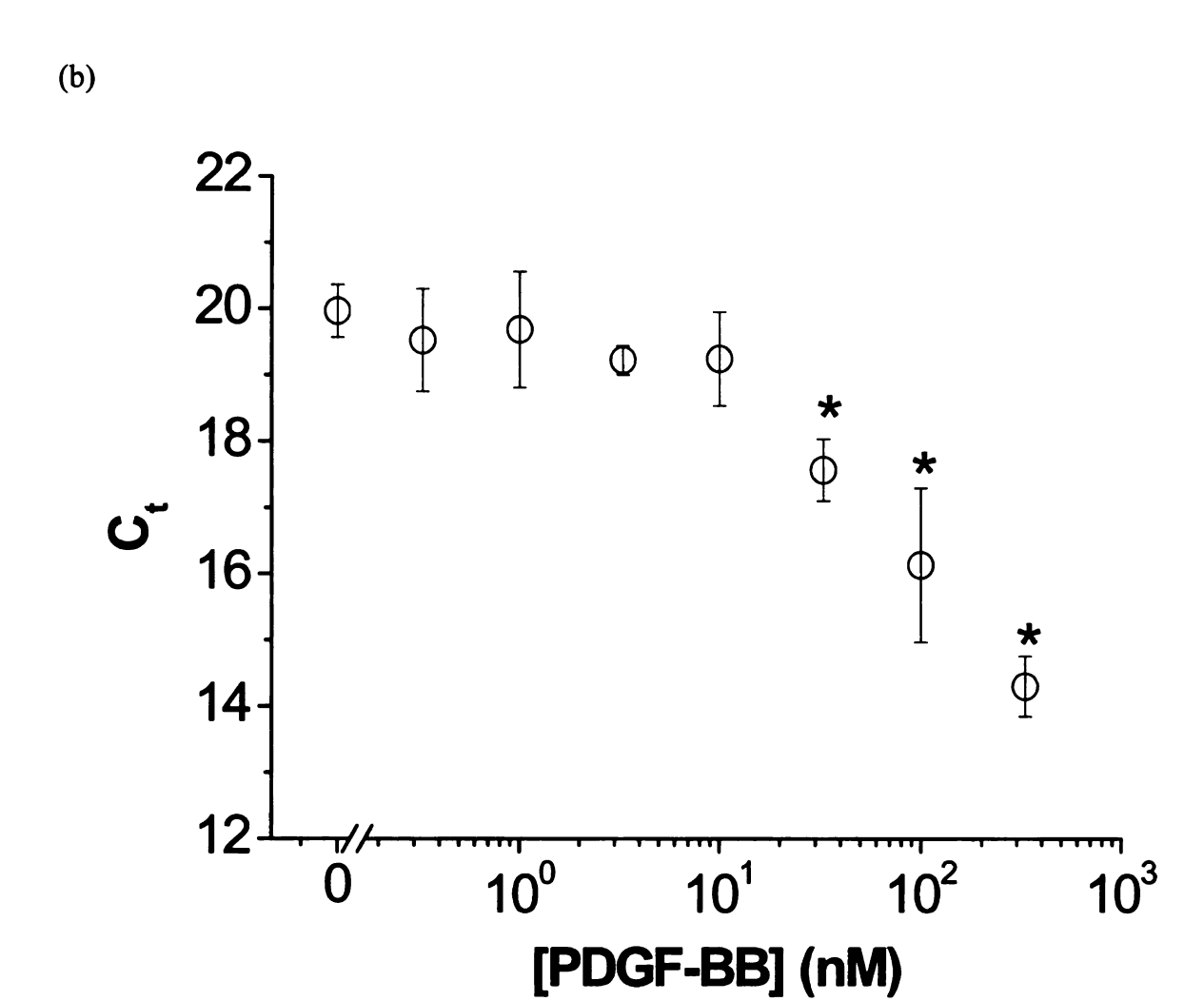


Figure 3.10 continued.

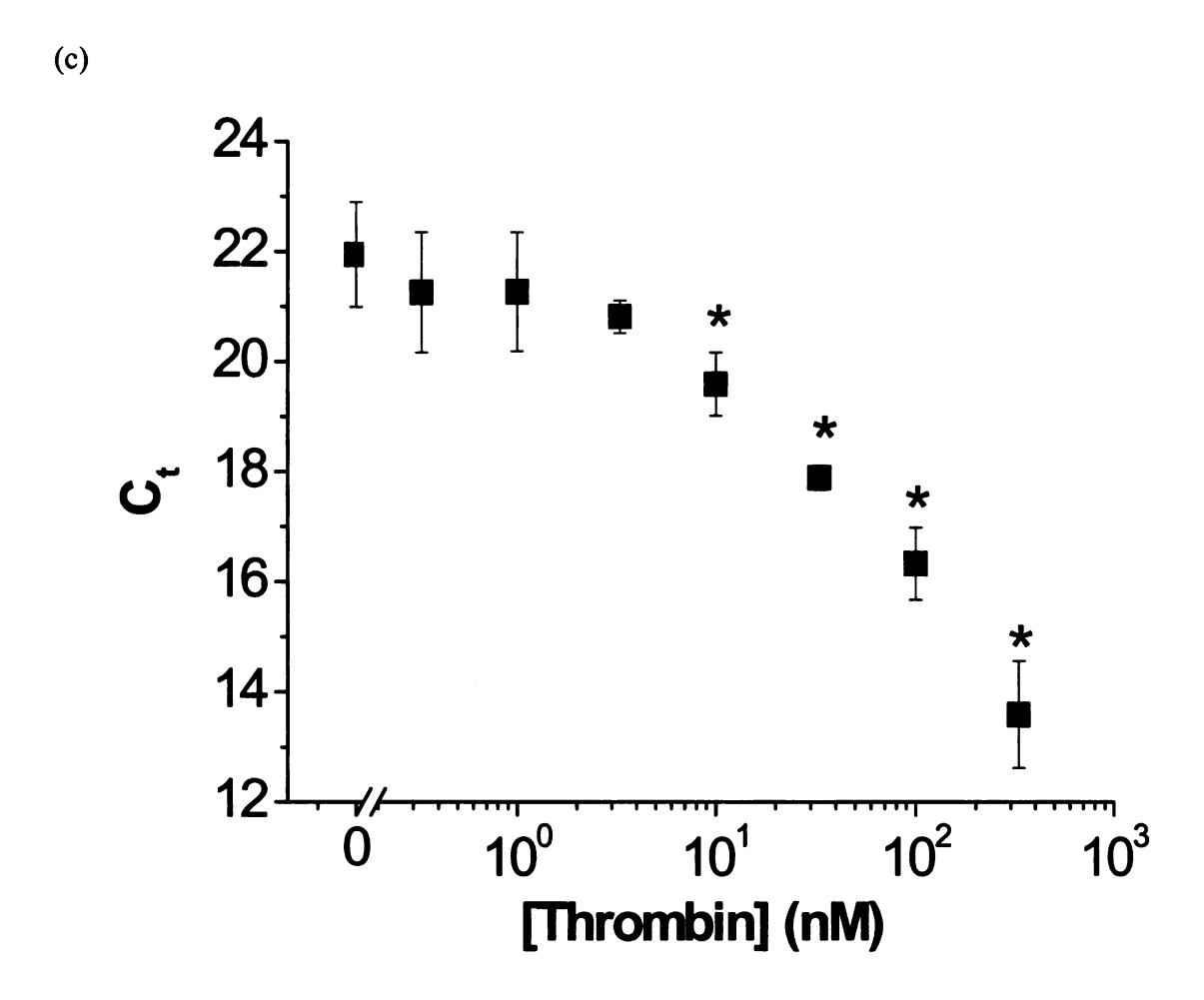
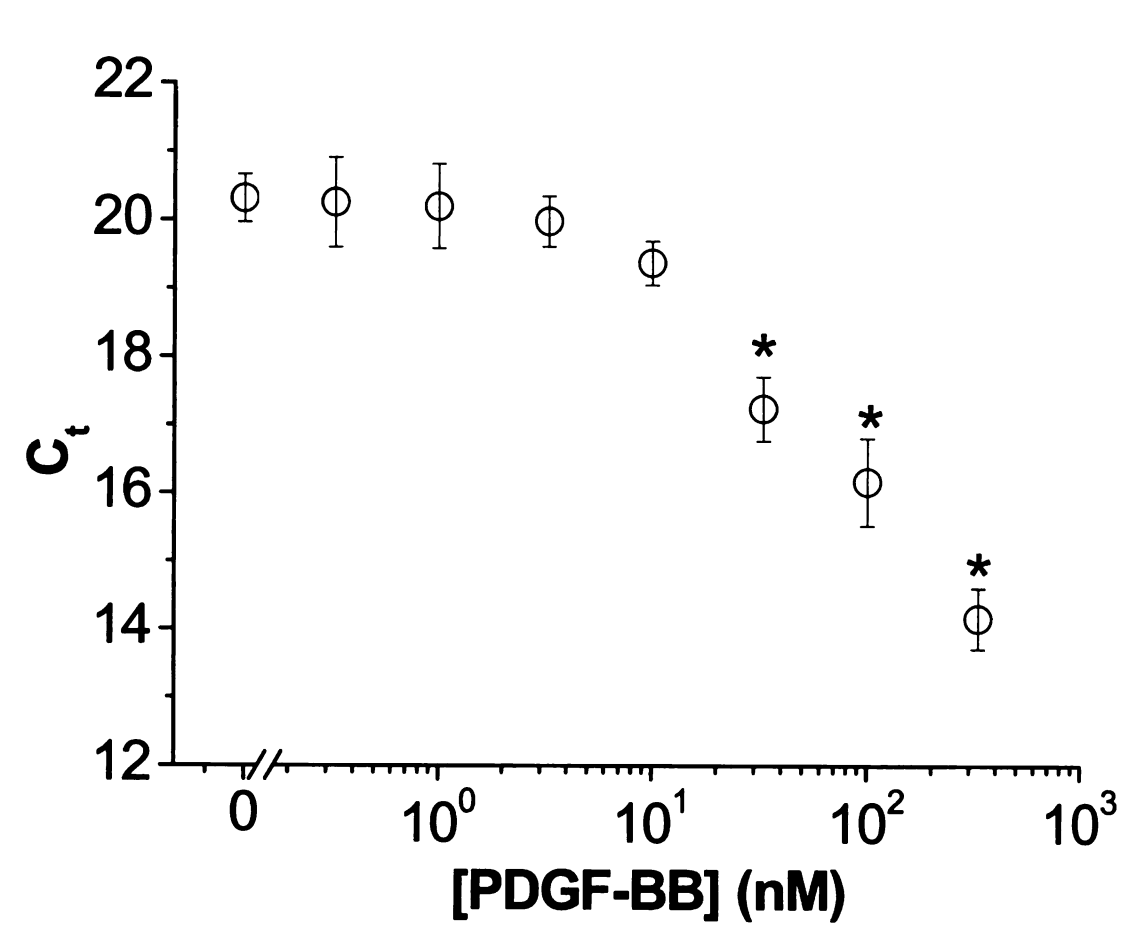


Figure 3.10 continued.







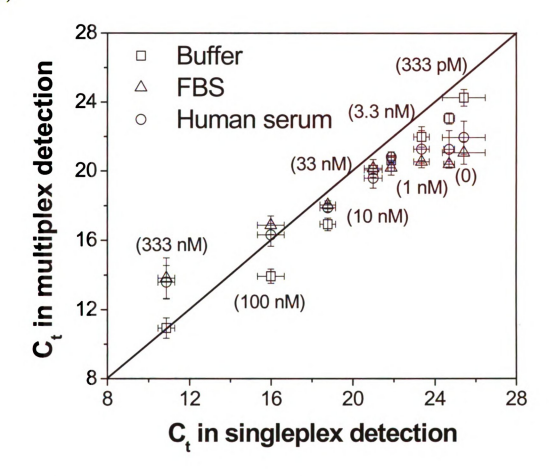
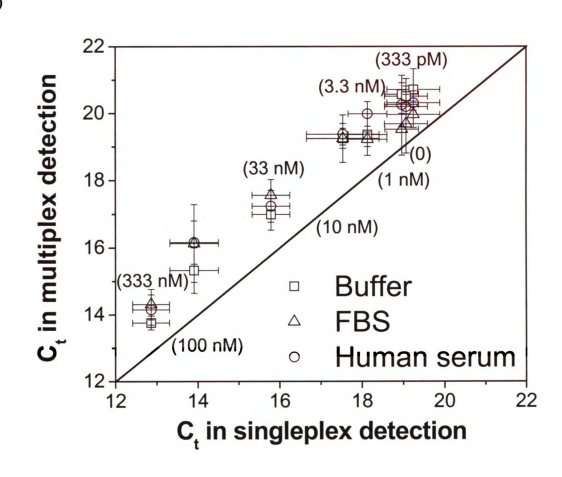


Figure 3.11: Correlation of various analyses. Multiplex  $C_t$  values derived in buffer or serum samples were plotted against the  $C_t$  value derived from singleplex experiments in buffer for thrombin (a) and PDGF-BB (b).

Figure 3.11 continued.





## References

- 1. O'Farrell PH. High resolution two-dimensional electrophoresis of proteins. Journal of Biological Chemistry, 250, 4007-4021 (1975).
- 2. MacBeath G. Protein microarrays and proteomics. *Nature Genetics*, 32, 526-532 (2002).
- 3. MacBeath G, Schreiber SL. Printing proteins as microarrays for high-throughput function determination. *Science*, 289(5485), 1760-1763 (2000).
- 4. Schweitzer B, Roberts S, Grimwade B *et al.* Multiplexed protein profiling on microarrays by rolling-circle amplification. *Nature biotechnology*, 20(4), 359-365 (2002).
- 5. Xie S, Moya C, Bilgin B, Jayaraman A, Walton SP. Emerging affinity-based techniques in proteomics. *Expert Rev Proteomics*, 6(5), 573-583 (2009).
- 6. Zichi D, Eaton B, Singer B, Gold L. Proteomics and diagnostics: Let's get specific, again. Current opinion in chemical biology, 12(1), 78-85 (2008).
- 7. Gloriam DE, Orchard S, Bertinetti D et al. Report: A community standard format for the representation of protein affinity reagents. Mol Cell Proteomics, (2009).
- 8. Breaker RR. Engineered allosteric ribozymes as biosensor components. *Curr Opin Biotechnol*, 13(1), 31-39 (2002).
- 9. Navani NK, Li Y. Nucleic acid aptamers and enzymes as sensors. Current opinion in chemical biology, 10(3), 272-281 (2006).
- 10. Lai RY, Plaxco KW, Heeger AJ. Aptamer-based electrochemical detection of picomolar platelet-derived growth factor directly in blood serum. *Analytical Chemistry*, 79(1), 229-233 (2007).
- 11. Lee JO, So HM, Jeon EK et al. Aptamers as molecular recognition elements for electrical nanobiosensors. Analytical and Bioanalytical Chemistry, 390(4), 1023-1032 (2008).

- 12. Swensen JS, Xiao Y, Ferguson BS et al. Continuous, Real-Time Monitoring of Cocaine in Undiluted Blood Serum via a Microfluidic, Electrochemical Aptamer-Based Sensor. Journal of the American Chemical Society, 131(12), 4262-4266 (2009).
- 13. Zuo XL, Xiao Y, Plaxco KW. High Specificity, Electrochemical Sandwich Assays Based on Single Aptamer Sequences and Suitable for the Direct Detection of Small-Molecule Targets in Blood and Other Complex Matrices. *Journal of the American Chemical Society*, 131(20), 6944-6945 (2009).
- 14. Lee J, Icoz K, Roberts A, Ellington AD, Savran CA. Diffractometric Detection of Proteins Using Microbead-Based Rolling Circle Amplification. *Anal Chem*, (2009).
- 15. Hianik T, Wang J. Electrochemical Aptasensors Recent Achievements and Perspectives. *Electroanalysis*, 21(11), 1223-1235 (2009).
- 16. Xie S, Walton SP. Application and analysis of structure-switching aptamers for small molecule quantification. *Anal Chim Acta*, 638(2), 213-219 (2009).
- 17. Ellington AD, Szostak JW. *In vitro* selection of RNA molecules that bind specific ligands. *Nature*, 346(6287), 818-822 (1990).
- 18. Tuerk C, Gold L. Systematic evolution of ligands by exponential enrichment: RNA ligands to bacteriophage T4 DNA polymerase. *Science*, 249(4968), 505-510 (1990).
- 19. Bock C, Coleman M, Collins B et al. Photoaptamer arrays applied to multiplexed proteomic analysis. *Proteomics*, 4(3), 609-618 (2004).
- 20. Collett JR, Cho EJ, Ellington AD. Production and processing of aptamer microarrays. *Methods*, 37(1), 4-15 (2005).
- 21. Cox JC, Hayhurst A, Hesselberth J et al. Automated selection of aptamers against protein targets translated in vitro: from gene to aptamer. Nucleic Acids Research, 30(20) (2002).

- 22. Taussig MJ, Stoevesandt O, Borrebaeck CAK *et al.* ProteomeBinders: planning a European resource of affinity reagents for analysis of the human proteome. *Nature Methods*, 4(1), 13-17 (2007).
- 23. Nimjee SM, Rusconi CP, Sullenger BA. Aptamers: An emerging class of therapeutics. *Annual Review of Medicine*, 56, 555-583 (2005).
- 24. Bang GS, Cho S, Kim BG. A novel electrochemical detection method for aptamer biosensors. *Biosensors & bioelectronics*, 21(6), 863-870 (2005).
- 25. Fischer NO, Tarasow TM, Tok JBH. Protein detection via direct enzymatic amplification of short DNA aptamers. *Anal. Biochem.*, 373(1), 121-128 (2008).
- 26. He J-L, Wu Z-S, Zhang S-B, Shen G-L, Yu R-Q. Fluorescence aptasensor based on competitive-binding for human neutrophil elastase detection. *Talanta*, 80(3), 1264-1268 (2009).
- 27. Lee J, Icoz K, Roberts A, Ellington AD, Savran CA. Diffractometric Detection of Proteins Using Microbead-Based Rolling Circle Amplification. *Analytical Chemistry*, 82(1), 197-202).
- 28. Peng YG, Zhang DD, Li Y et al. Label-free and sensitive faradic impedance aptasensor for the determination of lysozyme based on target-induced aptamer displacement. Biosensors & bioelectronics, 25(1), 94-99 (2009).
- 29. Gronewold TMA, Baumgartner A, Hierer J et al. Kinetic Binding Analysis of Aptamers Targeting HIV-1 Proteins by a Combination of a Microbalance Array and Mass Spectrometry (MAMS). J. Proteome Res., 8(7), 3568-3577 (2009).
- 30. Kim KS, Lee HS, Yang JA, Jo MH, Hahn SK. The fabrication, characterization and application of aptamer-functionalized Si-nanowire FET biosensors. *Nanotechnology*, 20(23), 6 (2009).
- 31. Yao CY, Qi YZ, Zhao YH et al. Aptamer-based piezoelectric quartz crystal microbalance biosensor array for the quantification of IgE. Biosensors & bioelectronics, 24(8), 2499-2503 (2009).
- 32. Fredriksson S, Gullberg M, Jarvius J et al. Protein detection using proximity-dependent DNA ligation assays. *Nature biotechnology*, 20(5), 473-477 (2002).

- 33. Seetharaman S, Zivarts M, Sudarsan N, Breaker RR. Immobilized RNA switches for the analysis of complex chemical and biological mixtures. *Nature biotechnology*, 19(4), 336-341 (2001).
- 34. Cho EJ, Collett JR, Szafranska AE, Ellington AD. Optimization of aptamer microarray technology for multiple protein targets. *Anal Chim Acta*, 564(1), 82-90 (2006).
- 35. Hesselberth JR, Robertson MP, Knudsen SM, Ellington AD. Simultaneous detection of diverse analytes with an aptazyme ligase array. *Anal. Biochem.*, 312(2), 106-112 (2003).
- 36. Stadtherr K, Wolf H, Lindner P. An aptamer-based protein biochip. *Anal Chem*, 77(11), 3437-3443 (2005).
- 37. Kirby R, Cho EJ, Gehrke B *et al.* Aptamer-based sensor arrays for the detection and quantitation of proteins. *Analytical Chemistry*, 76(14), 4066-4075 (2004).
- 38. Zhang HQ, Li XF, Le XC. Tunable aptamer capillary electrophoresis and its application to protein analysis. *Journal of the American Chemical Society*, 130(1), 34-35 (2008).
- 39. Macaya RF, Waldron JA, Beutel BA et al. Structural and Functional-Characterization of Potent Antithrombotic Oligonucleotides Possessing Both Quadruplex and Duplex Motifs. Biochemistry, 34(13), 4478-4492 (1995).
- 40. Tasset DM, Kubik MF, Steiner W. Oligonucleotide inhibitors of human thrombin that bind distinct epitopes. *Journal of Molecular Biology*, 272(5), 688-698 (1997).
- 41. Green LS, Jellinek D, Jenison R et al. Inhibitory DNA ligands to platelet-derived growth factor B-chain. *Biochemistry*, 35(45), 14413-14424 (1996).
- 42. Zuker M. Mfold web server for nucleic acid folding and hybridization prediction. *Nucleic Acids Res*, 31(13), 3406-3415 (2003).
- 43. Chamberlain JS, Gibbs RA, Ranier JE, Nguyen PN, Caskey CT. Deletion screening of the Duchenne muscular dystrophy locus via multiplex DNA amplification. *Nucleic Acids Res*, 16(23), 11141-11156 (1988).

- 44. Zangenberg G SR, Reynolds R. Multiplexed PCR: Optimization Guidelines. In: *PCR Applications: Protocols for functional Genomics*. (Academic Press, 1999) 73-94.
- 45. Shoemaker DD, Lashkari DA, Morris D, Mittmann M, Davis RW. Quantitative phenotypic analysis of yeast deletion mutants using a highly parallel molecular bar-coding strategy. *Nat Genet*, 14(4), 450-456 (1996).
- 46. Giaever G, Chu AM, Ni L *et al.* Functional profiling of the Saccharomyces cerevisiae genome. *Nature*, 418(6896), 387-391 (2002).
- 47. Walton SP, Mindrinos MN, Davis RW. Analysis of hybridization on the molecular barcode GeneChip microarray. *Biochem Biophys Res Commun*, 348(2), 689-696 (2006).
- 48. Shlyahovsky B, Li D, Katz E, Willner I. Proteins modified with DNAzymes or aptamers act as biosensors or biosensor labels. *Biosensors & bioelectronics*, 22(11), 2570-2576 (2007).
- 49. Hu J, Zheng PC, Jiang JH *et al.* Electrostatic interaction based approach to thrombin detection by surface-enhanced Raman spectroscopy. *Anal Chem*, 81(1), 87-93 (2009).
- 50. Zhang Z, Yang W, Wang J et al. A sensitive impedimetric thrombin aptasensor based on polyamidoamine dendrimer. *Talanta*, 78(4-5), 1240-1245 (2009).
- 51. Wang J, Meng W, Zheng X, Liu S, Li G. Combination of aptamer with gold nanoparticles for electrochemical signal amplification: application to sensitive detection of platelet-derived growth factor. *Biosensors & bioelectronics*, 24(6), 1598-1602 (2009).
- 52. Wang LQ, Li LY, Xu Y et al. Simultaneously fluorescence detecting thrombin and lysozyme based on magnetic nanoparticle condensation. *Talanta*, 79(3), 557-561 (2009).
- 53. Kajizuka M, Miyachi T, Matsuzaki H et al. Serum levels of platelet-derived growth factor BB homodimers are increased in male children with autism. Prog. Neuro-Psychopharmacol. Biol. Psychiatry, 34(1), 154-158 (2010).

54. Zhang YL, Huang Y, Jiang JH, Shen GL, Yu RQ. Electrochemical aptasensor based on proximity-dependent surface hybridization assay for single-step, reusable, sensitive protein detection. *Journal of the American Chemical Society*, 129(50), 15448-15449 (2007).

# CHAPTER 4 IN VITRO SELECTION OF APTAMERS TO ACUTE PHASE PROTEINS

#### 4.1 Abstract

Acute phase proteins (APPs) are secreted as part of the body's response to inflammation, and their concentrations can be greatly altered in response to a variety of abnormities. C-reactive protein (CRP) and fibrinogen are two widely studied APPs whose elevated concentrations are associated with an array of diseases. Thus, analytical techniques for quantifying these proteins are important for clinical diagnostics. In this study, RNA aptamers specific for CRP and fibrinogen were generated by *in vitro* selection. Two random RNA pools, R50 and R70, containing 50 and 70-nt random sequences respectively were used for fibrinogen aptamer selection, and a R60 pool containing a 60-nt random region was used for in the CRP aptamer selection. The selected aptamers were characterized by sequencing. Results showed one aptamer from each pool was selected to have nanomolar affinity for its target protein. In addition, two fibrinogen aptamers selected from two different random pools bind on the protein in non-competitive fashion. These aptamers will serve as affinity reagents for use in the multiplex protein analytical technique we have developed.

## 4.2 Introduction

Acute phase proteins (APP) are part of bodies' response to inflammatory signals and their circulating levels can be greatly altered in response to inflammation. As growing evidence has suggested that inflammation plays a strong role in the development of vascular diseases and cancers, APPs have began to be studied for their predictive roles in such disorders [1,2]. Among these important APPs are C-reactive protein (CRP) and fibrinogen.

CRP is elevated during the body's non-specific response to inflammation [3]. Recent research has shown that elevated CRP concentrations are also associated with increased risk of cardiovascular disease and reduced survival in metastatic cancer [1,4]; therefore, CRP was identified as a useful biological marker that can be used to guide treatment decisions [5,6]. Fibrinogen plays a key role in the coagulation cascade [7]. During the cascade, fibrinogen is converted to fibrin and insoluble fibrin aggregates to block the damaged blood vessel and prevent further bleeding [7]. Elevated fibrinogen levels have also been associated with a number of diseases including stroke, cancer, and diabetes [8-10]. Therefore, quantitative techniques for measuring these proteins are proving useful in the diagnosis of a variety of diseases.

As aptamers do not exist for these proteins, we sought to select high-affinity aptamers for CRP and fibrinogen. Aptamer sequences with nanomolar affinities were selected from three pools with different lengths of random sequence. The selected aptamers will be useful in designing analytical assays for these proteins. Moreover, competition

experiments showed that the selected fibrinogen aptamers bind the protein in a non-competitive fashion, making them well suited for use in the dual-aptamer analytical approach we developed (Chapter 3).

# 4.3 Experimental section

# 4.3.1 Synthesis of randomized RNA pool

The template used for preparing the single stranded RNA pool was 5' - TAA TAC GAC TCA CTA TAG GGG ATG TCC ACG AGG TCT CTGA TGC GGC ACT ATC GCT CAT<N50>C GTA CGC TGC AGG TCG AC - 3' for R50, and 5' - TAA TAC GAC TCA CTA TAG GGG ATG TCC ACG AGG TCT CTCCT GCG TGCAAA TCT AAC AA<N60>C GTA CGC TGC AGG TCG AC - 3' for R60 (Underlined: T7 promoter, italicized: MB sequence). The primers for PCR amplifications were 5'-TAATACGACTCACTATAGGGGATGTCCACGAGGTCTCT-3' (p46) and 5'-GTCGACCTGCAGCGTACG-3' (p47). p47 was also used for Klenow fill-in reaction and reverse transcription. The template for preparing R70 RNA pool was 5'-TTCTAATACG ACTCACTATA GGATGCGTAG GCGTGTAACT TG<N70>CACATTACAA GCTCGCCAGT-3' (Underlined: T7 promoter). The primers for PCR amplification of R70 pool were 5'-

TTCTAATACGACTCACTATAGGATGCGTAGGCGTGTAACTTG-3' (R70-5'p) and 5'-ACTGGCGAGCTTGTAATGTG-3' (R70-3'p).

Double stranded DNAs were prepared by annealing single stranded oligo templates and 3' primers at 95°C for 5 min in Klenow annealing buffer (100 mM Tris-HCl, pH 8.0 and 100 mM MgCl<sub>2</sub>) followed by cooling on ice for 5 min. Klenow fill-in reactions were performed by adding dNTP (0.8 mM each) and Exo- Klenow fragment (NEB, Ipswich, MA) to the annealed reactions and incubating at 37 °C for 1 hr.

Phenol/Chloroform extraction was performed to purify the enzymatic reactions. The reactions were added with 1/10 volume of 3M sodium acetate and extracted with equal volume of phenol/chloroform followed with an equal volume of chloroform. The aqueous phase was recovered and added with 2.5 volumes of 100% ethanol to precipitate the DNA. The reactions were frozen at -80 °C for 15 min and centrifuged at 4 °C for 15 min. The pellets were dried and resuspended in TE 8.0.

Double stranded DNAs were *in vitro* transcribed using Ampliscribe T7 *in vitro* transcription kits (Epicentre, Madison, Wisconsin) at 42 °C for 2 hrs. After incubation, DNase was added to remove the DNA templates at 37 °C for 30 min. Transcribed RNAs were loaded onto 10% polyacrylamide urea gels and electrophoresed at 100 V for 1 hr.

The RNAs were purified by UV shadowing, and gel fragments were soaked in TE buffer (pH 7.0) overnight at room temperature and ethanol precipitated.

#### 4.3.2 In vitro selection

A negative selection in the absence of protein was performed in each round before a positive selection. Purified RNA pools in 1x binding buffer (20 mM HEPES, pH 7.5, 150 mM NaCl, 5 mM MgCl<sub>2</sub>) were heated to 65  $^{\circ}$ C for 5 min and cool to room temperature over a 30-min period. The 0.45 mm HAWP filters (Millipore, Bedford, MA) were assembled into the filter holder and pre-wetted with 100- $\mu$ L of 1x binding buffer. Binding reactions were then loaded onto the filters to exclude filter binding species. Liquid flow-through was collected and added with target proteins for the positive selection. The reactions were incubated at room temperature for 30 min and subjected to filter separation. The filters were washed 3 times with 100  $\mu$ L 1x binding buffer and eluted twice each with 200  $\mu$ L elution buffer (25 mM EDTA and 5 M Urea) at 95  $^{\circ}$ C for 5 min.

Eluted RNAs were ethanol precipitated by adding 1/10 volume of 3 M NaOAc, 3  $\mu$ L glycogen and 2.5 volumes of 100% ethanol, and frozen at -80 °C for 15 min. The RNAs were centrifuged at 13000 rpm at 4 °C for 30 min. The supernatant was decanted and the pellets were washed slowly with 100  $\mu$ L of 70% ethanol. The reactions were chilled on ice for 5 min and centrifuged for 5 min. The liquid was removed and the pellets were dried in a speed-vac and resuspended in nuclease-free water.

Selected RNA were reverse transcribed with Superscript II (Invitrogen, Carlsbad, CA) at 42 °C for 50 min and heat inactivated at 70°C for 15 minutes. Reverse transcription reactions of 1-μL aliquots were PCR amplified with Taq polymerase in 10x PCR buffer (100 mM Tris-HCl, pH 8.3, 500 mM KCl, 20 mM MgCl<sub>2</sub>) in 100 μL reactions. Every 2-3 cycles, a 5-μL aliquot was sampled and analyzed by Electrophoretic Mobility Shift Assays (EMSA) to decide the optimum cycle number. An 800-μL large scale PCR was assembled with 8-μL reverse transcription reaction and cycled for the optimum cycle number. PCR products were pooled and ethanol precipitated as described and resuspended in 30 μL nuclease-free water. PCR products were *in vitro* transcribed and the RNAs were purified and subjected to another round of selection.

# 4.3.3 Cloning and sequencing

After selection, the pools were cloned using the TOPO TA cloning kit (Invitrogen, Carlsbad, CA). Fresh PCR products were incubated with TOPO vectors for 30 min on ice. Ligated vectors were transformed into One Shot competent *E. coli* cells (Invitrogen, Carlsbad, CA). The cells were grown on X-gal coated agar plates at 37 °C overnight. White colonies were selected and grown in liquid culture overnight. The cultures were harvested and the plasmids were extracted by Plasmid Miniprep kits (Qiagen, Valencia, CA). The plasmids were sequenced by standard dideoxy-sequencing methods.

Selected clones were PCR amplified by p46 and p47. PCR products were *in vitro* transcribed and purified as described. Affinities of the derived RNA sequences were characterized by filter binding assays.

#### 4.3.4 Affinity characterization by filter binding assays

Affinities of selected RNA pools were characterized by filter binding assays. The RNAs were dephosphorylated by Calf Intestinal Alkaline Phosphatase (CIAP) (Ambion, Austin, TX) at 37 °C for 1 hr, 5' end-labeled with <sup>32</sup>P-γ-ATP using T4 polynucleotide kinase (Ambion, Austin, TX) and purified by Quick Spin Columns (Roche, Indianapolis, IN). To monitor the pool affinity improvement progression, labeled RNAs were incubated with 500 nM of proteins in 1x binding buffer at room temperature for 30 min. To determine the dissociation constants, labeled RNA was incubated with increasing concentrations of proteins in 1x binding buffer for 30 min at room temperature. The reaction products were passed through a vacuum manifold (Schleicher & Schuell) equipped with a nitrocellulose membrane (Whatman, Piscataway, NJ) over a piece of hybond nylon membrane (Amersham, Piscataway, NJ). After the separation, both membranes were exposed to phosphorimaging screen followed by quantification of the signal intensity. The fractional binding of the pool or clone to the proteins were calculated as the signal retained on the nitrocellulose membrane divided by the total signals of the two membranes. The dissociation constant  $(K_D)$  of the aptamer protein interaction was determined by curve fitting using equation (4.1)

$$f = \frac{C_{\text{max}} P_0}{K_D + P_0} \tag{4.1}$$

where f is the fraction bound as calculated from the quantified dot blot image.  $C_{max}$  is the extrapolated maximal retention of RNA-protein complex on the filter.  $P_0$  is the initial concentration of the protein added to each binding reaction.

# 4.3.5 Competition assays

Competitions between the random pools R50, R70 and R70-3 for R50-9 were performed by mixing 100 nM fibrinogen with 1 μM each unlabeled RNA in binding buffer followed by addition of 2 nM <sup>32</sup>P end-labeled R50-9. Binding assays were incubated for 30 min at room temperature. Competition assays between the random pools R50, R70 and R50-9 for R70-3 were performed under the same conditions. The separation between protein bound and free RNA were performed on a vacuum manifold and the fractional binding was calculated as described.

# 4.4 Results and discussion

Fibrinogen and CRP from human plasma were used in the aptamer selection. *In vitro* selection for fibrinogen was initiated from two RNA pools with different randomized sequence lengths. The R50 pool contained a 50-nt randomized region and was labeled with an MB sequence for future multiplex analytical applications. Another pool, R70, contained a 70-nt randomized sequence and was used in a separate selection for fibrinogen aptamers to compare the outcome sequences selected for the same protein

using different pools. The RNA pool designed for CRP, R60, contained 60 randomized positions and was also labeled with a MB sequence.

In each round of selection, RNA pools were incubated with the proteins and bound sequences were separated from the unbound ones by nitrocellulose filter membranes. Protein-bound RNAs were retained on the filters, eluted, and amplified for the subsequent round of selection. A negative selection was incorporated in each round to minimize the enrichment of filter binding species. As the selection progressed to higher rounds, the optimum cycle numbers determined for PCR cycle course decreased (data not shown). To increase the selection stringency, the amount of protein used was reduced as the selection progressed to higher rounds (Tables 4.1, 4.2 and 4.3).

Table 4.1: Summary of in vitro selection for the R50-fibrinogen pool.

Round of selection	Input RNA (nM)	Input protein (nM)	[RNA]: [Protein]	% bound to protein	% bound to filter
1					
1	2000	320	6.25:1	0.48	0.26
2	2000	320	6.25:2		
3	2000	320	6.25:3		
4	2000	320	6.25:4		
5	2000	320	6.25:5	14.04	0.26
6	800	32	25:1	15	0.71
7	800	32	25:1	10.57	0.98
8	800	32	25:1	10.55	1.32

(Round highlighted in bold was selected for further characterization.)

Table 4.2: Summary of in vitro selection for the R70-fibrinogen pool.

Round of selection	Input RNA (nM)	Input protein (nM)	[RNA]: [Protein]	% bound to protein	% bound to filter
1	2000	320	6.25:1	0.42	0.12
2	2000	320	6.25:2		
3	2000	320	6.25:3		
4	2000	320	6.25:4		
5	2000	320	6.25:5		
6	2000	80	25:1		
7	2000	32	62.5:1	2.79	0.21
8	800	32	25:1	2.51	0.18
9	800	32	25:1	2.42	0.22
10	800	32	25:1	2.65	0.22

(Round highlighted in bold was selected for further characterization.)

Table 4.3: Summary of in vitro selection for the R60-CRP pool.

Round of	Input RNA	Input protein	[RNA]:	% bound	% bound
selection	(nM)	(nM)	[Protein]	to protein	to filter
1	2000	2000	1:1	0.6	0.27
2	2000	2000	1:1		
3	2000	2000	1:1		
4	2000	2000	1:1		
5	2000	2000	1:1		
6	2000	500	4:1		
7	2000	200	10:1	26.65	0.61
8	800	32	25:1	15.3	0.76
9	800	32	25:1	34.69	2.6
10	800	32	25:1	37.09	4.21

(Round highlighted in bold was selected for further characterization.)

The progression of the selection was also monitored by filter binding assays (Figure 4.1). For the R50-fibrinogen selection, the fractional binding of the RNA pool in the presence of 500 nM of fibrinogen increased to 15% at round 6 and started to decrease with further selection, while the filter binding fraction started to increase to 1.32% at round 8 (Table 4.1 and Figure 4.1 (a)). The results indicated further selection was unable to increase the pool binding affinity and non-specific filter binders were enriched instead. Therefore, round 6 from R50 pool was chosen for further characterization. Filter binding assays performed with the R70-fibrinogen pool selected against the same protein target showed a plateau of affinities from round 7 to round 10, though with a smaller fractional binding of ~ 2.5% (Table 4.2 and Figure 4.1 (b)). The fractional binding of the selected R60 pool for CRP decreased at round 8 and then increased gradually and ultimately yielded 37.9% binding at round 10 with a background binding of 4.21% (Table 4.3 and Figure 4.1 (c)).

Round 6 of R50-fibrinogen and Round 10 of R70-fibrinogen and R60-CRP (highlighted in Tables 4.1-4.3) were cloned and sequenced. 15 clones were selected from the R50-fibrinogen selection pool (Table 4.4). R50-20 and R50-9 were the most abundant clones, each represented 6 times. Therefore, they were selected for further affinity characterization by filter binding assays. 13 clones were selected for sequencing from the R70-fibrinogen selection pool, with two primary aptamer families represented by the clones R70-1 and R70-3. Both of these were selected for affinity characterization (Table 4.5). 17 clones were selected from the R60-CRP selection pool, and the most abundant clones R60-5 and R60-7 were chosen for affinity characterization (Table 4.6).

(a)

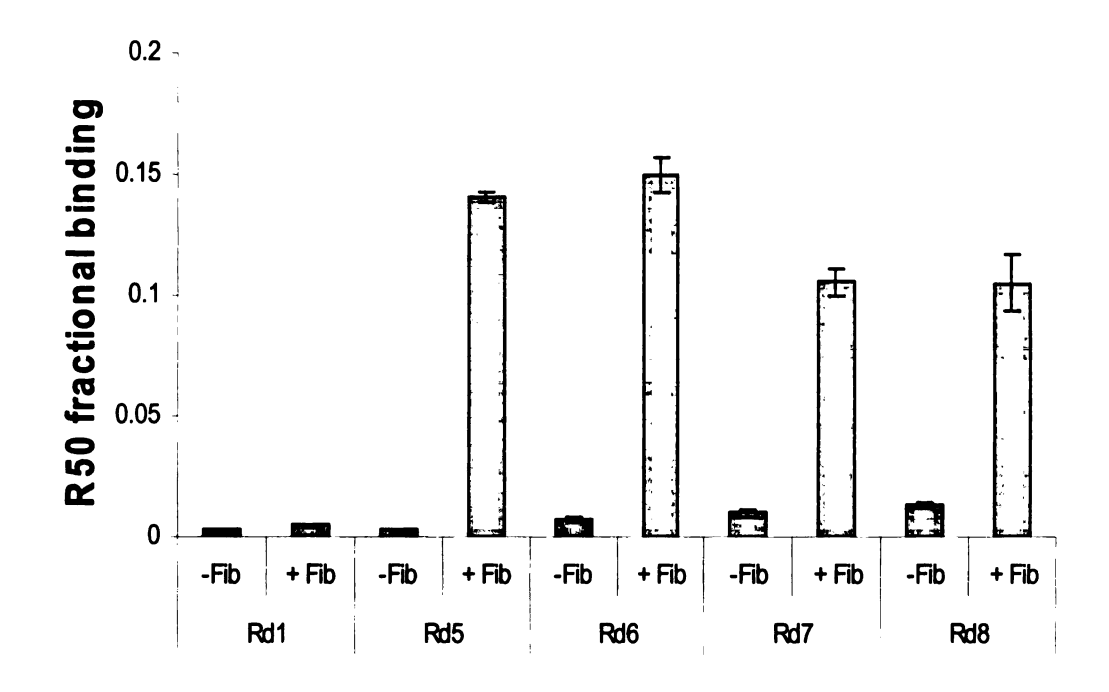
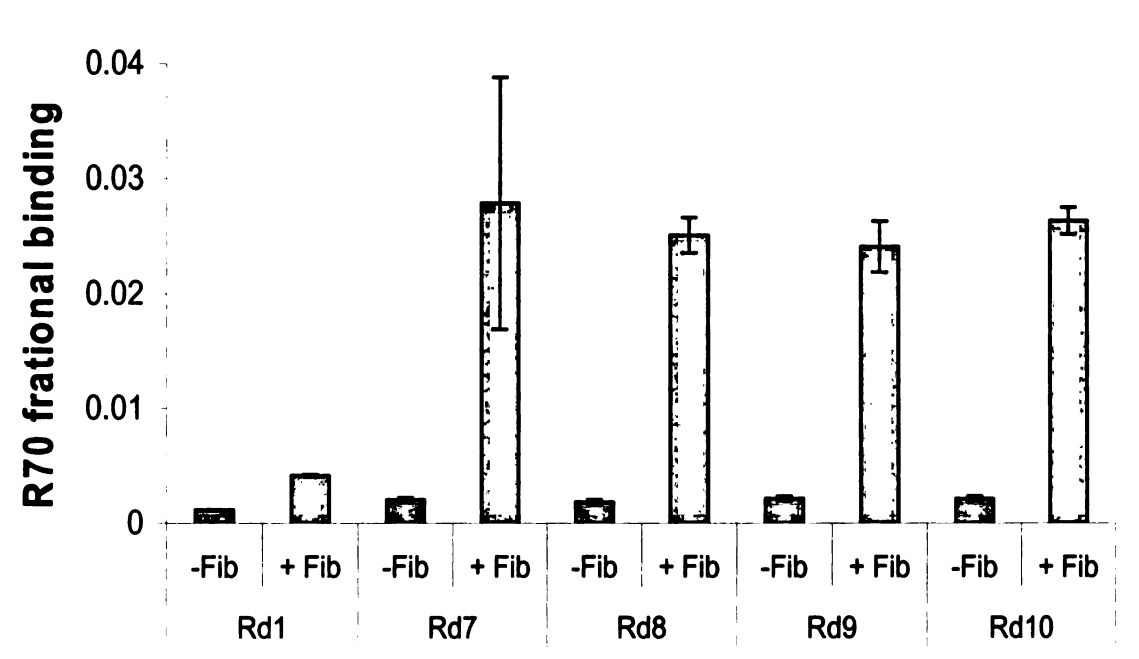


Figure 4.1: Affinity improvement of selected pools. Selected pools were radiolabeled and incubated with target proteins. The mixtures were then passed through a vacuum manifold. The fractional binding in the presence (+) and absence (-) of proteins were plotted for R50-fibrinogen (a) and R70-fibrinogen (b) and R60-CRP (c)

Figure 4.1 Continued.





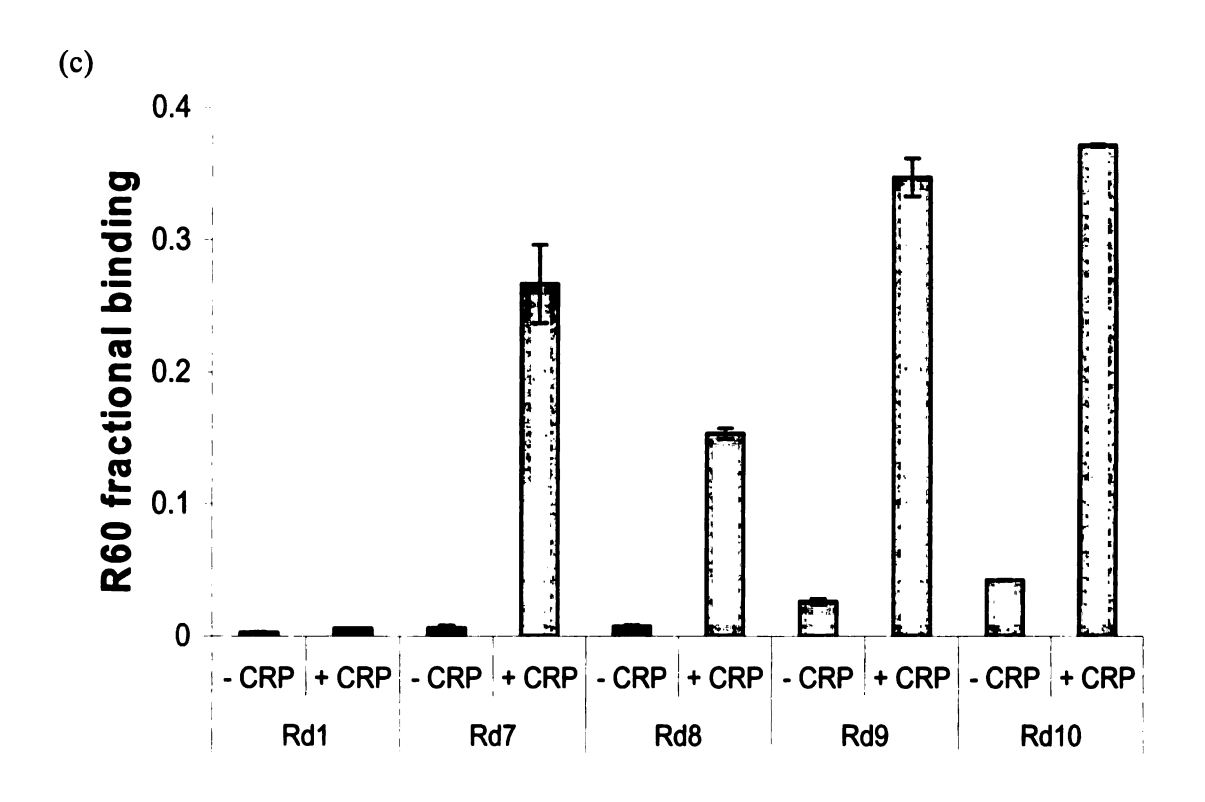


Table 4.4: The sequences of the random regions from selected clones of round 6 of the R50-fibrinogen selection pool.

Clone ID	Random region sequence	Repeats
R50-20	tggtcggagggaggggagagggtgagatgcctttgggagactagtc	6
R50-9	gacttagggcaccaggaactttagcatttgggttaaatgtcatgggagtg	6
R50-5	cgcggtatgtcagaaacatcagagggcctgcttgccgtttgagaacgact	1
R50-6	gcaatgagcattttggtcgcactggctgggtctcaggctgcagggcactt	1
R50-8	ccgcggcaaatgccgcgattgagctgtagatggtcgtacaggctgggtct	1

(Clones highlighted in bold were selected for affinity characterization)

Table 4.5: The sequences of the random regions from selected clones of round 10 of the R70-fibrinogen selection pool.

Clone ID	Random region sequence	Repeats
R70-1	ggaattcaaaacccagatcaaaaaaattactcaatcgtcagattatgctttg ttctttgcgttgaactgc	10
20,02	gctctcaaatttgattactaactcgctagttagtcttacaaagttcatccaag	20
R70-3	cagtcgccttgagtca	3

(Clones highlighted in bold were selected for affinity characterization)

Table 4.6: The sequences of the random regions from selected clones of round 10 of the R60-CRP selection pool.

Clone ID	Random region sequence	Repeats
R60-5	cttatgcagaggttcgtactaagggtagagggagagtggaatgtattgcacccgttggta	7
R60-7	a a a gatt t c t a c g gatt a g g c t g t a c t a a t g g t t g g t g t g g g g t g t	4
R60-19	tagatcgtacggtctcgtaagaaatggagggtagggtattaaagggcagaaaatagaaac	1
R60-2	tagtatgatcgatttagcagcgaagtgacggttaagtgggtgg	1
R60-6	ccggtatacagttcacaggtcgtgggtgggtggaggaaagtgaatgagatgcggattgtg	1
R60-3	tttcagcattaggccgttggcgtactcttgggatggaggggcaatttagggggagtggtg	1
R60-4	tggtgtcgaatggtgtgtggggaatggtaccattaaagttgattgctcttaacatgtag	1
R60-13	ggatcgtggtggaagttactggatgttggagagcgcggttttgaattgtctaacattagc	1

(Clones highlighted in bold were selected for affinity characterization)

The selected clones were PCR amplified and the PCR products were *in vitro* transcribed. The resulting RNAs were purified and radiolabeled for use in the filter binding assays. Filter binding assays were performed with limiting amount of RNA and increasing concentrations of respective proteins for all six selected sequences (Figure 4.2). R50-20 showed constant background binding at varying protein concentrations and was determined to be a filter binder. R50-9 showed a fibrinogen dose response with increasing protein concentrations from 0 to  $1\mu$ M. The dissociation constant  $K_D$  of R50-9 was determined by non-linear least square fitting (as described in the experimental section (Chapter 4.3.4)) to be 91.6 nM with a  $R^2$ = 0.93 (Figure 4.2 (b)).

For the selection with R70 pool, both R70-1 and R70-3 showed fibrinogen-responsive binding. R70-3 was determined to have a  $K_D$ =416 nM with  $R^2$ = 0.99 (Figure 4.2 (b)). The affinity of R70-1 was too weak (>1  $\mu$ M) and was not selected for further analysis. The affinity of R50-9 was higher than that of R70-3 and was consistent with the pool affinity characterization (compare 4.1 (a) and (b)). Through selection, the R70 pool seemed to have converged so much that only two sequences dominated the final pool and this could also explain the affinity saturation at higher rounds (Figure 4.1 (b)). Saturation of the pool at a lower binding affinity was perhaps due to the R70-fibrinogen pool aptamers targeting the protein on a surface less favorable for aptamer binding

For the selection with the R60-CRP pool, clone R60-5 showed a CRP dose response in the filter-binding assays (Figure 4.2 (a)). The affinity was determined to be 109.0 nM

with R<sup>2</sup>=0.97 (Figure 4.2 (c)). The other sequence, R60-7, was determined to be a filter binder. It is worthwhile to note that filter binders were still selected, even with negative selection during the SELEX process. This may be due to imperfect binding and separation using the filters, even in the absence of protein. Thus, the sheer number of filter binding sequences relative to specific binding sequences would give them an advantage throughout the process.

The two aptamers selected against fibrinogen, R50-9 and R70-3, showed no sequence homology. It was therefore of interest to investigate further their interaction with their target protein fibrinogen. A competition assay was performed for R50-9 and R70-3 (Figure 4.3). Radiolabeled R50-9 or R70-3 was incubated with 100 nM of fibrinogen and added with unlabeled R50-9, R70-3, round 0 of R50 randomized pool and round 0 of R70 randomized pool. The fractional binding in the presence of different competitors was determined (Figure 4.3). It was observed that R50-9 did not compete for binding with R70-3 or any of the randomized sequences (Figure 4.3 (a-b)). This was true for either R50-9 or R70-3 being labeled. These results demonstrated that R50-9 and R70-3 bind in a non-competitive fashion on fibrinogen, and they likely bind at distinct epitopes on the protein.

(a)

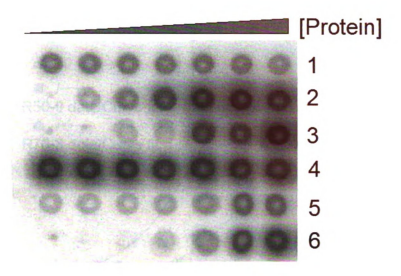
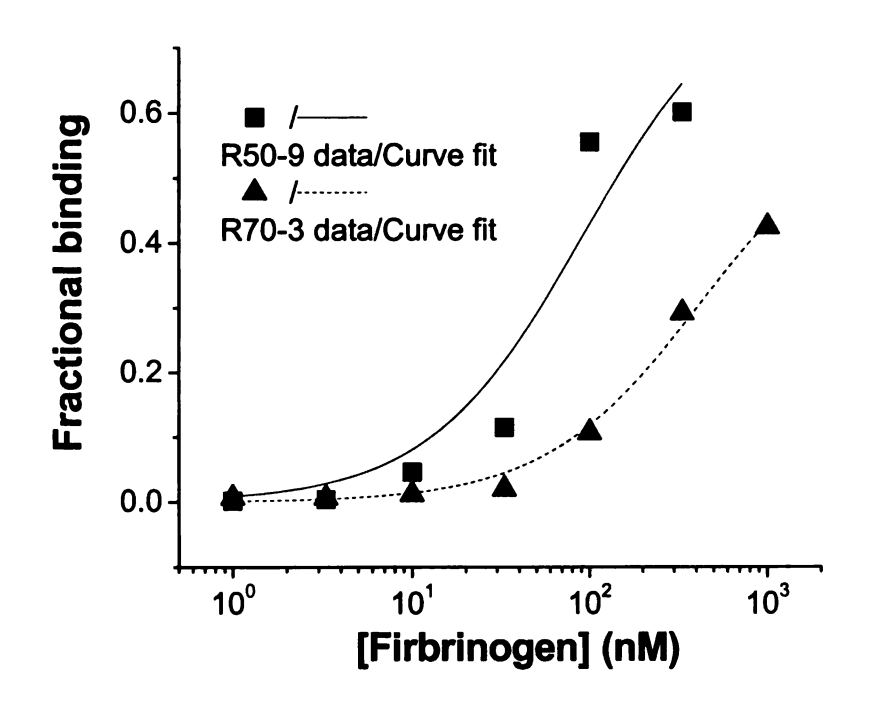


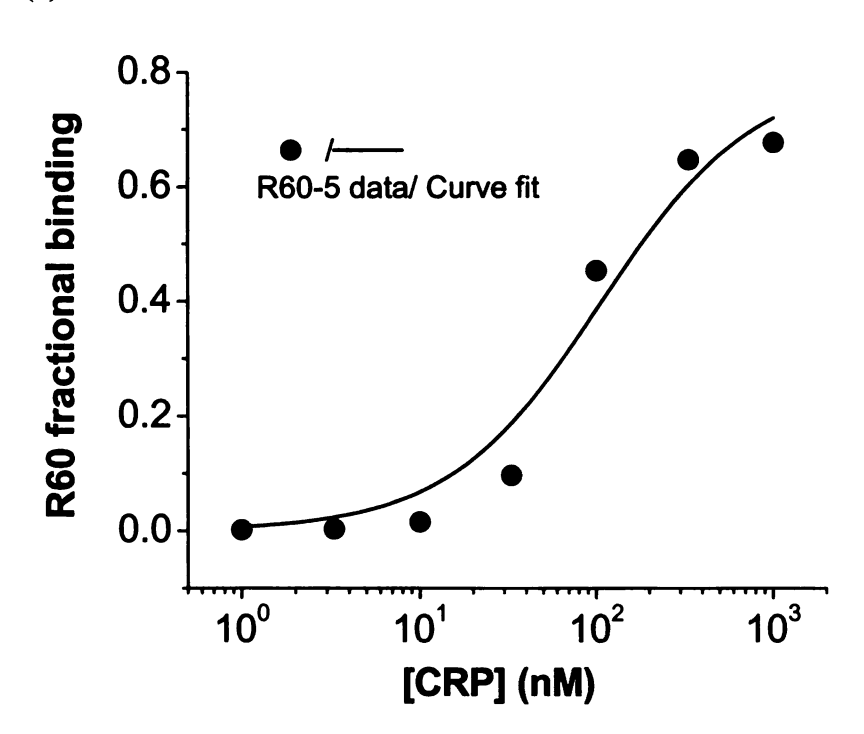
Figure 4.2: Affinity characterization of selected clones. The RNA sequences from selected clones were synthesized, radiolabeled, and incubated with increasing concentrations of protein. (a) Nitrocellulose membrane image obtained for R50-20, R50-9, R60-5, R60-7, R70-1 and R70-3 (row 1 through row 6), protein concentrations increased from left to right. (b) Aptamer R50-9 and R70-3 fractional binding at increasing fibrinogen concentrations. (c) Aptamer 60-5 fractional binding at increasing CRP concentrations. Curve fits were derived with non-linear least square fitting as described in the experimental section (Chapter 4.3.4).

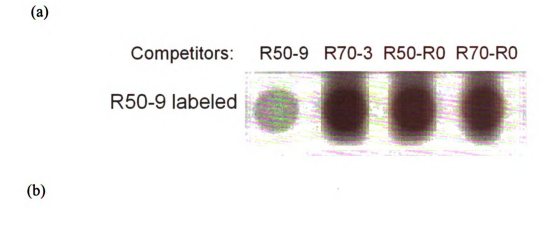
Figure 4.2 Continued.

(b)



(c)





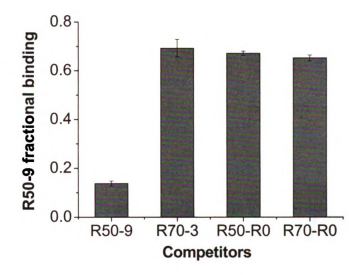


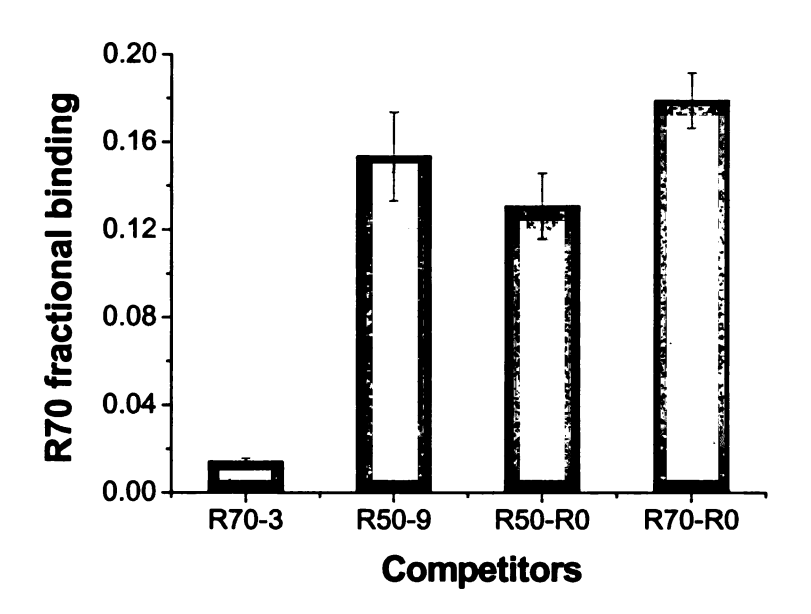
Figure 4.3: Competition assays for fibrinogen aptamers. (a) Aptamer R50-9 was radiolabeled, incubated with 100 nM fibrinogen, and added with unlabeled R50-9, R70-3, round 0 of the R50 randomized pool, or round 0 of the R70 randomized pool. Binding reactions were separated by filter binding, and fractional binding in the presence of each competitor was quantified (b). (c) Aptamer R70-3 was radiolabeled, incubated with 100 nM fibrinogen and competed with unlabeled R70-3, R50-9, round 0 of the R50 randomized pool, or round 0 of the R70 randomized pool. Binding reactions were separated by filter binding, and fractional binding in the presence of each competitor was quantified (d).

Figure 4.3 continued.

(c)



(d)



# 4.5 Conclusions

In conclusion, RNA aptamers were generated for potential cancer biomarker proteins, fibrinogen and CRP, from pools with varying lengths of random sequence. Two fibrinogen aptamers R50-9 from the R50 pool and R70-3 from the R70 pool were selected. R50-9 and R70-3 were characterized to bind fibrinogen with K<sub>D</sub> of 91.6 and 416 nM, respectively. The CRP aptamer R60-5 selected from the R60 pool has an affinity of 109.0 nM. Moreover, fibrinogen aptamers generated from two randomized pools showed no homology, and competition assays demonstrated that the aptamers bind fibrinogen in a non-competitive fashion. These aptamers can serve as biosensing elements for designing biosensing assays for measuring these proteins.

#### References

- 1. Clearfield MB. C-reactive protein: a new risk assessment tool for cardiovascular disease. *J Am Osteopath Assoc*, 105(9), 409-416 (2005).
- 2. Coussens LM, Werb Z. Inflammation and cancer. *Nature*, 420(6917), 860-867 (2002).
- 3. Mazlam MZ, Hodgson HJF. Why Measure C-Reactive Protein. *Gut*, 35(1), 5-7 (1994).
- 4. Crumley ABC, McMillan DC, McKernan M, Going JJ, Shearer CJ, Stuart RC. An elevated C-reactive protein concentration, prior to surgery, predicts poor cancerspecific survival in patients undergoing resection for gastro-oesophageal cancer. *British Journal of Cancer*, 94(11), 1568-1571 (2006).
- 5. Pierce BL, Ballard-Barbash R, Bernstein L *et al.* Elevated biomarkers of inflammation are associated with reduced survival among breast cancer patients. *Journal of Clinical Oncology*, 27(21), 3437-3444 (2009).
- 6. Hashimoto K, Ikeda Y, Korenaga D *et al*. The impact of preoperative serum C-reactive protein on the prognosis of patients with hepatocellular carcinoma. *Cancer*, 103(9), 1856-1864 (2005).
- 7. Walsh PN. Platelet coagulation-protein interactions. Seminars in Thrombosis and Hemostasis, 30(4), 461-471 (2004).
- 8. Welin L, Svardsudd K, Wilhelmsen L, Larsson B, Tibblin G. Analysis of risk-factors for stroke in a cohort of men born in 1913. New England Journal of Medicine, 317(9), 521-526 (1987).
- 9. Haffner SM. Insulin resistance, inflammation, and the prediabetic state. Am. J. Cardiol., 92(4A), 18J-26J (2003).
- 10. Jones JM, McGonigle NC, McAnespie M, Cran GW, Graham AN. Plasma fibrinogen and serum C-reactive protein are associated with non-small cell lung cancer. *Lung Cancer*, 53(1), 97-101 (2006).

# **CHAPTER 5 CONCLUSIONS AND FUTURE WORK**

The motivation for this work was to provide new technologies for the analysis of proteins and small molecules in parallel. The approach we chose was to leverage existing nucleic acid analytical technologies such as PCR and standardized oligonucleotide microarrays for proteomic and metabolomic analyses. To do this, we chose to use aptamers for affinity capture of the analytes and readout of the signal. Each aptamer was designed in advance for parallel applications through the incorporation of unique MB sequences.

To this end, an SSA was first designed to develop a theophylline biosensor in combination with scintillation counting and qPCR. The SSA converted the analyte signal into a nucleic acid signal for subsequence amplification and quantification. Analysis of the controlling parameters of the system indicated that further performance enhancements may be achievable through careful SSA design and protocol optimization. The theoretical framework for analyzing SSA biosensing performance can be easily adapted to other SSA-based *in vitro* biosensor designs, as these usually require multiple constructs to be tested experimentally to identify the best biosensors, based on some metric such as S/N. This work can also guide the design of non-natural riboswitches used for *in vivo* sensing and gene expression control. This work further provides a foundation for future parallel measurements of small molecules using SSAs. It is expected that SSAs composed of aptamers targeting other analytes can be labeled with other MBs, and the PCR amplification products can be analyzed simultaneously by microarray or other parallel readout.

Furthermore, a novel parallel protein measurement technique was developed using dualaptamer recognition. It was demonstrated that the technique is flexible and has the
potential for straightforward customization to sets of proteins. The sensitivity and
dynamic response of the approach warrants further selection and characterization of
aptamer pairs and their use in the described approach. Continued development of this
technology in combination with a microarray-based readout will provide a valuable
platform for screening of biomarker proteins in a robust, sensitive, and multiplexed
fashion. This platform will greatly facilitate the development of diagnostics for disease
detection and treatment decisions.

The dual-aptamer based biosensor is also uniquely suited for studying protein-protein interactions. Similar to the design rationale for PDGF-BB analysis, aptamers targeting each component of a pair of interacting proteins can be used to quantitatively measure the existence and persistence of their interaction. By specifically capturing a single protein and adding sensing aptamers for a variety of potential binding partners, the composition of protein complexes that form could be identified from the recovered aptamers, with the strength of the interaction described by the number of recovered sensing aptamers. This technique can provide a systematic analysis of protein interactions involved in cell signaling and uncover new connections in cellular pathways. Moreover, as aptamers can be selected to bind specifically with post-translationally modified (e.g., phosphorylated) proteins [1], it is straightforward to envision how the dual-aptamer approach would be extended to the analysis of the relative quantities of modified and unmodified protein.

This technology would add another layer of information to proteomic research, which is important for the complete understanding of cellular activity.

We have demonstrated that two aptamers can be selected that bind on distinct epitopes on a protein. This suggests that our multiple affinity detection approach would also be useful for detecting still larger targets such as cells, spores and bacteria, as these targets also have multiple surface protein markers. Pairs of aptamers selected against different epitopes on these targets would be useful in a variety of cell biology, biodefense, and biosensing applications.

The current experiments were performed in idealized laboratory conditions. A key future direction would be the continued optimization of processing and development of the mechanical details of the assay. For instance, the dual-aptamer based assays are currently performed in batch reactions but could be applied in a continuous format, such as on a microfluidic device. With continued improvement of techniques for high-throughput aptamer selection, this technique can mature to an automatic, durable, portable and economic biosensor in high-throughput format. Ultimately, the flexibility, sensitivity, and specificity of the multiplexed analytical technologies developed in this dissertation could not only enable convenient and more accurate monitoring of biological systems with reduced experimental costs and time, but also could facilitate development of a larger variety of sensors as point-of-care analytical tools.

# References

1. Li MY, Lin N, Huang Z et al. Selecting aptamers for a glycoprotein through the incorporation of the boronic acid moiety. *Journal of the American Chemical Society*, 130(38), 12636-12638 (2008).

